THE AGGLOMERATION OF NICKEL LATERITE ORE

by

Adirek Janwong

A dissertation submitted to the faculty of
The University of Utah
in partial fulfillment of the requirements for the degree of

Doctor of Philosophy

Department of Metallurgical Engineering

The University of Utah

December 2012

The University of Utah Graduate School

STATEMENT OF DISSERTATION APPROVAL

The dissertation of **Adirek Janwong**

has been approved by the following supervisory committee members:

Michael S. Moats	, Chair	**8/14/2012** Date Approved
Sanja Miskovic	, Member	**8/14/2012** Date Approved
Michael L. Free	, Member	**8/14/2012** Date Approved
Chen-Luh Lin	, Member	**8/14/2012** Date Approved
Erich Petersen	, Member	**8/14/2012** Date Approved

and by **Jan D. Miller**, Chair of the Department of **Metallurgical Engineering**

and by Charles A. Wight, Dean of The Graduate School.

ABSTRACT

Nickel laterites are becoming more attractive for nickel production due to the depletion of high grade nickel sulfide ores. Since the nickel content in laterites is relatively low, processes to recover nickel from these resources must be economical and robust. Heap leaching has been commonly used to treat low grade copper and gold ores due to its low capital and operating costs. Therefore, research and development in nickel heap leaching technology is compelling. However, nickel laterites typically contain significant quantities of fine particles and clay minerals which could contribute to heap leaching difficulties.

Agglomeration has been used to improve heap performance in copper and gold heap leaching. Experiments have been conducted to evaluate the performance of agglomeration in nickel heap leaching. In this study, nickel laterite ores were agglomerated with various conditions, including moisture content, acid concentration, retention time and drum rotation speed. Size distribution, permeability and electrical conductivity data of agglomerates were collected to study the effects of agglomeration conditions on agglomerate qualities. The agglomerates were then leached with diluted sulfuric acid for 90 days. Nickel and other interested element extraction rates were obtained by ICP-OES. Mineralogy of feeds, agglomerates and leached residuals were also investigated.

From the experimental data, we found that agglomerate size distributions (ASD) correlated with the agglomeration volume of solution added agglomeration. The drum rotation speeds did not a have significant effect on agglomerate size distribution. Increasing mixing times during agglomeration led to increases in agglomerate sizes. Hydraulic conductivity (permeability) of the agglomerate bed is related to the agglomerate size distribution. The electrical conductivity of nickel laterite agglomerate beds depends on the sulfuric acid concentration used during agglomeration, solution addition, external compression and nature of the ores. Nonetheless, the values depend heavily on the sulfuric acid concentration.

The highest extraction rate of nickel, cobalt, iron, aluminum, magnesium and manganese in these experiments are 58%, 38%, 22%, 28%, 48% and 27%, respectively. The feed contains mainly silico-ferruginous plasma, goethite and clay minerals along with other minor phases. In agglomerates, a new sulfate phase was observed. The main element in this phase is sulfur. The "sulfate" phase and clays appear to dissolve during leaching. The nickel that remained unleached predominantly resides in the silico-ferruginous plasma.

For my supportive parents, brothers and lovely wife

TABLE OF CONTENTS

ACKNOWLEDGEMENTS

I would like to express my sincere gratitude to my advisor, Professor Michael S. Moats, for his abundantly helpful guidance, assistance and financial support through the entirety of this research work. I also owe my deepest gratitude to my supervisory committee, Professor Erich U. Petersen, Professor Michael L. Free, Professor Chen L. Lin and Professor Sanja Miskovic, for their suggestions, time and support.

I would also like to express my thankfulness to Professors Jan D. Miller and Raj K. Rajamani for their useful suggestions and advice. Special thanks to my friends, especially AMIRA project members, Michael J. Peoples, Thien Vesodrosakda, Nikhil Darwan, Francis Elnathan, Brent Randall and Blaine Wilson for their invaluable assistance.

Finally, I am indebted to my parents, my wife, my family and my friends for their moral and physical support through the duration of my study.

CHAPTER 1

INTRODUCTION

Nickel is one of the more common metallic elements used among iron and copper. The main nickel-bearing minerals can be divided into sulfides and oxides. In the past, nickel production was highly dependent on sulfide ores. Since high-grade nickel sulfide ores are becoming depleted, nickel oxide or laterite ores are becoming more attractive to the nickel production industry.

The most common method of extraction leading to the eventual production of high-purity nickel from laterite ores is high-pressure acid leaching (HPAL) (Dalvi et al. 2004). However, the process has to perform in high temperature and pressure. Moreover, the autoclaves used in this process are costly. Several processes have been introduced as alternative methods to extract nickel, such as Caron, atmospheric leaching, chloride leaching, nitric leaching and heap leaching. Among these, heap leaching has the potential to be a low-capital option and thus is of interest to nickel production companies.

Heap leaching is routinely used in gold and copper extraction from low-grade ores. Low capital and operating costs are the advantages of heap leaching; however, long leaching time and low recovery rates are potential disadvantages. Nickel laterites normally contain significant quantities of fine particles which can lead to poor

percolation within the heap, low heap strength and low recovery rate. Agglomeration of laterite ores has the potential to overcome these difficulties.

Agglomeration is basically the process of adjusting the size distribution of the material placed on a heap. In wet agglomeration, as used in heap leaching, the particles are attached to each other mainly by capillary forces. The other bonding mechanisms, such as attractive forces between solid particles and interlocking, contribute less to bond particles in wet agglomeration.

In order to improve the percolation within the heap, the agglomerate size distribution should be optimum and the strength of the agglomerates should be reasonable. The preferable size and strength of agglomerates varied depending on type and initial size distribution of ores. To investigate the agglomeration process and its effects on leaching, the agglomeration, electrical conductivity, permeability, column leaching and mineral phase analysis of a nickel laterite ore from Piaui, Brazil was investigated.

CHAPTER 2

LITERATURE REVIEWS

Nickel Laterite Ore Mineralogy

Nickel is one of the common metals, as it is fairly abundant in the earth. Nickel ranks fifth in abundance in the earth, following iron, oxygen, silicon and magnesium, respectively (Boldt Jr. 1967). The earth is comprised of about 3% nickel. Most nickel is found in basic or mafic rocks. The mafic rocks are dark, dense and high in iron and magnesium. Relatively low nickel content is found in acid or silicic rocks which are high in silicon and light in color. Generally, the more iron and magnesium and the less silicon and aluminum the rocks contain, the higher the nickel content is.

The main nickel-bearing minerals can be divided into two categories: sulfide and oxide. About 70% of the world's land-based nickel resources is in laterite (oxide) minerals. Sulfide minerals contain 30% of nickel resources. The most common nickel sulfide mineral is pentlandite; it accounts for a majority of the nickel mined in the world. The other important nickel sulfide minerals are millerite, heazlewoodite and polydymite. Garnierite and nickeliferous limonite are the commonly mined nickel oxide minerals. The nickel contents in the oxide minerals are relatively low and variable compared to the sulfide minerals. The oxide ores are usually called lateritic ores due to the formation process of the ores.

The weathering process or laterization involves the dissolution of the original minerals, movement of the elements in solution and precipitation of the elements in another location (Golightly 1979, 1981). This process plays a vital role in the development of nickel laterite deposits. The process begins with the dissolution of peridotite by acidified groundwater. Peridotite is composed mainly of olivine ($(Mg,Fe,Ni)_2SiO_4$), a silicate of iron and magnesium which normally contains 0.3% of nickel by weight. Prolonged weathering of olivine releases iron, magnesium, nickel and silicon into solution. Iron oxidizes and precipitates out first to goethite ($FeO(OH)$) and hematite (Fe_2O_3). Therefore, these iron oxides form near the earth surface, while nickel, magnesium and silicon are carried downward with the solution. As long as the water remains acidic, these elements remain in solution. When the solution is neutralized by reacting with surrounding rock and soil, these elements tend to precipitate as hydrous silicates. The nickel is less soluble than magnesium so the first precipitates contain more nickel than magnesium. The magnesium which is still in the solution is often carried off to the ground water.

The precipitated minerals can be attacked by fresh acidic ground water repeatedly due to the erosion of the earth surface. This constant weathering enhances the nickel concentration in the precipitated minerals. The nickel concentration is highest near bedrock at the bottom of the deposits.

Several factors influence the formation of the nickel-bearing minerals in laterite deposits. These include the mineralogy of the peridotite and its tectonic setting, the climate, the topography and the geomorphic history. These factors control the movement of water and the initial nickel concentration (Golightly 1979, 1981). Normally, the nickel

laterite deposits are divided into 3 different zones: limonite, nontronite (intermediate or smectite-quartz) and saprolite zones, as shown in Figure 1.

The limonite zone contains mostly goethite and amorphous ferric hydroxide. Silica and magnesium are low in this zone. Sometimes, this zone is separated into two subzones: Ferricrete or iron cap and limonite zones. Nickel contents increase downward in the limonite zone. Nickel is mostly found in iron-manganese oxide or poorly crystalline lithiophorite and cryptomelane. This zone generally has a red, fragmental or rubble appearance. Depending on locations, typical concentrations are 0.6-1.7 wt% Ni, 0.1-0.2 wt% Co, 1-4 wt% Mg and more than 40 wt% Fe that are found in this layer.

Iron Cap			
Limonite Zone	Goethite (FeO(OH)) and ferric hydroxide	Ni Co Mg Fe	0.6-1.7% 0.1-0.2% 1.0-4.0% > 40%
Nontronite Zone	Smectite clays, usually nontronite ($Fe_2O_3.2SiO_2.2H_2O$), quartz (SiO_2) and a mineral possibly belong to the chlorite groups ($(Mg, Fe, Ni, Mn,Al)_6(AlSi_3)O_{10}(OH)_8$)	Ni Co Mg Fe	1.2% 0.08% 3.5% 18%
Saprorite Zone	Bed rock fragments, garnierite ($(Ni, Mg)_6Si_4O_{10}(OH)_8$), quartz ($SiO_2$) and saprolized rims of the boulders	Ni Co Mg Fe	0.4-3.0% 0.02-1.0% 10-30% 9-25%

Figure 1. Typical laterite ore profile

The nontronite zone is the intermediate zone between the limonite and saprolite zones. It consists of soft smectite clays, usually nontronite, and quartz. This zone develops in dry climate areas and the presence of this layer is not typically found in humid areas. The nontronite zone is soft and has a low bulk density. Generally, 1.2 wt% Ni, 0.08 wt% Co, 3.5 wt% Mg and 18 wt% Fe are found in this zone.

The saprolite zone has the highest nickel grade when compared to the limonite and nontronite zones. The mineralogy and chemistry of saprolites in this zone are highly variable due to differences in bed rock geology, climate environment, laterization process time, the degree of serpentinization of the bed rocks and the drainage ability of the area. The last two factors seem to have more effects on the mineralogy and chemistry of the saprolite. The zone normally is composed of fragments of bed rocks, saprolitic rims, veins of precipitated garnierite, nikeliferrous quartz and manganese wad (Golightly 1979, 1981). 0.4-3 wt% Ni, 0.02-1 wt% Co, 10-30 wt% Mg and 9-25 wt% Fe are observed in this zone.

Nickel Laterite Ore Processing

The mineralogy and chemistry of nickel laterite ores are complex and are not amenable to significant upgrading and concentrating. This often leads to complicated extraction processes. Pyrometallurgical and hydrometallurgical processes have been commercially used for nickel production. About 35% of the laterite ores are treated pyrometallurgically with the remainder processed by hydrometallurgical processes (Norgate & Jahanshahi 2010).

Prior to processing via pyrometallurgy or hydrometallurgy, nickel content in the nickel laterite ores is normally upgraded by the following steps: crushing, separating

small, soft and nickel rich materials from coarse, hard and low nickel content materials by screening, hydrocyclone or spiral classifiers and finally rejecting the nickel lean particles from the ore body. Upgrading nickel laterite ores prior to the main processes reduces a requirement of energy, reagent and equipment usages during further nickel production processes (Crundwell et al. 2011).

Pyrometallurgical Processes

Pyrometallurgical processes are typically used for saprolite ores. Relatively low iron and high nickel contents in saprolite ores ensures that nickel-bearing products do not contain excessive iron content which reduces the flexibility of their uses and increasing transportation costs (Reid 1996). The final nickel-bearing product depends on the slag melting point which is affected by the SiO_2/MgO ratio of the saprolite ore. For an ore with low melting point slag, with the SiO_2/MgO ratio in the range of 1.8 to 2.2, the production of nickel sulfide matte is more preferable. High melting point slag ores, SiO_2/MgO ratio either < 2 or > 2.5, are suitable to produce ferronickel. Ores having SiO_2/MgO ratio between 2.3 to 2.5 are very corrosive to the furnace lining and require a modification to the feed chemistry prior to smelting (Dalvi et al. 2004).

Dewatering and calcination are typical processes before smelting of nickel laterite ores. Nickel laterite ores almost always contain high moisture content. However, the smelting feed requires dry ores to avoid explosions within the furnaces. Wet ores are continuously fed to a sloped rotating kiln. Hot air at about 800 ^{o}C is blown into the rotation kiln at the same time and direction with the ores along the rotating kiln. The

dewatered ores are then screened and crushed before transferring to the calcination process (Crundwell et al. 2011).

Calcination removes any remaining water and partially reduces the nickel and iron minerals. Calcination is performed in a rotating kiln. Dewatered ores are fed continuously to the kiln. Coal and recycled dust pellets are added to the kiln continuously. Hydrocarbon fuel provides both energy and reducing gas to the rotating kiln. The hot reducing gas heats, dries the feed and also partially reduces nickel and iron minerals in the feed. The products of calcinations are dry, partially reduced and coal-bearing calcine at a temperature of 900^{o} C. For the dewatered ores preparing for the nickel sulfide matte smelting process, liquid sulfur is also sprayed into the discharged end of the rotating kiln. The sulfur reacts with nickel and iron within the dewatered ores, producing nickel and iron sulfides (Crundwell et al. 2011).

These processes consume significant quantities of energy due to the fact that all the moisture and combined water have to be removed in the process and required high temperatures to melt the minerals. Electrical and hydrocarbon power have been used to provide the necessary energy.

Smelting to ferronickel

The preferable ores for ferronickel production have relatively high nickel content (>2.2%); however, >1.5% nickel content ores can also be used to produce ferronickel. Ferronickel can be produced with low or high carbon content, depending on the Fe/Ni ratio in the ores. High Fe/Ni ratio (6-12) ores are used to produce low carbon ferronickel. Low Fe/Ni ratio (5-6) ores are used to make high carbon ferronickel (Dalvi et al. 2004).

Calcination products are fed continuously to an electrical furnace where they are melted and reduced. Layers of molten crude ferronickel at 1450 ^{o} C and molten slag at 1550 ^{o} C are the products of the process. Hot carbon monoxide and nitrogen gas is also produced. The molten crude ferronickel is composed of 20-40% of nickel and 60-80% of iron. The molten slag consists of SiO_2, MgO, FeO and 0.1-0.2% of nickel. Due to the immiscibility of molten slag and crude ferronickel, they are tapped intermittently out of the furnace from different tap holes.

The impurities within molten ferronickel are then removed or reduced in concentration before the ferronickel is used. The main impurities are phosphorus and sulfur. The acceptable phosphorus and sulfur contents are 0.02% and 0.03%, respectively. Lime is used to remove phosphorus from molten ferronickel while sulfur is removed by reaction with calcium carbide and/or other calcium and sodium compounds. The ferronickel then is cast into ingots or granulates, depending on the application (Crundwell et al. 2011).

Smelting to nickel sulfide matte

The suitable ores should have relatively high Fe/Ni ratio (>6) and low melting point slag (<1600 ^{o}C), SiO_2 / MgO ratio between 1.8 and 2.2 (Dalvi et al. 2004). The nickel sulfide matte is usually made into melting grade nickel and used in the ferrous alloy industry.

The sulfided calcine produced via calcination is fed into an electrical furnace. Matte, slag and hot off gas are the products of the smelting process. The matte and slag are then tapped from the furnace by different holes. The slag which has lower density is

tapped out of the furnace via higher tap holes and discarded. The matte which has higher density is removed from the furnace via lower tap holes and delivered to further purification. The matte usually contain 26% Ni, 63% Fe, 0.8% Co and 10% S. Air is then blown into the molten matte to remove iron. Silica is also added as a flux to produce an immiscible slag. The product from this converting process is 78% Ni, 20% S, 1% Fe and 1% Co.

Sulfur is another impurity which has to be removed from the matte products prior to use in the steel-making industry. Therefore, a roasting process is used to oxidize the sulfur in the matte. Enriched oxygen air is blown upward into the roasting chamber along with the granular matte. Sulfur in the matte reacts with oxygen to form sulfur dioxide gas. Nickel oxides are also products from this process. Normally, the roasted nickel oxides are reroasted to further decrease sulfur down to 0.003%. The final process is to reduce the oxidized products to metal. The process is similar to the roasting process; however, kerosene is used to produce reducing gas. The nickel granules are then cooled and sent to the steel-making industry (Crundwell et al. 2011).

Hydrometallurgical Processes

Hydrometallurgical processes play a vital role in the treatment of nickel laterites due to the depletion of the sulfide ore deposits. Lower grade nickel laterite, limonite, is not suitable for the pyrometallurgy processes due to its high iron and low MgO contents. Several processes have been commercially used and/or proposed in the last few decades. Some of them are currently operated and some are still under development.

Caron process

The Caron process is the oldest limonitic ore hydrometallurgical process. However, it can also be used to treat a mixture of limonite and saprolite ores. Ores are ground and dried then heated to over 700^{o} C in a reducing atmosphere. This changes nickel and cobalt to their metallic state. The metallic nickel and cobalt are leached by ammoniacal-ammonium carbonate to dissolve nickel and cobalt as ammine complexes (Moskalyk & Alfantazi 2002). The nickel and cobalt is precipitated from the solution as carbonate when the ammonia is removed by boiling. Calcination of carbonate at 1200^{o} C produces nickel oxide (Reid 1996).

The Caron process has high energy consumption due to the fact that it involves the pyrometallurgy processes; drying, calcining and reducing in ore pretreatments. The recovery of nickel and cobalt are low, normally 80% for nickel and 55% for cobalt (King, 2005). The recovery of nickel and cobalt decrease as the amount of saprolite increases because nickel and cobalt are locked in silicates and are difficult to reduce at 700^{o} C (Dalvi et al. 2004).

High pressure acid leach (HPAL) and pressure acid leach (PAL)

HPAL and PAL are the main commercial alternative processes to the Caron process in the treatment of limonite ores. Nickel and cobalt recoveries are higher than the Caron process. Limonite ores are suitable for these processes due to their low magnesium content (usually less than 4%). The ores can contain some saprolite or clay. The disadvantages of the processes are the uses of expensive titanium autoclaves, high leach

temperature: varying in the range of 245 to 270 ^{o} C and narrow leachable ore types (Dalvi et al. 2004).

The feed to HPAL is a heated slurry of nickel laterite ores. The slurry is then leached with sulfuric acid in the autoclave for 1 to 2 hours to achieve 95% nickel extraction. After leaching, the slurry is sent to flash cooling, neutralization, liquid/solid separation, solution purification and nickel and cobalt recovery. The solid liquid separation is carried out by Counter Current Decantation (CCD). Various processes have been used to separate nickel and cobalt out of the leaching solution, such as mixed sulfide precipitation, nickel carbonate precipitation, mixed hydroxide precipitation and solvent extraction (Crundwell et al. 2011).

During HPAL, goethite continuously dissolves and releases nickel into the leach solution. The ferric iron precipitates as hematite in between goethite pores. Nickel is also found in magnesium silicate structures and in manganese particles. High temperature enhances the dissolution of nickel and results in rapid extraction of nickel. Cobalt is normally found in manganese phases. It also dissolves rapidly and extraction of 90% can be achieved.

The shrinking core model cannot be used as a model in the HPAL of limonite ores due to the porous nature of the ores even through the model is fit mathematically. The grain model was introduced for use in the nickel dissolution during HPAL of limonite ores. The model assumes that solid particles are visualized as pellets consisting of individual dense grains compacted together. Each grain reacts individually following an unreacted shrinking core pattern. The fluid reactant diffuses through the pores of solid grains while reacting (Georgiou & Papangelakis 1998).

X. Guo et al. (2011) investigated the effects of sulfuric acid addition, leaching temperature and time, liquid/solid (L/S) ratio on metal extraction from a limonite ore using HPAL. The limonite ores were ground to less than 180 μm and mixed with water and Na_2SO_3. The sulfuric acid was added to the slurry and then the mixture was injected into the reactor. The mixture was then heated up to the desired temperature. In order to extract nickel, the goethite phase had to dissolve. At high temperatures, the acid consumed by the dissolution of iron is equal to the acid produced by hydrolization of ferric iron. Therefore, at high temperature (>240^{o}C) and high pressure, the transformation of goethite to iron oxide does not consume acid. Ferrous ion and chromium (III) enhance the dissolution of cobalt and manganese oxide. The nickel extraction efficiency increases with increasing of sulfuric acid addition. The cobalt extraction increases slightly with increasing acid addition. As the leaching temperature increases, the extraction of nickel, cobalt, manganese and magnesium increase. In contrast, iron extraction decreases. Nickel, cobalt, manganese and magnesium extraction increase as the leaching time increases up to 1 hour. Extended leaching time had only a small effect on metal extraction. A negative effect of increment of leaching time can be observed on iron extraction. The L/S ratio has a slightly positive effect on the metal extraction except for iron. The optimum conditions for the process used in the experiments are as follow: 250 kg/t ore sulfuric acid addition, 250^{o}C, 1 hour and 3/1 of L/S. 97% nickel, 96% cobalt, 93% manganese, 95% magnesium and less than 1% iron can be obtained from these conditions.

Inco Technical Services Limited has developed pressure acid leaching in the horizontal autoclaves process which requires limited ore upgrading for nickel laterite ores

from Goro. Because of the relatively low saprolite to limonite ratio and low magnesium content of saprolite in the Goro ore body, the leaching of a mixture of both ore types can be processed by pressure acid leaching. The ores were mixed with water to create slurry and then fed to the agitated autoclave where the ores were leached with sulfuric acid at 270^{o} C (Mihaylov et al. 2000). The goethite is dissolved and then iron precipitates as hematite. The CCD process was used to separate the leach residual. Sulfur dioxide and lime was used to increase the pH and precipitate impurities. The solvent extraction was used to extract nickel, cobalt and zinc into the hydrochloric acid strip solution. Cyanex 301 was used as a new reagent. The zinc and cobalt were selectively removed from the solution using strong or weak base ion exchange resin and tertiary octyl amine, respectively. The nickel containing hydrochloric acid solution is subjected to the pyro-hydrolysis in order to produce nickel oxide products and recover hydrochloric acid.

Atmospheric leaching (AL)

Atmospheric leaching (AL) is the competitive process to the HPAL. AL is operated at lower temperature and in open vessels which can avoid the expensive autoclave used in the HPAL. However, the nickel and cobalt extraction and the postprocesses of the PLS are the important issues that need to improve. Several methods have been proposed to improve the leach kinetics of the nickel and cobalt by AL, including increasing temperature and leaching time, using redox-control, adding salt (NaCl), reducing the particle size, roasting and sulfating the ores prior to leaching (McDonald & Whittington 2008a).

S. Chander (1982) investigated the effects of several acids to the extraction of nickel in AL. He found that the extraction of nickel depends on different types of acids in

order: oxalic > hydrochloric ≈ hydrofluoric > sulfuric > nitric > perchloric. Sodium chloride, calcium chloride and diluted sulfuric acid leach solution can increase the extraction of nickel. Chloride ions do not form a complex with nickel but form a complex with ferric ions. He also found that the extraction of nickel and the dissolution of iron phase are correlated.

I. Halikia (1991) performed leaching experiments on Greek iron-nickel laterite which had hematite as the primary mineral. She found that the agitation rate has no effect on the rate of leaching of nickel. The sulfuric acid concentration influences the kinetics of nickel extraction only in the initial stages of leaching and becomes less influential as time increases. Particle size had no obvious effect on the kinetics of nickel extraction, especially with coarser particles. Finer particles have some effect, but only in the initial stages of leaching. Only temperature had a demonstrated effect on the rate of nickel extraction, particularly at high temperature.

In a leaching study of Greek serpentine ores, S. Agatzini-Leonardou and I. G. Zafiratos (2004) found that nickel recovery increases with sulfuric acid concentration independently from temperature and particle size. Cobalt, iron and magnesium recoveries follow similar trends. 74% and 51% extraction of nickel and cobalt, respectively, were obtained within 2 hours. The Fe/Ni ratio in the solution was low relative to the ores; Mg/Ni in the solution was equal to that in the ores. These indicate that nickel comes into the leach liquor from the dissolution of serpentine, not hematite or goethite.

The Anglo Research Nickel (ARNi) Process was developed to exploit the advantages of both chloride and sulfide processes at atmospheric temperature. Sulfuric acid, water and strong $MgCl_2$ are used as the leach solution. The resulting hydrochloric

acid acts as the main leach agent. 95% of nickel and cobalt can be extracted from ferruginous ores (Steyl et al. 2008).

H. Liu et al. (2005) presented a laterite atmospheric leaching process in United States Patent No. US 2005/0226797 A1. The laterite ores were separated into low magnesium (limonite) and high magnesium (saprolite). The limonite is subjected to primary leaching with concentrated sulfuric acid at 105 ^{o}C. The saprolite fraction and goethite seeds are then added to the slurry. The iron is precipitated out as goethite. The excess ferric iron in the secondary leach solution can be removed as jarosite by adding jarosite forming ions and jarosite seed materials. The excess ferric iron can also be treated by adding a reductant such as sulfur dioxide to reduce it to the ferrous state. More than 80% and 90% of nickel and cobalt can be extracted via this proposed process.

H. Liu (2006) also introduced another process in which nickel sulfide slurry is leached with the leach solution of the laterite ores. The combination of HPAL and AL processes can be used to treat both low and high magnesium ores. The low magnesium ore was subjected to HPAL to produce primary leach solution. The high magnesium slurry was added to the primary slurry to promote the precipitation of iron as goethite or hematite and release free acid for secondary leaching.

In the Triple A process (Curlook 2004), highly serpentine ores were crushed to smaller than 48 mesh, and pulped with water to a pulp density of about 15 to 20% solids. Saline water can be used instead of fresh water. Sulfuric acid was then added to the pulp in the amount of 85% or more by weight of the dry ores. The pH should be between 1.5 and 2.0. The mixtures were then heated up to 100 ^{o}C for 1 hour. Limestone was then added to the leach solution in order to bring the pH up to 4.0 and precipitate iron out of

the solution. The nickel and cobalt can be extracted out of the solution by raising the pH up to 8.5 by adding magnesia, lime, sodium compounds or sulfide compounds. 96 and 97% of nickel and cobalt extraction can be achieved via this process

Chloride leaching

Leaching of nickel laterites by chloride media has been studied for more than a decade. Most chloride media used in nickel laterite leaching are hydrochloric acid and magnesium chloride. The use of hydrochloric acid has several advantages compared to sulfuric acid. Firstly, the hydrochloric acid is a more powerful lixiviant for extracting nickel and cobalt at atmospheric pressure and the acid can be recycled by spray roasting. Secondly, the leach solution can be purified by direct solvent extraction (DSX) with Versatic 10 and Cyanex 301. Finally, the production of hematite, a stable phase for iron disposal, and magnesia, a pH adjustment reagent, are useful for the process (Gibson & Rice 1997).

Hubler and Ratcliffe (1938) indicate the use of dilute hydrochloric acid (4 to 20%) in nikeliferous ore leaching. The ores were crushed to - 4 mesh and then leached by the dilute hydrochloric acid to form metal chlorides. The leach continues until the acid concentration decreases to below 1% to obtain the selective extraction of nickel over iron. The magnesia is added to precipitate nickel out of solution after iron and aluminum have been removed. The extracted nickel is calcined to produce nickel oxides as a final product.

Amer and Ibrahim (2001) used hydrochloric acid to leach Egyptian iron ores and investigate the effects of temperature, leaching time, acid concentration, particle size and agitation rate on the extraction of iron and nickel. As temperature and acid concentration

increase, the extraction of the iron and nickel increases. As expected, smaller particles dissolve faster in the leach solution. The agitation rate does not have significant effect on the metal recovery. Iron and nickel extraction can reach 90 and 96%, respectively, during the experiments.

Concentrated magnesium chloride and hydrochloric acid solution was used in leaching experiments by Chesbar Resource Inc. for their laterite project in Guatemala. More than 90% recovery of nickel and cobalt can be achieved in the chloride leaching process at atmospheric ambient. Acid and chloride can be recovered by pyrohydrolysis and high grade magnesia is obtained as the end products. The use of concentrated chloride has two benefits as the activity of water is very low and the activity of the hydrogen ions is significantly increased. The leaching process was performed at temperatures of 80 to 105^{o}C (Harris & Magee 2003). In a patent proposed by Harris, Lakshmanan and Sridhar (2004), more details of the process are described. The concentration of magnesium chloride and hydrochloric acid are at least 200 g/L and 4.5 to 14 M, respectively. The pH of the lixiviant solution is between 0.4-2.5 to enhance the precipitation of iron as hematite.

Due to the high energy consumption of the pyrohydrolysis process, the later process seems to use other approaches. The leach condition is designed to take all the iron, nickel, cobalt, and magnesium into the solution. 500 kg/tonne hydrochloric acid and 360 g/L magnesium chloride are used as a leach solution. The distillation of the hydrochloric acid and hydrolysis of the iron as hematite are effective in the system with the presence of concentrated magnesium chloride. The vapor pressure of hydrochloric

acid over the concentrated magnesium chloride is high and this condition promotes the hydrochloric acid distillation process (Harris et al. 2006a; 2006b).

Leaching of nickeliferous laterite with ferric chloride solution was examined by Munroe (1997). He indicated that 96% extraction of nickel can be achieved. The experiments were performed in titanium autoclaves and nitrogen atmosphere. The ores used were ground in a mortar until all particles were smaller than 150 μm. The ferric chloride concentration was 1 M. The results show that an extraction of metals increases as the temperature increases. However, at temperatures beyond 423 K, the extraction of the metals began to decrease.

Nitric leaching

Nickel content of the Orissa deposit in India is approximately 1%. These nickel ores were mixed with 10% of coke and then roasted at 650^{o} C for 1 hour. The roasted ores were cooled in the nitrogen atmosphere to prevent reoxidation of the nickel. The cooled ores then were leached by 0.7N nitric at 80^{o} C for 2 hours. More than 70% recovery of nickel can be achieved. The nitric acid selectively leaches nickel without largely dissolving oxides of iron, aluminum and chromium (Sarojini et al. 1972).

Nossen (1959) performed nitric leaching experiments of nickel laterite ores to support his patent. The laterite ores were roasted at 650^{o} C for 30 minutes and then cooled. The cooled ores then leach with diluted nitric acid at 80^{o} C until the pH of solution is at about 2. The solution is then separated from the undissolved gangue. Precipitation was used to recover nickel and cobalt and get rid of contaminated elements. The nickel and cobalt recovery of ~80 % can be obtained. The acid recovery was 96%.

Heap leaching

Heap leaching is commonly used in gold and copper extraction from low grade ores due to its low capital and operating costs. However, the low recovery, acid waste and long leaching times are disadvantages of the heap leaching process (Robertson & Van Staden 2009). The diminution of high-grade nickel sulfide ore deposits and high capital costs for smelting processes are stimulating research and development in nickel laterite heap leaching technology. High acid consumption, potential breakdown of the aggregated mineral structures, poor selectivity of nickel over iron and magnesium and high swelling clay content are the primary issues that need to be resolved relating to nickel laterite heap leaching (McDonald & Whittington 2008a).

European Nickel (Oxley et al. 2007) constructed three heaps at its Caldag nickel laterite atmospheric heap leach project and demonstrated the feasibility of the process. The flow diagram is illustrated in Figure 2. The ore was crushed to less than 25 mm. Heaps 1 and 3 were irrigated from ponds 1 and 3 which had an acid concentration of 75 g/L H_2SO_4. A bleed from the underflow of heaps 1 and 3 was fed to heap 2. The PLS of heap 2 was collected in pond 2 for further processes. After 548 days of leaching, the extractions were 79.4% Ni, 82.7% Co, 30.0% Fe, 78.9% Mn, and 37.1% Al.

Metallica Minerals (Gillies 2005) has reported the initial heap leach on its NORNICO nickel laterite ores. The crushed ore, which was 80% less than 25 mm, was agglomerated with water and sulfuric acid and then the agglomerates were allowed to cure for 24 hours in air. Nickel extraction was 34% after 34 days of leaching.

Another group (Duyvesteyn et al. 2001) crushed nickel ores to less than 2.54 cm (1 inch) and agglomerated with 20-100 kg sulfuric acid /tonne of ore. The agglomerates

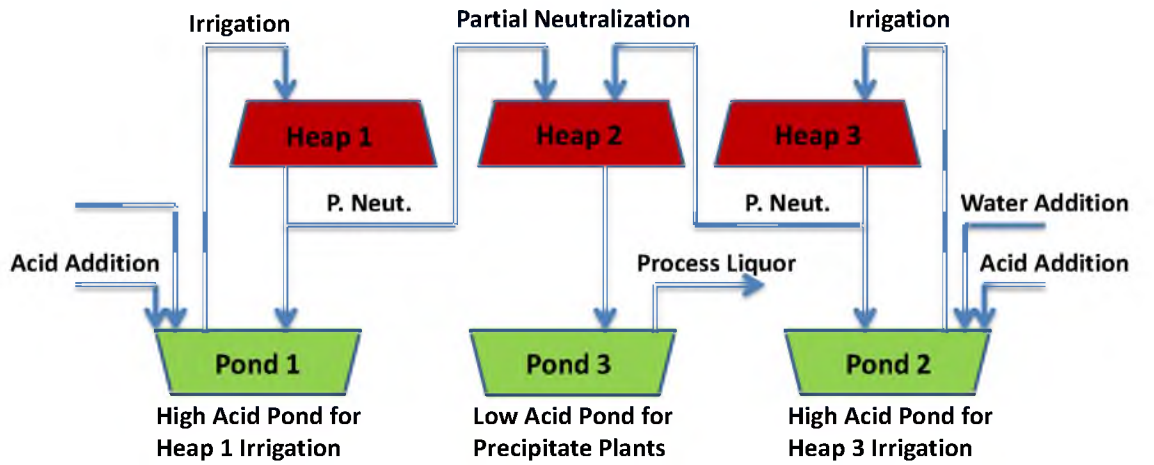

Figure 2. Flow diagram of Caldag nickel laterite atmospheric heap leach trail. Adapted from Oxley et al. 2007.

were then cured for 2-3 days. The agglomerates were formed into a heap having a height of 11-13 ft. The raffinate solution containing 20-100 g/L sulfuric acid was then applied to the heap at 10-100 $L/h/m^2$. 65-66% Ni recovery can be achieved. However, adding 27 g/L of NaCl to the raffinate enhanced the nickel recovery. The nickel recovery increased to 86% by adding NaCl into solution.

H. Liu (2006) performed experiments to improve the heap leaching processes by enhancing the leach solution with hyper saline water or mixing fluorspar into the ores prior to preparing the heap. The ores were crushed to minus 25 mm and agglomerated with sulfuric acid. The agglomerates were then loaded into 100 mm diameter columns. The extraction of nickel improved when hyper saline water was added into the leach solution.

Miller and Liu (2005) separated nickel laterite ores into limonite and saprolite fractions. The low-grade limonite ores were subjected to heap leaching while saprolite

was subjected to the PAL&AL process. The limonite ores were loaded into 75 mm diameter columns of 4 m height. The feed solution was 50 g/L sulfuric acid in brine containing 56 g/L total dissolved salt. The feed flow rate was progressively increased to $120\,L/m^2h$. The nickel recovery can be more than 80% within 292 days.

Rodriguez and Wedderburn (2007) separated nickel laterite ore into fine and coarse fractions. The fine ore fraction was processed by pressure acid leaching. The coarse ore fraction was agglomerated with 10 to 300 kg of sulfuric acid per tonne and then cured for 1 to 20 days. The liquor from the treated slurry was used as the leach solution for the heap leaching. Nickel and cobalt recoveries of between 60 to 95% were achieved.

In an Australian patent by J. William (2005), nickel laterite ores are mixed with inert substrate to provide more strength to the heap structure during the leaching period prior to agglomeration. Binder(s) are used during agglomeration along with the agglomeration solution. The lixiviant which can be hydrochloric, nitric or sulfuric acid with alkaline metal chloride and/or alkaline earth chloride at a concentration of 100 to 200 g/L is heated to hotter than 50^o C. The preferred concentration of sulfuric acid is 1M. However, it can vary from 0.2M to 5M. The nickel and cobalt can be separated and recovered from pregnant solution using known procedures.

Column leaching is a common method to study heap leaching. Many researchers have conducted column leach tests with nickel laterite ores. Leach test work of nickel laterite performed by Murrin Murrin Operation Pty Ltd (Readett et al. 2006) indicates that Ni and Co recoveries of greater than 80% can be achieved. A. Elliot et al. (2009) performed column leaching on several nickel laterite ores from Australia. The ores were

agglomerates with water and sulfuric acid in a rotating drum. The agglomerates then were loaded into 150 mm diameter columns with a bed depth of ~ 1 m. The columns were irrigated with 200 g/L sulfuric acid solution at the rate of 10 $L/h/m^2$ without recycle. Extraction of 10-98% Ni and 12-97% Co were achieved within 120 days of leaching. The extraction of nickel and cobalt depended on the mineralogy of laterite ores. Nickel and cobalt extraction are high in laterite ores containing low goethite and moderate smectite.

Agatzini-Leonardou and Dimaki (1994) performed column leaching tests on a low-grade limonitic laterite from the Litharakia deposit in Greece. The ores were wet with water and then loaded into 100 mm internal diameter columns and with heights ranging from 1 to 2.5 m. Two different processes were performed, one with no solution pH adjustments and the other with solution pH adjustments. The raffinate solutions in the tests were recirculated. Maximum nickel and cobalt recoveries were 86% and 70%, respectively, in 40 days by 3N (~147 g/L) sulfuric acid solution. They also found that solution containing 2N (98 g/L) sulfuric acid was adequate to obtain the maximum nickel recovery. Particle size showed no effect on nickel recovery.

Nickel and cobalt recoveries achieved during column leaching performed by Agatzini-Leonardou and Zafiratos (2004) were 60% and 45%, respectively, in 10 days. The ores were crushed to smaller than 15 mm and agglomerated with water to raise the total moisture content to 10%. The concentration of the sulfuric acid leach solution was 2N or 3N. The solution was pH adjusted to predetermined values and recirculated. The iron/nickel ratio is 5:1 for limonite ores and 1.4:1 for serpentine ores. Percolation problems occurred at 190 cm column height with -1 mm particle sizes. The calcite content and high solution flow rates were the main suspects for the problems.

In the experiments of Horizote and Horizonte (2007), nickel laterite ores were crushed to obtain maximum particle sizes of approximately 12.5 mm and 6.3 mm. Sulfuric acid was used to agglomerate the crushed ores. The agglomerates were loaded into 1 and 4 m height column. The irrigation rate was $10\,L/h/m^2$. Sulfuric acid concentration in the leach solution was 20 to 200 g/L. Their results indicate that higher acidity leads to faster kinetics. The recoveries of nickel and cobalt reached 84% and 70%, respectively, within 150 days.

Agglomeration

In the early period of commercial heap leaching, percolation within the heap was a major problem when ores contained a considerable amount of fine particles. The fine particles would migrate down along with the raffinate and eventually block the pores within the heap. This led to percolation problems which in turn reduced the efficiency of heap leaching.

Agglomeration was adopted over time to overcome that problem. The agglomeration process is generally used as the intermediate process between crushing and stacking. Fine particles are attached to the coarser particles or bonded together to form coarser particles during the agglomeration.

Agglomeration produces several advantages. Agglomeration improves the physical structure of the heap by reducing the amount of fines (Moats & Janwong 2008). Ponding, solution channeling and slope failure problems decrease. Slumping problems are also reduced since fines are stuck together and do not migrate within the heap. Agglomerated ores provide more porosity both within the heap and agglomerated particles which allow better solution and, in some cases, air distribution. This can

enhance heap leaching performance (e.g. shorten leaching time or achieve higher metal extraction rate).

For ores containing more than 5% by weight of -74 μm (-200 mesh), agglomeration with at least water is recommended (Garcia & Jorgensen 1997). If the ores contain more than 10-15 wt.% of -74 μm, the uses of a binder during agglomeration is also recommended (Chamberlin 1986; Garcia & Jorgensen 1997). Binders in agglomeration enhance the bonding between particles either chemically or physically. Organic or inorganic compounds can be used as binders in the agglomeration processes. In the alkaline system such as gold and silver heap leaching, Portland cement has often been used effectively. For the acidic heap environment, sulfuric acid or raffinate has been used. A benefit of using concentrated sulfuric acid during the agglomeration process is to predistribute a leach solution to the ore body. This will often increase the initial recovery rate (Bouffard, 2005).

Conveyor belts and drums are the most common equipment used in the agglomeration of crushed ores. Conveyor belts are suitable for agglomerating ores containing less than 15wt.% of -104 μm fines (Bouffard 2005). There are three typical systems of conveyor belts using in the industries. First, the conveyers are inclined about the same angle (15^{o}) and are moving in the same direction. The agglomerates occur when the particles touch each other at the transfer point or when they bounce on the belts upon landing. The belt speed is between 1.25 and 1.5 m/s. The number of transfer points increases as the fine content increases. Agglomerated solution can be applied at the transfer point. Second, the low angle and speed belts carry the ores to a high-angle belt with high speed in the opposite direction to the low angle belt. The agglomerates occur at

the transfer point and on the high velocity belt due to the opposite forces in action: the upward movement of the belt and the gravity force. Finally, low angle belts carry the ore to a vibrating conveyor. The agglomerates occur at the transfer point and on the vibrating conveyor.

Drum agglomeration is suitable for high fines content ores. The crushed ores are delivered to an inclined and rotating cylinder drum. Agglomerated solution is applied to the ores via nozzle or perforated pipe located along the first 2/3 of the drum length. The rotational speed, the drum inclination and retention time are important factors in drum agglomeration. The agglomerates occur as the results of rolling, cascading and tumbling motion within the drums (Bouffard 2005).

Binding Mechanisms of Agglomeration

Agglomeration is a process in which particles attach to each other via several methods. These methods are known as binding mechanisms. The binding mechanisms of agglomeration have been defined by Rumpf (1962) into five major categories: (1) solid bridges, (2) adhesion and cohesion forces, (3) interfacial forces and capillary pressure, (4) attraction forces between solid particles and (5) interlocking bonds.

Solid Bridges

Solid bridges can be formed by sintering, chemical reaction, hardening binders, partial melting, crystallizing substances and deposition of colloidal particles. These are shown schematically in Figure 3. Sintering and partial melting usually form solid bridges at high temperatures. The molecules diffuse from one particle to another particle at the contact point as the temperatures increase, resulting in solid bridges.

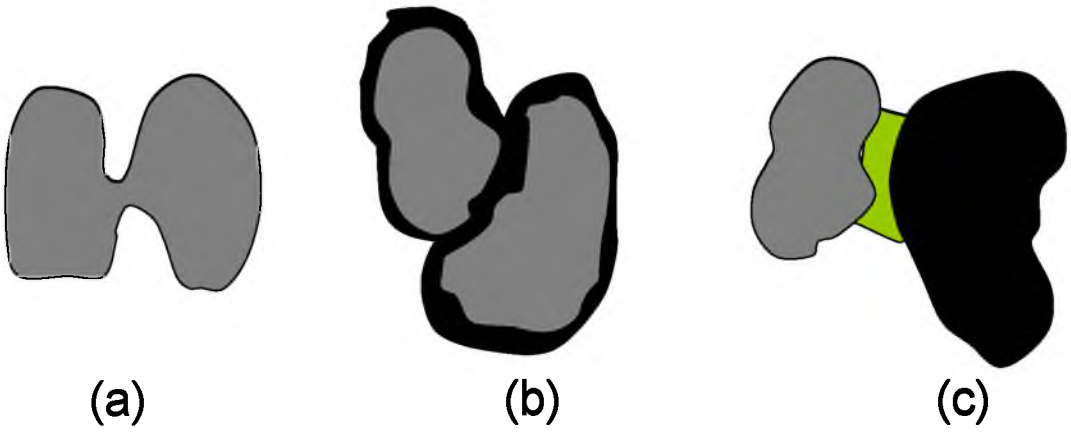

Figure 3. Example of solid bridges formed between two particles; (a) Solid bridges formed by sintering, partial melting or crystallizing substance, (b) Solid bridges formed by chemical reaction or hardening binders, and (c) Solid bridges formed by chemical reaction, hardening binders, disposition of colloidal particles or crystallizing substance.

Crystallizing substances usually form as the temperature drops. Chemical reactions and hardening binders often form solid bridges as moisture is present in the system.

Adhesion and Cohesion Forces

Adhesion and cohesion forces occur at the solid-liquid interfaces when highly viscous binders are applied. Most small divided particles easily attract free atoms or molecules from the neighboring atmosphere to their surface, forming absorption layers. These thin absorption layers are not freely movable; however, they can contact or penetrate each other (Pietsch 1991). If these layers are thinner than 3 nm, the molecular forces are often high enough to deform the films at the contact points, leading to larger contact areas and higher strength of the bonds between the two particles.

Interfacial Forces and Capillary Pressure

Interfacial forces and capillary pressure are a common binding mechanism of wet agglomeration and are shown schematically in Figure 4. The agglomerates are bonded by liquid bridges at the coordination points between the particles. Liquid bridges can be developed from free water or by capillary condensation. Liquid bridges are often the precondition for the formation of solid bridges (Tibbals 1987; Pietsch 1991). If the entire pores between particles are filled with liquid and concave menisci form at the pore ends on the surface of the system, a negative capillary pressure will develop in the interior, causing agglomeration. As the liquid consumes more pore space between the particle systems, the contribution of interfacial forces to the total strength of the system decreases while the capillary pressure contribution increases.

Figure 4. Example of liquid bridges between particles; (a) the two particles are bonded by the liquid bridge and (b) the agglomerates are bonded by capillary pressure.

Attraction Forces Between Solid Particles

Van der Waals electrostatic and magnetic forces can play an important role in binding mechanism (see Figure 5). These forces are very high at very close distance between the particles; however, they decrease quickly with increasing distance. The adhesion in small particles is much higher than large particles due to the surface roughness of the particles. The van der Waals force is the attractive or repulsive force between molecules. This force is very weak and influences only in very short distances (< 10 Å). The electrostatic force is nearly always present in particulate systems (Sherrington & Oliver 1981). It is mainly produced by interparticle friction. The electrostatic force is greater than the van der Waals forces as the surface roughness decreases in a small particle environment. For a relatively large dry particle, electrostatic forces are decisive for initial adhesion of the materials. The magnetic force is the attractive or repulsive force between the two particles; however, the particles have to be intrinsically magnetic.

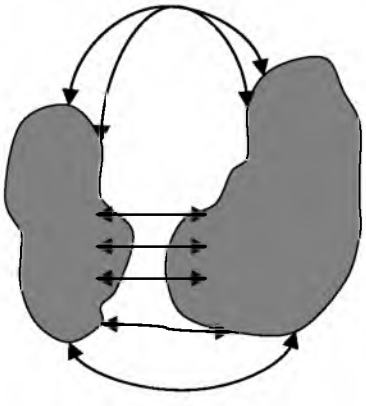

Figure 5. Example of attraction forces between solid particles.

Agglomeration occurs when the combinations of these three forces are sufficiently negative.

Interlocking Bonds

Fibers, as well as flat and bulky materials, can interlock with each other in the disperse system due to their shape, as depicted in Figure 6. A compression or shear force must always act on the system to enhance the interlocking bonds. The strength of the agglomerates depends upon the type of interaction and the material characteristics.

Mechanism of Agglomerate Growth

There are two stages of the agglomeration growth: initial growth and secondary growth stages, as shown in Figure 7 (Schaafsma 2000). Firstly, when the solution droplet hits a particle bed, the droplet is sucked into the bed by capillary forces. The wetted particles are attached to the surrounding particles, forming an initial agglomerate (nuclei). The void area of the initially formed agglomerates is filled with the solution. In the second stage of growth, the liquid is move from inside the agglomerates to the free

Figure 6. Example of the interlocking bonds between particles.

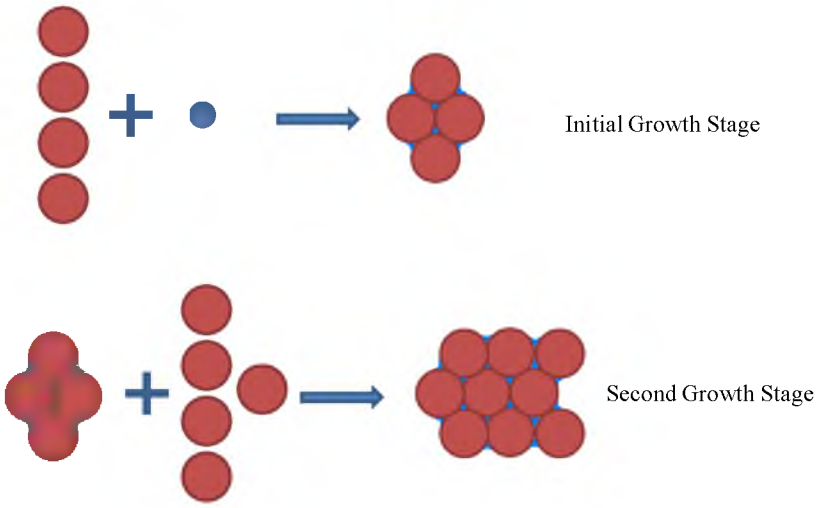

Figure 7. The growth stages of agglomeration.

particles surrounding the agglomerates. The liquid flow is induced by the difference between the capillary forces of the pores inside agglomerates and those of the pores near the surface of the agglomerates. The surrounding particles attach to the nuclei by capillary forces, leading to the growth of agglomerates. The agglomerates grow continuously; as long as the pores at the surface of agglomerates are sufficiently filled with solution, a free particle can reach the liquid phase and the liquid bridge can be formed. The second growth stage takes place until saturation reaches a minimum point, as shown in Figure 8.

The particle size distribution and porosity play a vital role in the final size of the agglomerates. Broad size distribution of the primary ores results in larger agglomeration since small particles fill in the gaps between larger particles. These small particles can act like bridges for the wetting phase, as shown in Figure 9.

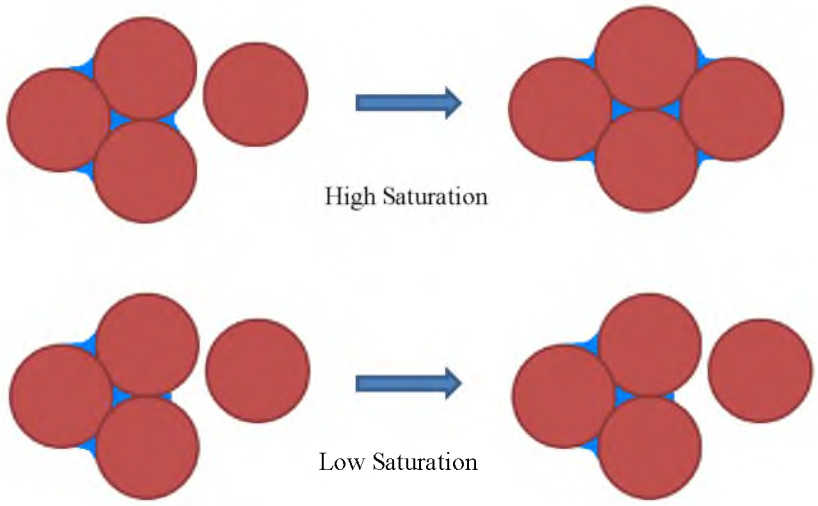

Figure 8. The limitation of the growth of agglomerate.

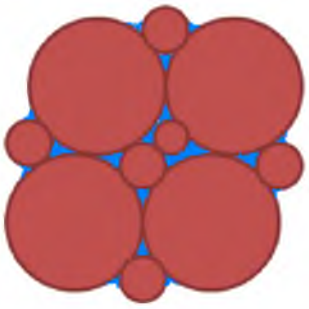

Figure 9. The fine particles act as the bridges for the larger particles.

Agglomerate Quality Evaluation Techniques

Agglomerate quality can be defined in term of agglomerate size distribution, agglomerate moisture content, agglomerate strength or stability and agglomerate internal porosity (Bouffard 2005). To achieve control of the preferred agglomerate quality, several techniques have been developed. The techniques vary from a simple glove test to a more complicated percolation column.

Glove Test

The glove test is commonly used test to evaluate the agglomerate quality in the field operation. The test involves the visual inspection of the agglomerate by the operator. The effectiveness of this technique completely depends on the experience of operators. It provides very limited indication of agglomerate quality (Velarde 2005).

Size Distribution

Size distribution of agglomerates is another method used in the heap leaching industry. Both moist and dry agglomerates can be screened by sieving to obtain the agglomerate size distribution. This method is practical in the laboratory and in the field during periodic sampling. Nonetheless, few records were found in the literature (Bouffard 2005). The preferred agglomerate size distribution may vary from ore to ore. However, there are some recommendations. Lipiec and Bautista (1998) suggested that agglomeration should remove fines and produce uniform size agglomerates. Chamberlin (1986) added that particles smaller than 104 μm should not remain in the ore body. Bouffard (2008) found that a narrower agglomeration size distribution can be obtained as the ore size distribution is narrowed. Higher moisture content in a batch agglomeration

process produced a narrower size distribution of agglomerates. When the ores contain a high amount of fines, larger amounts of small agglomerates (- 1/4") are normally formed.

Attrition Test

The attrition test was introduced by Southwood (1985). The objective of the test is to simulate the abrasion occurring during agglomerate handling. The test was performed in a 200 mm diameter pan with a soft rubber lining for 20 minutes. Particles smaller than 9.5 mm were collected after the test was finished. The 9.5 mm particle percentage was used to compare for different test conditions.

Drop Test

The shatter drop test was developed to imitate an agglomerate dropping from a conveyor belt during heap stacking. Agglomerates were dropped at 1.83 m height onto a steel plate. The numbers of drops taken to break an agglomerate was recorded (Southwood 1985). Southwood found that dropping numbers of agglomerates have an inverse relationship to the size of the agglomerates. The test result also showed that agglomerates must have equal size to be comparable.

Compaction Test

Agglomerates at different height in the heaps are subjected to different compaction loads. To investigate the agglomerate ability to withstand the compaction forces, and the agglomerate strength, the compact test was developed. The minimum load that the agglomerate must be able to resist can be calculated from the following equation.

$$M = \rho h A \quad (1)$$

where M = The agglomerate minimum withstand load

ρ = The bulk density of the heap

h = The height of the heap

A = The cross-sectional area of the agglomerate

A load cell was used to determine the strength of agglomerates. The larger particles can tolerate greater loads than the smaller particles. However, the breakage of the coarser particles was not consistent and had a large variation. The 9.5 mm pellets were preferable for this test (Southwood 1985).

Soak Test

One of the common techniques uses to analyze the strength of agglomerates is to submerge the agglomerates into a solution for a period of time. This method has been performed by various researchers. Name and processing details of the techniques may be slightly different. Chamberlin (1986) suggested that good agglomerates should not disintegrate for many hours when the agglomerates are submerged in water. The Bouffard (2008) "dip test" consists of placing a known amount of -1/2" + 3/8" agglomerates onto a 10 mesh screen (1.7 mm) submerged in water for 24 hours. After the test was finished, the agglomerates remaining on the screen were weighted. Milligan and Engelhardt (1983) measured the amount of fines generated when dipping the agglomerates in water 10 times. The agglomerates must be previously dried for 6 hours at 90^{o} C and cooled before dipping.

A research group at Michigan Technological University performed a "soak test" to analyze the strength of agglomerates in an acidic environment. Approximately 500 grams of agglomerates was placed on a Tyler 10 mesh (1.7 mm) screen and allowed to cure for 24 hours in an ambient condition. The screen was then submerged into a 6 g/L sulfuric acid solution for 30 minutes (Eisele et al. 2005; Lewandowski & Kawatra 2007a, 2007b). The fines passing through the screen were dried and weighted. The fine migration was calculated via equation 2.

$$Fine\ migration = \frac{Weight\ of\ ore\ migrated\ out\ of\ the\ sample}{Total\ weight\ of\ -10\ mesh\ fines\ available\ in\ the\ sample} \quad (2)$$

Southwood (1995) submerged the agglomerates in sulfuric acid solution (pH 1.0) for extended times. The agglomerate breakdown times were noted. He found that many agglomerates disintegrated in less than 1 minute, but some remained intact for several days. The good agglomerates should remain intact for more than 24 hours.

Electrical Conductivity

The electrical conductivity has been studied for use as a tool to identify the moisture content of agglomerates. This use of electrical conductivity is based upon the drastic changes in conductivity which occur after moisture is added to crushed ores to produce a film around the particles. This moisture leads to the particle agglomeration through liquid bridging which at the same time forms an electrical connection between the particles. The values of the electrical conductivity form an exponential curve with respect to moisture content. Preceding the film formation, increasing moisture content

results in a very small increase in the electrical conductivity values. The biggest change of a slope in the curve indicates the presence of a moisture film (Velarde 2005)

Stacking Test

Robertson et al. (2009) designed a stacking test to analyze relationships between electrical conductivity, bulk density and heap height. The agglomerates were placed in the test cell and then mechanical loads were applied to the agglomerates. The loads were increased in a stepwise pattern. The agglomerate bed was allowed to stabilize at each step prior to electrical conductivity and bulk density measurement. Lower strength agglomerates produce a steep bulk density profile while higher strength agglomerates produce a relatively flat bulk density profile with increasing compaction.

Permeability

Permeability is one of the most important parameters in heap leaching. It is the particle bed's ability to allow water to flow through voids. There are two common permeability tests that are performed in the laboratory to characterize beds of particles. These are constant head permeability or falling head permeability tests. The constant head permeability test is favored when measuring the permeability of a bed of particles that have relatively high permeability: sand, gravel, etc. ($k > 10^{-6} cm^2$). The falling head permeability test is more suitable for measuring the fine grain minerals and hence low permeability ($k < 10^{-6} cm^2$) (Wray 1986; Maclver & Hale 1986).

The percolation flooded column test designed by the Michigan Technological University research group (Lewandowski & Kawatra 2007a, 2007b) and hydrodynamic column test developed by Robertson et al. (2009) are other techniques attempting to

obtain permeability. The Michigan Technology University research group allowed agglomerates to dry under ambient temperature for 24 hours before performing the test. The solution was then dripped onto the top of the column at a controlled rate. The bulk density and hydraulic conductivity values were measured at various increments over 72 hours. After finishing the test, the column was allowed to drain for 1 hour. The agglomerates were then dried and weighted.

The Robertson group does not provide details regarding their hydrodynamic column test. Their test can provide various parameters, including saturated hydraulic conductivity, hydraulic conductivity, moisture retention, air conductivity, drain down curve and total micro and macro porosity.

Research Objectives

Nickel laterite heap leaching has been studied and developed for many years. However, one of the main difficulties in the process is permeability within the heap. This problem results from the high amount of fines in the ore. One technique to cope with excessive fines is to agglomerate the ores prior to construction of the heap. In order to achieve good permeability within the heap, agglomerates should possess good strength, be acid resisted, have proper sizes and reduce fines in the agglomerate body.

In this study, several techniques were used to investigate the qualities of agglomerates, including particle size distribution (PSD), electrical conductivity, permeability and bulk density. The nickel laterite ores were agglomerated with various agglomeration conditions prior to testing. Then, column leaching experiments were performed to investigate the effects of different agglomeration conditions on leaching performance.

Mineralogy of nickel laterite ores, agglomerates and leach residuals were also studied. The effects of sulfuric acid on the agglomerate qualities and the leach performance can be obtained by analyzing the samples with x-ray diffraction, QEMSCAN and EMPA. The results from both agglomerate quality measurements and mineralogy of nickel laterite ores, agglomerates and leach residuals are provided to help understand nickel laterite agglomeration mechanisms.

CHAPTER 3

EXPERIMENTAL PROCEDURES

To study the agglomeration process and its effects on leaching efficiency of nickel laterite ore, five experimental tests were performed: agglomeration, electrical conductivity, permeability, column leaching and mineral phase analysis. Nickel laterite ore samples provided by an industrial sponsor were agglomerated at different conditions to study the effects of these factors. Electrical conductivity and permeability values then were obtained from agglomerates at each condition. Column leaching experiments were performed to observe the leaching performance of the nickel laterite ore after agglomeration at different agglomeration conditions. Finally, x-ray diffraction, EMPA and QEMSCAN were used to study the mineral phase change after agglomeration and column leaching tests.

The nickel laterite ore received from an industrial sponsor has the general size distribution given in Table 1. The -12.5 mm material was used in this study to ensure that final agglomerate size is less than 1/6 of the diameter of the leaching column, as recommended by the industrial sponsor. As the leaching columns have a 203 mm inner diameter, the final agglomerate size needed to be smaller than -33.83 mm. The coarser materials were crushed to -12.5 mm size. The size distributions used in the experiments were the same as the original -12.5 mm size fraction.

Table 1. Industrial sponsor laterite ore as-received size distribution.

Size (mm)	Approximate mass (kg)	Retained (%)	Retained cum. (%)
+50.0	43.4	2.1	2.1
-50.0 +12.5	884.7	42.5	44.6
-12.5 +3.17	357.9	17.2	61.7
-3.17 +0.5	326.7	15.7	77.4
-0.5	470.1	22.6	100.0
Total	2,082.8	100.1	-

A more detailed particle size distribution for the nickel laterite ore is shown in Table 2. The fine particles which are less than 75 μm (#200) account for 17.6% by weight of the ore. Since the amount of -75 μm material in the ore is more than 10%, agglomeration would be recommended before heap leaching, based on the literature (Garcia & Jorgensen 1997).

The as-received nickel laterite sample is basically composed of quartz, silico-ferruginous plasma and chlorite/smectite/vermiculite. Serpentine, iron oxi-hydroxides, chromite and aggregates of kaolinite/iron oxi-hydroxides/quartz are also present (Castro & Pereira 2009). Nickel is commonly found in the finer fractions (-3.17+0.5 mm and -0.5 mm). Chlorite, smectite, vermiculite, silico-ferroginous plasma and manganese oxide are the main nickel-bearing minerals. Global content of nickel and cobalt are 0.97 and 0.04%, respectively.

Agglomeration

Moisture content, sulfuric acid concentration, drum rotation speed and retention or mixing time are important factors in the agglomeration process. Retention time for an

Table 2. Industrial sponsor laterite ore particle size distribution.

Size (μm)	Mass (g)	Retained (%)	Retained cum. (%)
50,000	1,481	2.8	2.8
25,500	12,040	22.7	25.5
12,500	12,280	23.1	48.6
6,300	5,120	9.6	58.2
4,000	2,460	4.6	62.9
3,170	630	1.2	64.1
1,700	2,117	4.0	68.0
1,000	1,532	2.9	70.9
500	1,057	2.0	72.9
250	1,549	2.9	75.8
150	1,188	2.2	78.1
106	1,120	2.1	80.2
75	1,175	2.2	82.4
37	1,755	3.3	85.7
30	423	0.8	86.5
21	841	1.6	88.1
15	1,050	2.0	90.1
12	824	1.6	91.6
<12	4,452	8.4	100.0
Total	53,092	100.0	-

industrial drum agglomerator has been reported to be 1 to 4 minutes (Chamberlin 1986; Bouffard 2005). As such, time was fixed at 3 minutes for the first set of experiments, and then to examine the effect of time, it was varied in the range of 3 to 6 minutes. Shorter mixing times could not be performed in this study due to the limitation of the solution application system.

Commercial drum speeds are typically between 30 to 50% of the critical speed (Bouffard 2005). In this study, 31.5% of the critical speed was used at the first stage and then in the second stage, 15.7, 23.6, 39.3 and 47.1% of the critical speed were considered to observe the effect of drum speed. The critical speed formula is $42.3/\sqrt{D}$ where D is the inside diameter of the drum in meters.

A plastic drum was used as the agglomerator. The drum had dimensions of 26.67 cm in diameter and 36.2 cm in length. The plastic drum had 4 lifters of 5.0 mm height, 20 mm width and 33 cm length spaced evenly around the circumference of the drum. The critical speed was calculated as 81.9 rpm and those for 47.1%, 39.3%, 31.5%, 23.6% and 15.7% of critical speed are 38.6, 32.2, 25.8, 19.3 and 12.9 rpm, respectively.

The industrial sponsor recommended 60-70 g/L sulfuric acid for the leaching solution which is generally used also as the agglomeration liquid. Sulfuric acid concentration in this study, however, ranged from 102 to 972 g/l in this study.

In nickel laterite ore agglomeration, the moisture contents reported lie within a wide range (10-30%) due to the nature of the ores (Agatzini-Leonardou & Dimaki 1994; Agatzini-Leonardou & Zafiratos 2004; Rodriguez 2007; Mora et al. 2010). Thus, in this study, the moisture content was varied between 10 to 25%. The moisture content is calculated from the following equation.

$$Moisture\ content\ \ (\mu, \%) = \frac{Mass_{wet} - Mass_{dry}}{Mass_{dry}} x100 \qquad (3)$$

where $Mass_{wet} - Mass_{dry}$ is the weight of the solution used in the agglomeration and $Mass_{dry}$ is the weight of the dry ore samples.

The natural moisture content of the nickel laterite ore was measured prior to experiments. 500 g. of nickel laterite ore sample was weighed and then baked in the oven at 110^{o} C for 24 hours. The samples were weighed again after drying. The natural moisture content of the samples can be calculated using equation (3).

The amount of the sulfuric acid solution required for agglomeration was firstly calculated, and then the obtained acid solution amounts were used to calculate the amount of sulfuric acid and water applied to the drum via different hoses.

The amount of acid solution in mL used in each experiment was calculated via the following equation.

$$Acid\ solution\ added\ (S);(mL/kg\,of\ ore) = \left(\frac{\frac{(A-B)}{100}}{\rho_{acid\,solution}} \right)(C) \qquad (4)$$

where A = Target moisture content of the agglomerates (%)

B = Natural moisture content (%); measured at 4% for the nickel laterite ore used in this study

$\rho_{acic\,solution}$= Density of the target solution (g/mL)

C = Ore amount (g);

The density of the target solution used in this equation varied depending on the acid concentration of the final solution. The density of solution was obtained via the density data as a function of sulfuric acid concentration provided in the CRC Handbook of Chemistry and Physics (Weast 1973). The relationship between the sulfuric acid concentration and its density is illustrated in Figure 10.

The empirical equation depicted in Figure 10 was used to calculate the sulfuric acid density in this study. The sulfuric acid concentration by weight and density used in the calculations in this study are listed in Table 3. The obtained sulfuric acid solution

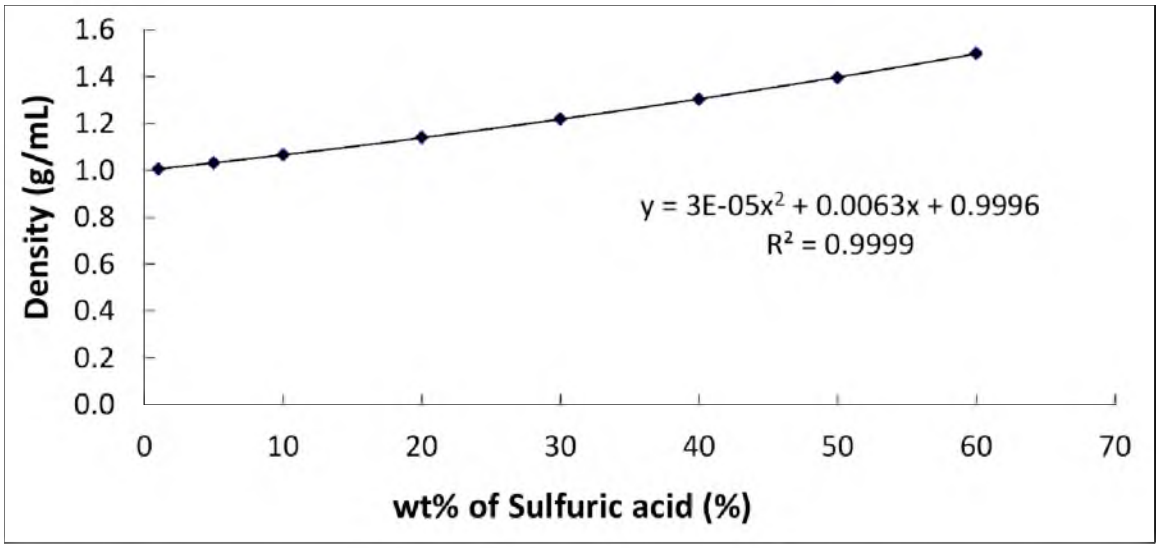

Figure 10. The relationship between density and concentration of the sulfuric acid.

amount was then used to calculate the concentrated sulfuric acid and water amount via the following equation.

$$Concentrated\ sulfuric\ acid\ \ (mL) = \left(\frac{SxT}{1766.4}\right) \tag{5}$$

$$Water\ \ (mL) = \frac{\left(\left(\left(\rho_{acid\,solution} x1000\right) - T\right)\right) xS}{1000 x \rho_{water}} \tag{6}$$

where S = The acid solution added (mL/kg of ores)

T = The acid concentration (g/L)

$\rho_{acicsolution}$ = Density of solution (g/mL)

ρ_{water} = Density of water (g/mL)

Table 3. The sulfuric acid solution wt% and calculated density at different concentrations.

Sulfuric acid solution concentration (g/L)	Sulfuric acid solution wt% (%)	Calculated sulfuric acid solution density (g/mL)
100	9.42	1.062
250	21.68	1.150
500	38.71	1.288
900	60.04	1.486

Tables 4 and 5 summarize the amount of concentrated sulfuric acid and water used to agglomerate 4 kg of nickel laterite ore, which was a typical batch size in this study.

For each batch, the drum was filled with 4 kg of sample (nickel laterite ore). To achieve homogeneity, the sample was mixed for 30 minutes in the drum at a pre-determined speed, corresponding to the speed used in the experiments. Then, about 350 g of randomly picked samples were subjected to size distribution analysis by hand screening to insure size distribution of the feed was consistent. Then, the sample was filled back into the drum.

The agglomeration solutions used in this study were composed of various amounts of the concentrated sulfuric acid and de-ionized water. Water and acid were applied separately to imitate industrial practice. Peristaltic pumps were used to control the addition rate of each liquid.

The solution applying time was 1/3 of the agglomeration time. Three batches of agglomeration were performed in order to obtain 12 kg of the agglomerates for each condition. After agglomerating, 500 g of agglomerates, obtained by the cone and quartering method, were baked at 225 ^{o}F ($110^{o}C$) for 24 hours to obtain a measured moisture content and to perform size distribution after agglomeration. The remaining

Table 4. The calculated amounts of concentrated sulfuric acid for agglomerating 4 kg of nickel laterite ore in mL at different moisture contents, and acid concentrations; the number in the parenthesis was the amount of acid used per tonne of ore.

Moisture content (%)	Acid solution concentration (g/L)			
	100	250	500	900
10	12.8 (5.7)	29.5 (13.0)	52.7 (23.3)	82.3 (36.3)
15	23.5 (10.4)	54.1 (23.9)	96.7 (42.7)	150.9 (66.6)
20	34.1 (15.1)	78.7 (34.8)	140.6 (62.1)	219.4 (96.9)
25	44.8 (19.8)	103.4 (45.6)	184.5 (81.5)	288.0 (127.2)

Table 5. The calculated amounts of water for agglomerating 4 kg of nickel laterite ore in mL at different moisture contents and acid concentrations.

Moisture content (%)	Acid solution concentration (g/L)			
	100	250	500	900
10	217.5	187.8	146.8	94.6
15	398.7	344.3	269.1	173.5
20	580.0	500.7	391.4	252.4
25	761.2	657.2	513.7	331.3

agglomerates were left for 1 hour and 45 minutes before performing other measurements on the agglomerates.

Size Distribution

Size distribution measurements are designed to determine the relative amount of particles present, sorted according to size. The size distribution of the agglomerates in this study was determined by hand screening. The hand sieving method was used to limit the breakage of agglomerates during the test. 350 g of agglomerates was collected by the cone and quartering technique. The agglomerates were then air dried for 24 hours to stabilize the agglomerates. The very fine particles which are smaller than 1.7 mm are difficult to determine by the hand screening method. Therefore, in this study, the smallest

sieve size is 1.7 mm. The agglomerate size distribution (ASD) curve, D_{10} and D_{50} of the agglomerates were obtained from the sieve data.

Electrical Conductivity

Electrical conductivity is a measurement of a material's ability to conduct an electric current. When a voltage is applied between two electrodes which has a bed of particles between them, ions or electrons between them will move and produce a current depending on the resistance of the materials.

To measure electrical conductivity, 650 g of agglomerated sample was placed in a specially designed electrical conductivity measurement cell shown in Figures 11 and 12. The cell needs to be dry prior to introduction of the sample to avoid changes in output voltage due to extra moisture. Five different direct current voltages were applied to the circuit with a maximum voltage of 3 V to avoid corrosion of the stainless steel electrodes. The measured current was recorded and then plotted versus the applied voltage. Resistance values were obtained from the slope of the current vs. voltage curves.

The resistivity of the bed of agglomerates was calculated using equation (7):

$$\rho = \frac{RA}{l} \tag{7}$$

where ρ = resistivity (Ω.m), R = resistance (Ω), A = area of electrode (m^2), l = distance between electrodes (m).

Conductivity is simply the inverse of resistivity and is expressed in Siemens per meter ($S\ m^{-1}$).

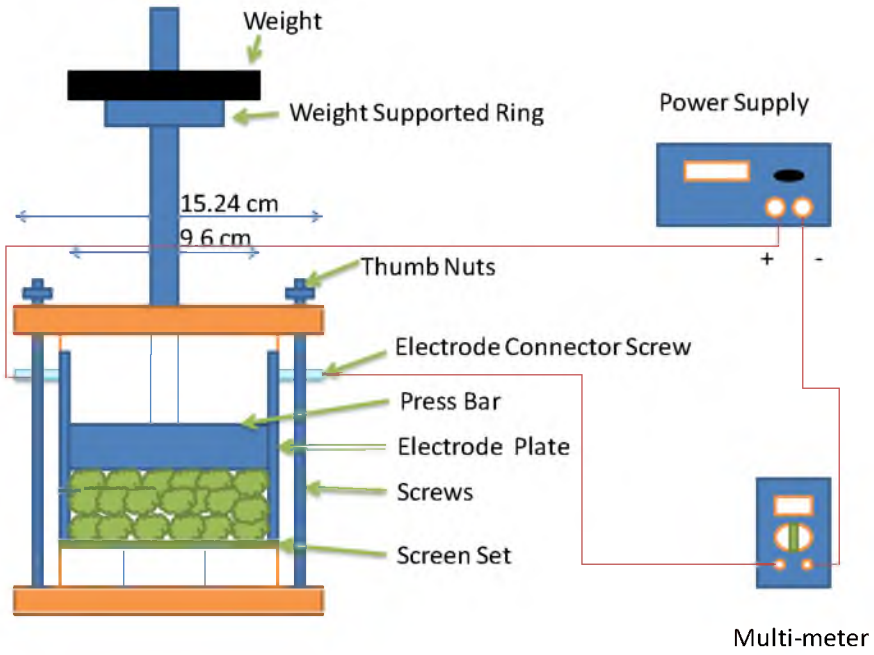

Figure 11. The schematic diagram of the electrical conductivity test setup.

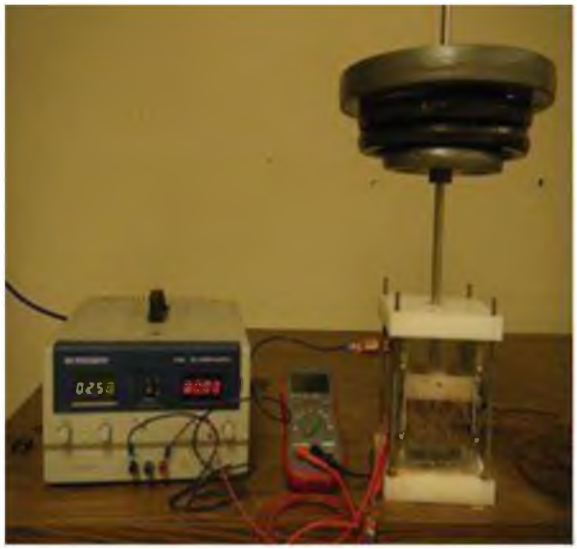

Figure 12. The electrical conductivity test system.

After finishing the first conductivity tests with no mechanical load applied, a second conductivity test was performed at a load of 20.4 kg (this simulates the weight that the agglomerates face at about 2 m height in the real heap). The amount of load was calculated from the bulk density of the ores. The experimental procedures were the same as when no load was applied. After finishing the conductivity tests, a hydraulic permeability test was carried out.

Permeability

The ability of a bed of particles to permit water to flow through its pores or voids is called permeability (k). A correct and uniform permeability of agglomerates in the heap is necessary to prevent channeling and ponding, enhance recovery and decrease leaching time.

After finishing the electrical conductivity tests, a hydraulic permeability test was performed based on ASTM D 2434-68. 10 kg of agglomerates was filled into a 19.05 cm inner diameter test column. The test setup is shown schematically in Figure 13 and shown as a photograph in Figure 14. Then, water was flowed through the test cell downward. A head change between the agglomerate bodies can be obtained by reading a manometer. The values of area and the height of the agglomerated ore bed could be measured and therefore, the hydraulic permeability could be calculated using equation (8) (Darcy's Equation).

The system must be in equilibrium, $Q = Q_{in} = Q_{out}$, for Darcy' law to be valid for this experiment.

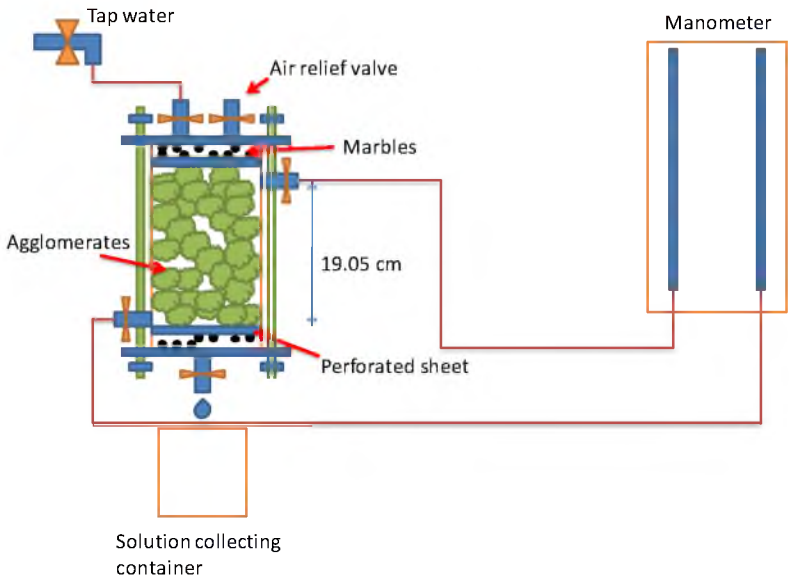

Figure 13. The schematic diagram of permeability test setup.

Figure 14. The permeability test system.

$$Q = AK\frac{\Delta h}{L} \tag{8}$$

where Q = Volumetric flow rate (cm^3/s)

A = Flow area perpendicular to L (cm^2)

K = Hydraulic permeability (cm/s)

L = Flow path length (cm)

Δh = Change in hydraulic head (cm)

The saturated permeability (k) of the ore body can be calculated from equation (9).

$$K = k\left(\frac{\rho g}{\mu}\right) \tag{9}$$

where K = Saturated hydraulic permeability (cm/s)

k = Permeability (cm^2)

ρ = Solution density (water); $1000\frac{kg}{m^3} = \frac{kg}{1000cm^3}$

g = Earth gravitational constant; $9.81\frac{m}{s^2} = 981\frac{cm}{s^2}$

μ = Solution viscosity (water);

$$1 centipoise = 0.001 Pa(s) = 0.001\frac{kg}{m.s} = 0.00001\frac{kg}{cm.s}$$

Therefore, the permeability (k) is equal to $k = K\left(\frac{\mu}{\rho g}\right) = K\left(\frac{0.00001}{981/1000}\right) = \left(1.02x10^{-5}\right)K$

Bulk Density

Bulk density is defined as the mass of the materials divided by the total volume that they occupied. The total volume includes particle volume, interparticle void volume and internal pore volume. It is inversely related to the porosity of the same samples. Increased porosity in the agglomerates lowers the bulk density of the agglomerates.

During the permeability experiments, the bulk density of the agglomerated nickel laterite ore was obtained both at the beginning and at the end of the test. The bulk density was calculated using equation (10).

$$Bulk\ Density\,(g/mL) = \frac{Mass\ of\ agglomerates\,(g)}{Volume\ of\ agglomerates\,(mL)} \tag{10}$$

The porosity of the ore body can also be calculated using equation (11).

$$Porosity = 1 - \frac{Bulk\ density\ of\ agglomerates\,(g/mL)}{Particle\ density\ \ (g/mL)} \tag{11}$$

For nickel laterite agglomerates, the average particle density is 2.24 g/mL as measured by Micromeritics Model 1305 multivolume pyncometer.

Column Leaching

Column leaching experiments were performed in order to investigate the relationship between the agglomeration-related parameters and the column leaching results: nickel and other minerals recovery rate, ponding and channeling and ore body slump. To develop this correlation, a 2^2 full factorial experimental design with a midpoint performed in triplicate was utilized. The two factors were moisture content and acid

concentration. The drum rotation speed and mixing time were fixed at 31.5 %NC and 3 minutes, respectively. Table 6 shows the proposed experimental design details.

A 30 gal drum was used for agglomeration to produce material for column leaching experiments. The drum was equipped with 4 lifters of 0.5 cm thickness. The lifters were spaced equidistant around the circumference of the drum. The drum was filled with 25 kg of crushed nickel laterite ores. The samples were then mixed for 30 minutes to assure homogeneity. Concentrated sulfuric acid and de-ionized water were applied through different pipes (0.635 cm in diameter).

Peristaltic pumps were used to control the rate of the solution flow. The solution application time and drum rotation speed were 1/3 of agglomeration time and 31.5% NC, respectively. Two batches of agglomeration were performed in order to obtain 50 kg of agglomerates. Approximately 800 g of agglomerated ores were collected by cone and quartering method and used to measure the agglomerate size distribution. The remaining agglomerates were left to cure for 1 hour and 45 minutes before performing the quality control tests and loading to a column of a diameter of 20.32 cm. The column consisted of 3 sections of 50.8 cm, as drawn schematically in Figure 15.

Table 6. The column leaching experimental conditions.

Factors	Levels		
	Low	Midpoint	High
% Moisture (dry basis)	12	15	18
Acid Concentration (g/L)	300	600	900

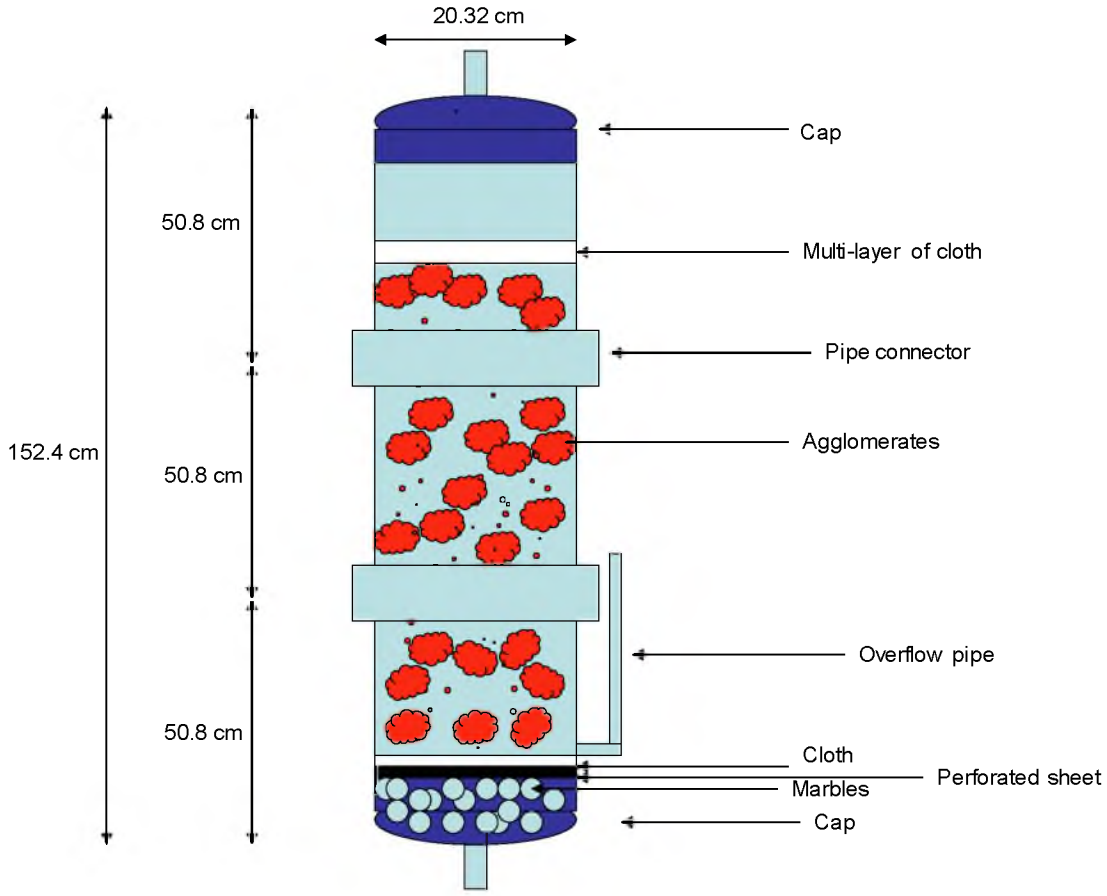

Figure 15. The schematic diagram of column test setup.

A layer of marbles, perforated sheet and cotton cloth were placed at the bottom of the column to prevent the migration of fines out of the column. Multi-layers of cotton cloth were placed on top of the agglomerates to achieve equal solution distribution within the column. The agglomerates were cured for 3 days prior to leach. A leach solution of 65 g/L sulfuric acid was applied through a hose at the top of the column and pregnant leaching solution (PLS) was collected at the bottom of the column. The raffinate flow rate was 4.2 to 6.2 mL/min. The PLS was sampled everyday within the first two weeks, then once every 3 days for the following month and finally once a week for the rest of the experiments. Each column was leached for 90 days. pH and oxidation reduction potential (ORP) of the PLS were measured. Inductively coupled plasma optical emission spectrometry (ICP-OES) was used to analyze the concentration of interested elements. The PLS was diluted to various concentrations in order to obtain the concentration of different elements in the PLS.

After the column leaching experiments were completed, representative samples of agglomerates from the top, center and bottom of each column were collected. The samples were analyzed by QEMSCAN to study the mineral phase changes and effects of these changes during agglomeration and leaching to the agglomerate quality and leaching efficiency. Particle size distribution data of agglomerates at different positions in the column were collected to study the breakage of the agglomerates and the migration of fine particles.

Mineral Phases Analysis

Mineral phase analyses were used to investigate the phases of the nickel laterite ores as they changed during the agglomeration and leaching processes. X-ray

diffraction, QEMSCAN and EMPA were used to characterize samples. The nickel laterite ores received from an industrial sponsor contain more than 20 wt.% clay mineral and more than 50 % of the nickel was found in the clay minerals. XRD was used to initially investigate the types of clays found in feed, agglomeration and leached residual samples.

For x-ray diffraction, 50 g of feed, agglomerated ore and leach residual representative samples were ground until all particles were less than 10 μm. The ore powders were then placed on the x-ray holder and scanned from 5 to 50^{o} to obtain preliminary results.

Then, the crushed ores were mixed with water and Calgon in a blender for 2 minutes to disaggregate the sample further. Particles larger than 2 μm were removed by centrifugation at 1000 rpm and then the rest of the particles in the solution were settled by centrifugation at 4000 rpm. The residual settled in the tubes was applied to glass slides. The air-dried samples were analyzed by XRD (2-30^{o}) and then placed in a saturated ethylene glycol solution and heated at 60^{o}C for more than 8 hours. The samples were then analyzed by XRD again. The ethylene glycol was used to expand clay for conclusive identification.

For QEMSCAN and EMPA, 50 g of feed, agglomerated ore and leached residual samples were mounted in epoxy and polished. Two size fractions (-2.0 + 0.853 mm) and (-0.5 +0.297 mm) were examined. Larger size fractions were not examined due to the difficulty of sample preparation. The samples were then analyzed by QEMSCAN. The scanning parameters used in QEMSCAN are shown in Table 7. Figure 16 illustrates the examples of samples used in QEMSCAN analysis. In each sample, three areas were scanned across the samples, as illustrated in Figure 16A; however, in case of small

Table 7. The QEMSCAN scanning parameters.

Parameters	Values
Scan Areas	6800 μm by 7700 μm
Field Space	2500 μm
Field Size	800 μm
Point Across Field	400 μm

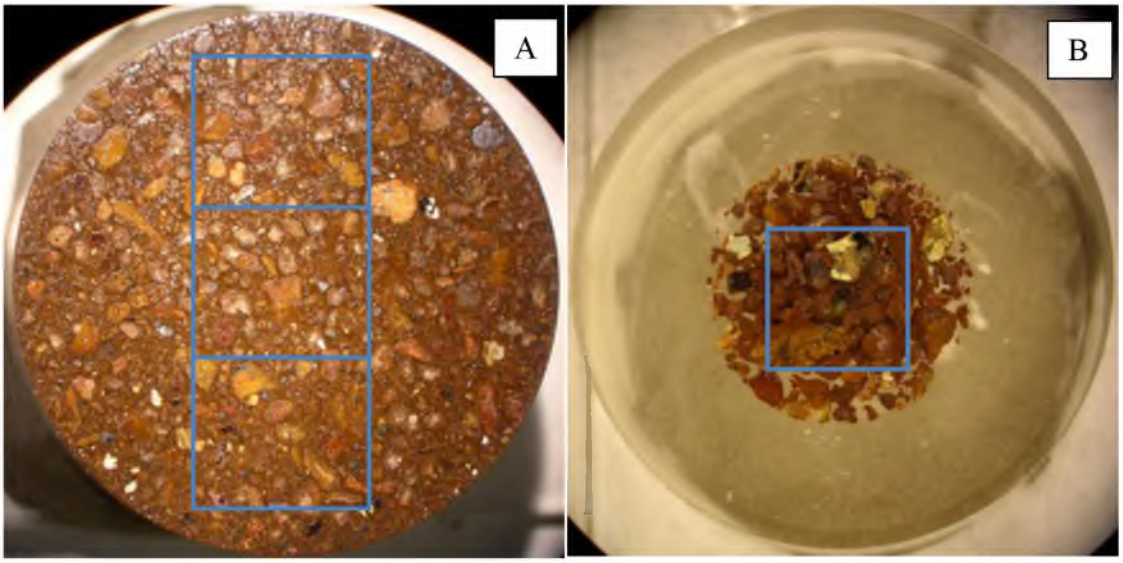

Figure 16. The scanning area of QEMSCAN samples, A) is regular samples and B) is small amount samples.

samples, as in Figure 16B, only one scanning area was scanned. The mineral phases that could not be identified by the QEMSCAN were subjected to EMPA to obtain the chemical formula of the unknown phases. EMPA allows for quantification of interested elements in phases that contain less than 5% of those elements and are below the detection limit of QEMSCAN.

CHAPTER 4

AGGLOMERATION QUALITY CONTROL TOOLS

Agglomeration has been used to improve the performance of heap leaching for many ores. Proper agglomeration improves permeability within the heap, prevents solution ponding and channeling, and increases the metal recovery. Suitable agglomerates for heap leaching can be considered from their quality. Agglomerate quality can be characterized using size distribution of the agglomerates, strength of agglomerates, and permeability of agglomerates and agglomerate bed.

In order to control the qualities of agglomerates, several techniques have been proposed such as electrical conductivity measurements (Velarde 2005), permeability of agglomerate bed measurements (Kinard & Schweizer 1987; Garcia & Jorgensen 1997), dip tests (Bouffard 2008) and soak tests (Lewandowski 2009).

The agglomerate size distribution, permeability of agglomerate beds and electrical conductivity of agglomerates were investigated in this study. It is believed that this is the first report of these parameters for a nickel laterite ore. Important agglomeration factors such as acid concentration, moisture content, drum rotation speed and mixing time were varied to obtain different agglomerates. Nickel laterite ores were used in the experiments. The acid concentration and moisture content used in the experiments are listed in Table 8.

Table 8. Moisture content, acid concentration and acid addition used in the agglomeration experiments.

Moisture Content (%)	Acid Concentration (g/L)	Acid Addition (kg/tonne)
10.6	972	39.14
10.6	532	25.15
10.4	259	13.75
10.2	102	5.80
16.1	972	71.76
16.0	532	46.10
15.7	259	25.21
15.3	102	10.63
21.7	972	104.38
21.5	532	67.06
21.0	259	36.67
20.4	102	15.46
27.2	972	137.00
27.0	532	88.02
26.3	259	48.13
25.6	102	20.30

Agglomerate Size Distribution

The main objective of agglomeration is to reduce the number of fine particles in the ore body and produce suitable agglomerate size distributions (ASDs). Therefore, the agglomerate size distribution is important and should be investigated. The preferable size of agglomerates varies from ore to ore. The amount of fines left unattached to other fines or coarser particles affects the permeability and bulk density of the agglomerate body. For this reason, unattached fine particles in the ore body should also be studied.

The effects of moisture content, acid concentration, drum rotation speed and mixing time to the agglomerate size distribution of nickel laterite ores were studied. In the agglomerate size distribution figures, the legends have the form of A: B: C. A represents the moisture contents in wt%. B represents the acid solution concentrations

(g/L). Finally, C represents special conditions; for example, NC is for drum critical speeds and min is for mixing times in minutes.

The effects of moisture content and acid concentration on the size of the nickel laterite agglomerates were studied first. Mixing time and drum rotation speed were keep constant at 3 minutes and 31.5% NC, respectively. Moisture contents were varied approximately from 10 to 25% on a dry basis. Acid concentration was varied from 102 to 972 g/L.

As expected, the size of agglomerates was coarser as moisture content increased, as shown in Figure 17. As the moisture content increases, obviously, the volume of liquid added during agglomeration also increases. The liquid fills the void space between the adjacent particles, creating capillary forces between those particles. The capillary forces provide enough force for nearby particles to attach to each other. If there is enough solution provided to the system, the liquid will go into the free surrounding surface of the nuclei agglomerates and attract free particles to attach to them and become coarser. The smaller particles and fines in the samples also play an important role in the agglomeration process. They can act as filling agents, filling the empty space between the coarser particles and bonding them together.

As the moisture content increases, the amount of smaller size agglomerates decreases and the amount of coarser size agglomerates increases. Bouffard (2008) also observed the same effects of moisture content as she mentioned that higher moisture content produced a narrower size distribution of agglomerates. The amount of agglomerates, smaller than 1.7 mm in size, decreased as the liquid in the system increased.

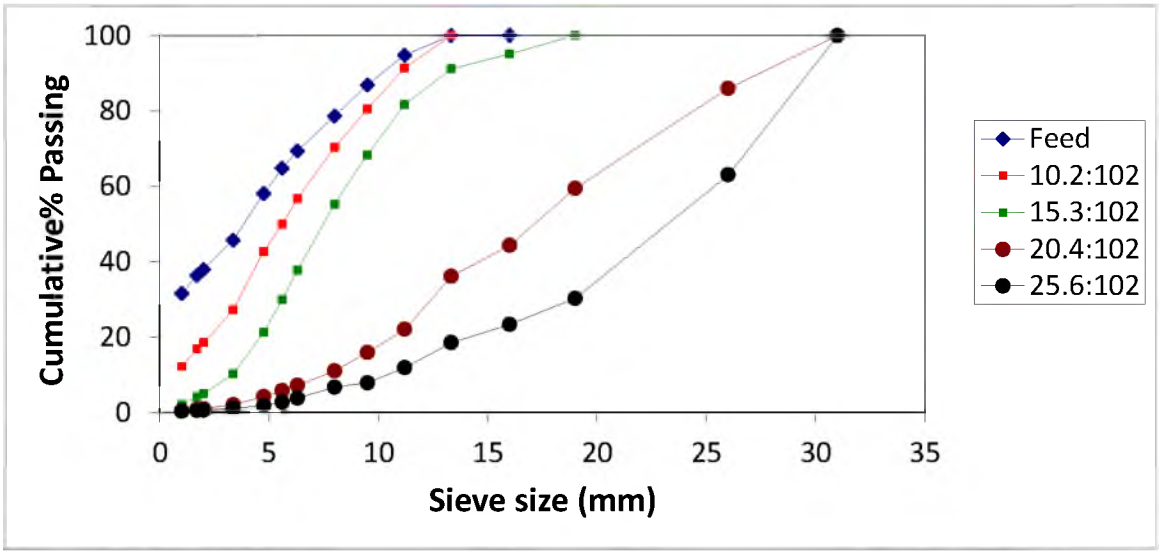

Figure 17. ASDs of agglomerates at different moisture contents (102 g/L acid concentration).

A significant decrease of less than one mm agglomerates can be observed when increasing the moisture content from 10.2 to 15.3 wt%. The agglomerates continue to grow as more liquid phase is introduced to the system. The coarse agglomerates which are larger than 13.33 mm can be observed as the moisture content increases from 15.3 to 20.4 wt%. The growth of coarser agglomerates as the moisture content increases is attributed to smaller agglomerates that attached to the larger agglomerates, and filled the void spaces between coarser agglomerates as the liquid phase or moisture content increases.

Figure 18 illustrates ASDs for batches produced with relatively constant moisture content while acid concentration was varied. From the graph, it is clearly seen that an inverse relationship exists between agglomerated size and acid concentration. Agglomerates become smaller as the acid concentration increases.

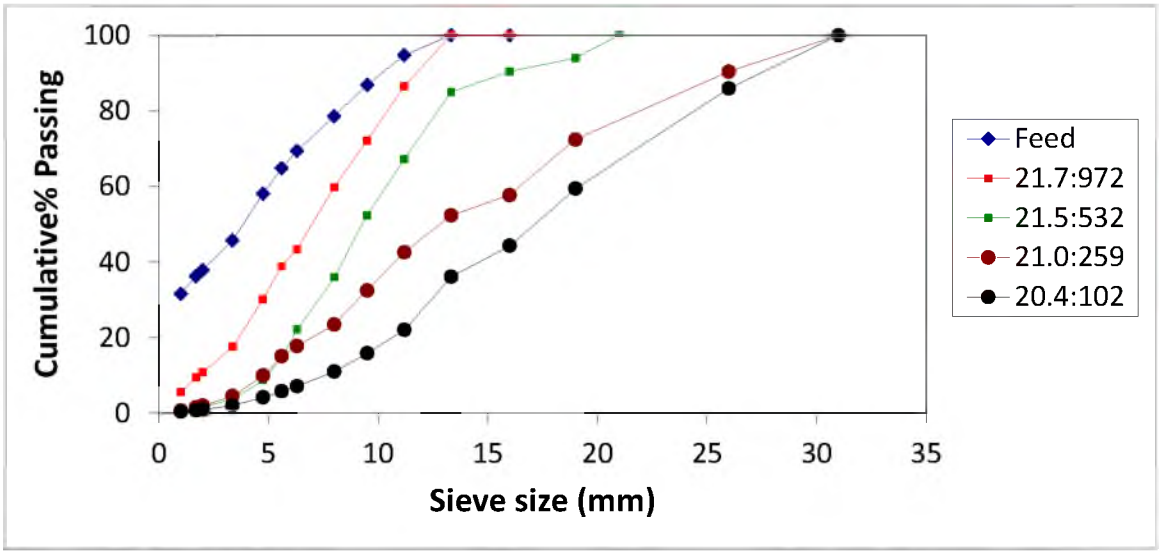

Figure 18. ASDs of agglomerates at different acid concentrations (20% moisture).

The liquid volume introduced to the agglomeration process decreases as the acid concentration increases with moisture content remaining constant. Therefore, the capillary force which helps to hold particles together decreases as less liquid is present in the empty spaces surrounding particles. This leads to smaller agglomerates observed.

Figures 19-21 summarize the effect of moisture content and acid strength on ASDs by displaying data for -1.7 mm material, D_{50}, D_{10}, respectively. Chamberlin recommends that no -150 µm (-100 mesh) fines remain unattached after agglomeration (Chamberlin 1986). To measure the amount of -150 µm particles, wet screening is needed. As the agglomerates are held together by a liquid bridge, wet screening will destroy the agglomerates. Thus, agglomerates which are smaller than 1.7 mm (-10 Tyler mesh screen) are considered as fines in this study. Increasing moisture content generally leads to less fines and larger agglomerates.

While the agglomerate size increases with increasing moisture, the -1.7 mm material eventually reaches a minimum.

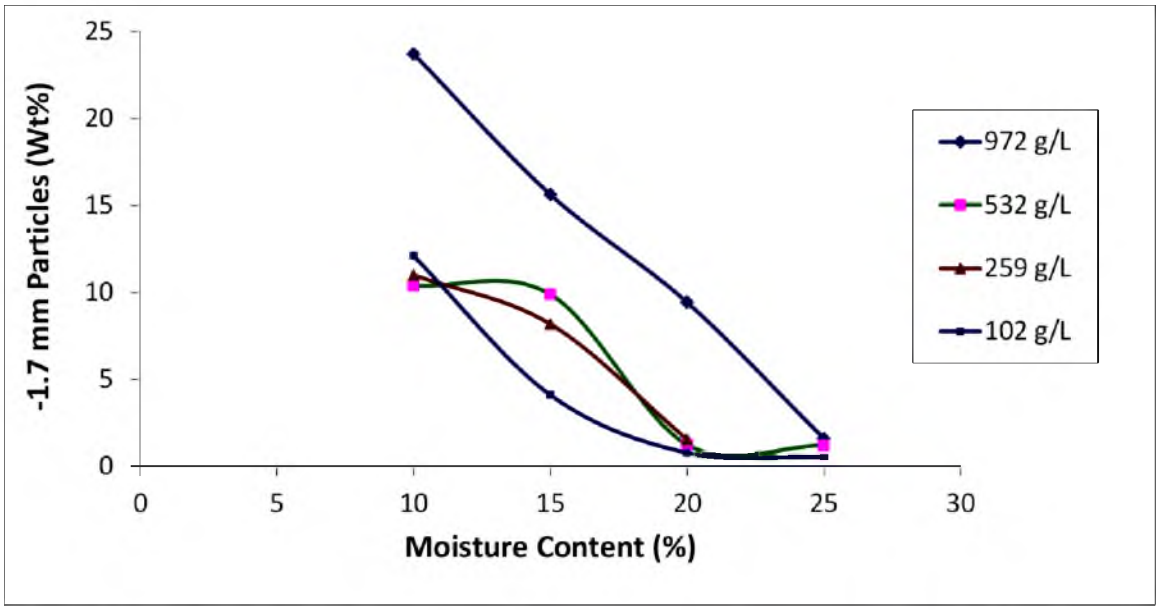

Figure 19. The relationship between moisture content and amount of fines left in the ore body at different acid concentrations as indicated in the legend.

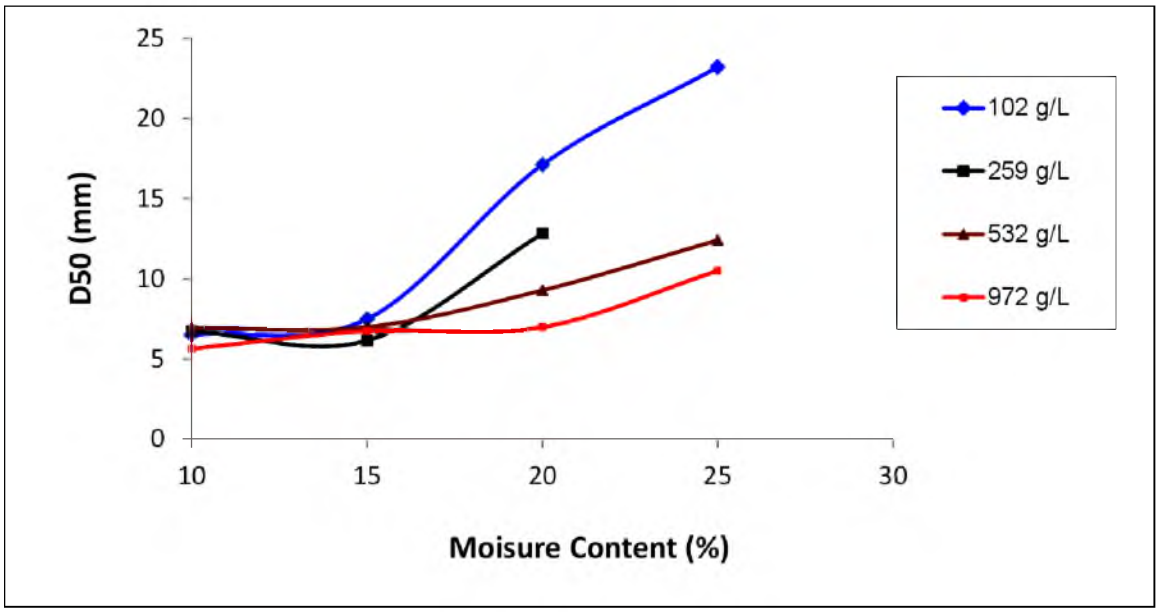

Figure 20. The relationship between D_{50} and moisture content of agglomerates at different acid concentrations as indicated in the legend.

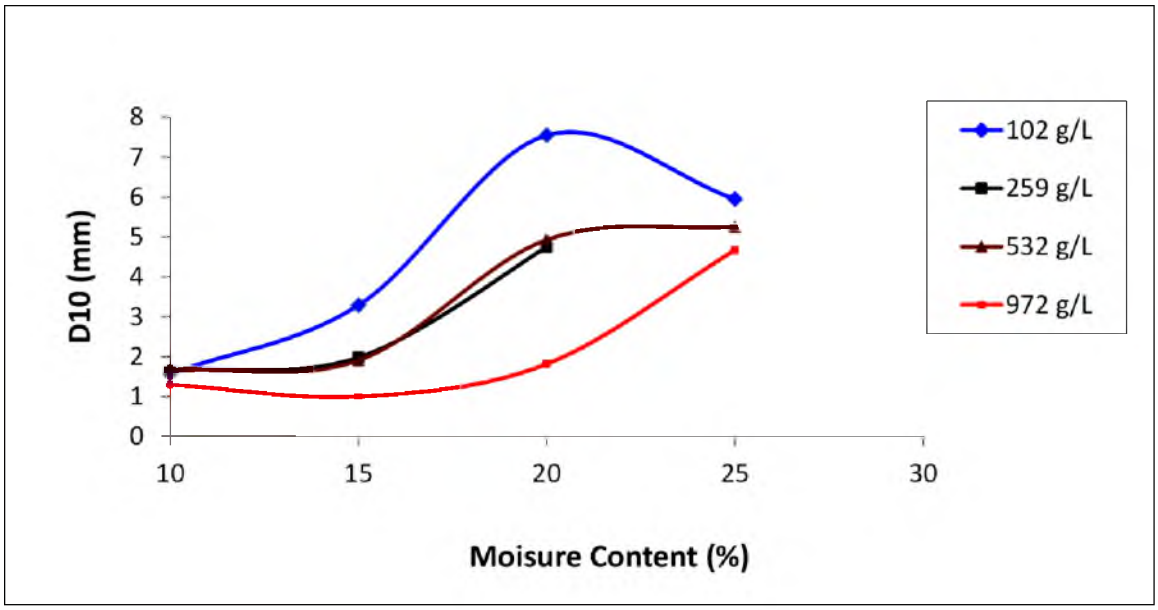

Figure 21. The relationship between D_{10} and moisture content of agglomerates at different acid concentrations as indicated in the legend.

Beyond this minimum, adding more liquid resulted in formation of "mud". Considering the results in the first phase of experiments, about 20% moisture content is the maximum moisture content for agglomeration (unless very high acid strength is used), as illustrated in Figure 19. Beyond this point, the fine amount was not further significantly decreased and mud formation occurred. This is shown in Figure 22 with pictures of agglomerates that are (a) too dry, (b) look good and (c) are too wet. In (a), fine particles are not attached to the other particles. In (b), fine particles were attached to coarser particles to form more coarser particles. In (c), mud formation has occurred.

Moisture content also has effects on both D_{50} and D_{10} of agglomerates. In Figure 19, the D_{50} of agglomerates is not significantly changed at low moisture content (<15% moisture content). At low moisture content, liquid phase is insufficient to create the liquid bridges between the particles, especially between coarse particles. As the moisture

content further increases beyond 15%, the D_{50} of agglomerates starts to rise. This change results from the available liquid in the agglomeration process. However, excess liquid phase will result in mud formation, as indicated above.

D_{10} is one of the parameters used to analyze particle size distribution. It considers small particle fraction in the systems. D_{10} also follows a similar trend as D_{50}. However, at an acid concentration of 102 g/L, the D_{10} of agglomerates seem to rise immediately. This may be due to more liquid solution used at a lower acid concentration than at higher acid concentration.

To illustrate that the volume of solution added is important, both D_{50} and D_{10} are plotted in Figure 23 versus the volume of solution applied during agglomeration. While there is scatter in the data, a general trend is observed that shows agglomerate size increases with increasing solution volume addition. At low solution addition, both D_{50} and D_{10} are not significantly changed. As the liquid volume increase beyond a point (~100 L/tonne), the D_{50} and D_{10} begin to increase. At this point, the solution addition volume is sufficient to provide a capillary force necessary for agglomeration.

In the next part of the scoping experiments, drum rotation speed was examined while moisture content, acid concentration and mixing time were held constant at 20.4%, 102 g/L H_2SO_4 and 3 minutes, respectively. The drum rotation speeds were changed from 15.7 to 47.1% of the critical speed.

Figure 24 shows the ASD curves for agglomerates produced at different drum rotation speeds. The -1.7 mm weight percentage, D_{10} and D_{50} of these agglomerates are summarized in Table 9.

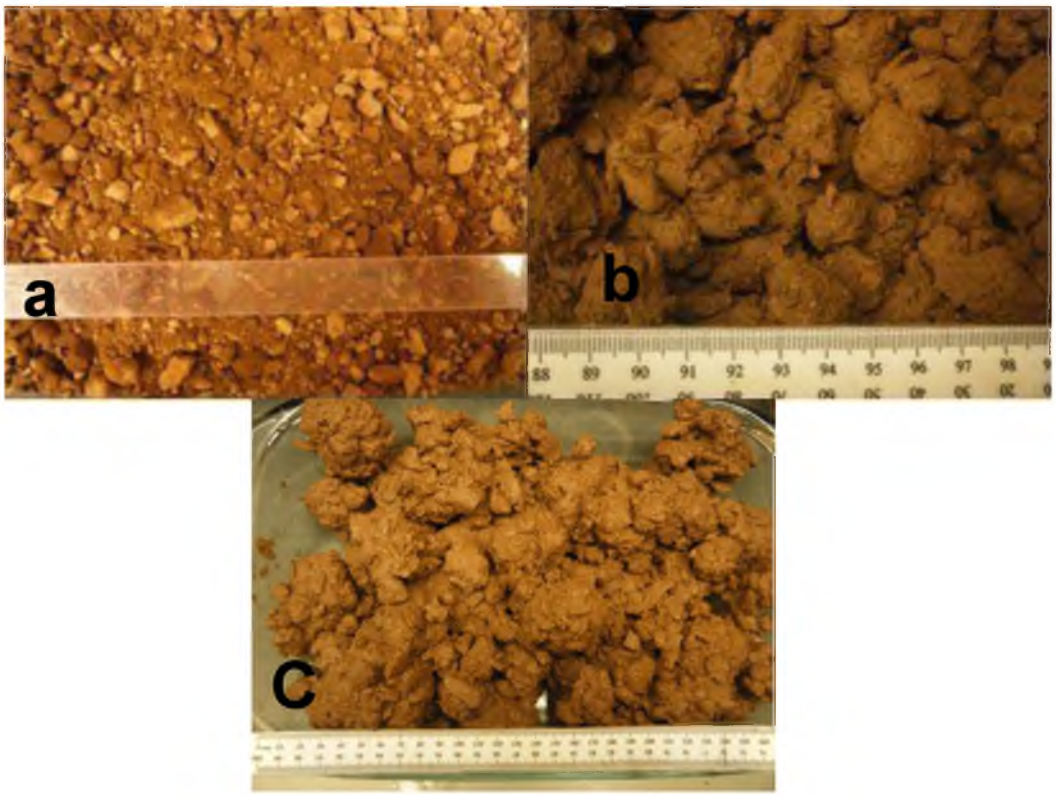

Figure 22. Pictures of agglomerates (a) 10% moisture content and1840 g/L acid concentration, (b) 20.4% moisture content and 102 g/L acid concentration sample, (c) 25.6% moisture content and 102 g/L acid concentration sample.

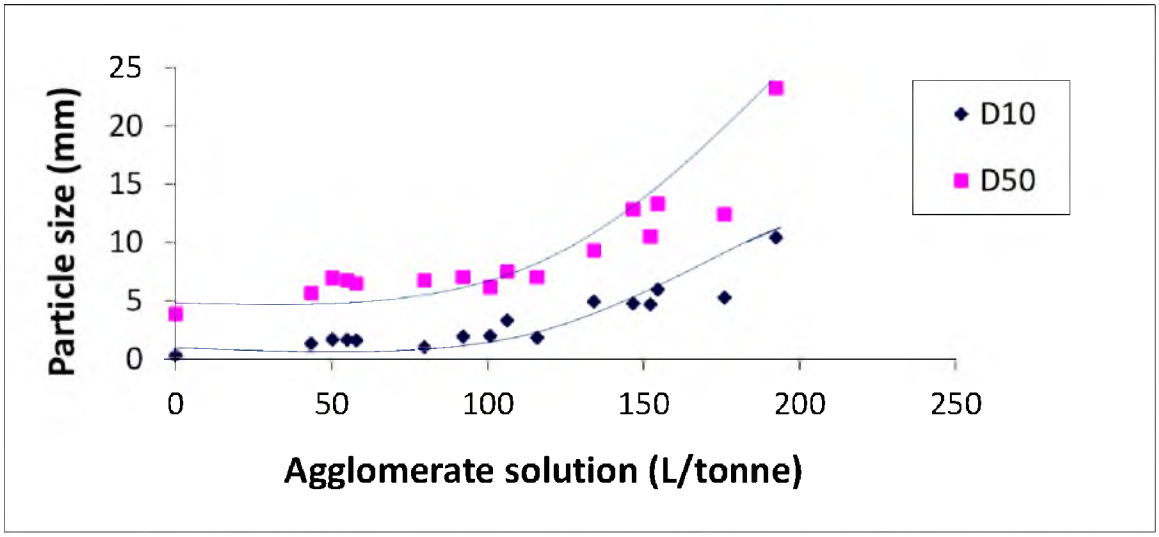

Figure 23. The relationship between agglomerate solution amount and the particle size distribution.

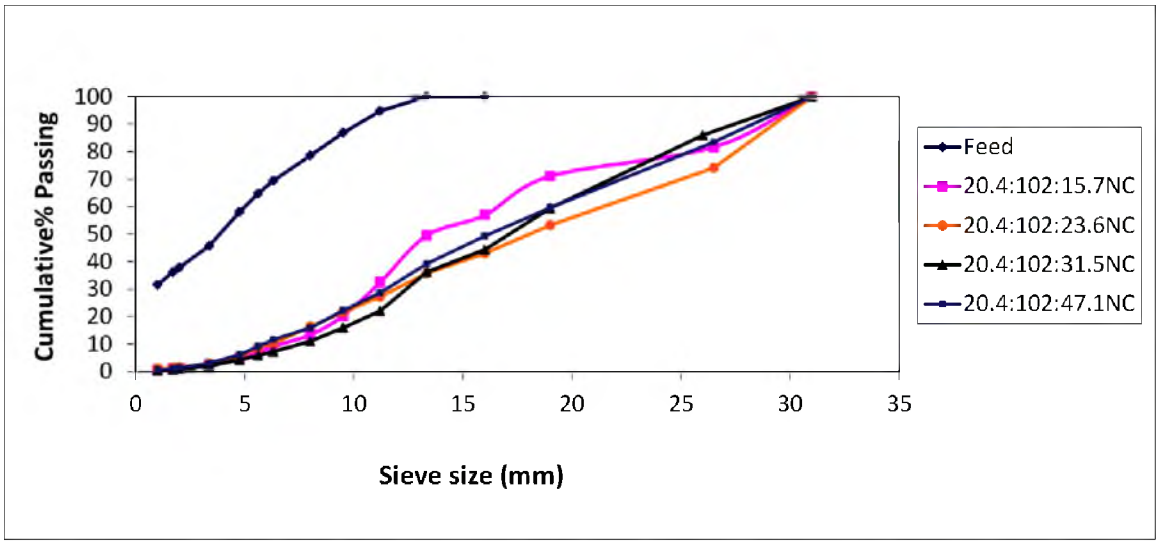

Figure 24. The ASDs of agglomerates produced at different drum rotation speeds using 20.4% moisture and 102 g/L H_2SO_4.

Table 9. Fine particles, D_{10} and D_{50} of agglomerates at different drum rotation speeds.

Drum rotation speed (%NC)	Fine particles less than 1.7 mm (%)	D_{10} (mm)	D_{50} (mm)	Percent of +19 mm particles (%)
15.7	1.03	6.63	13.53	28.90
23.6	1.39	6.21	18.05	46.80
31.5	0.77	7.55	17.12	40.54
47.1	1.03	5.86	16.18	40.40

From the data, the agglomerate size distribution curves versus drum rotation speed are not significantly different.

In the last part of the scoping experiments, mixing time was studied while drum rotation speed, moisture content and acid concentration were fixed at 31.5%NC, 20.4% and 102 g/L. Mixing times were examined over the range of 3 to 6 minutes. Figure 25 shows the agglomerate size distribution curves of agglomerates at different mixing times. The -1.7 mm weight percentage, D_{10} and D_{50} of these agglomerates are summarized in

Table 10. In general, for the conditions examined, mixing time had some effect on the resulting agglomerate size distribution. The ASDs of the agglomerates increased slightly as the mixing time increased and a maximum was achieved at 5 minutes.

Considering the proportion of each agglomerate size within each agglomerate condition, increasing mixing time obviously leads to coarser agglomerates. As time increases, the smaller size agglomerate proportion decreases and the larger agglomerate proportion increases. The rolling action within the drum along with adequate liquid phase during agglomeration promotes the growth of agglomerates as the rolling time increases. However, the maximum point is reached at 5 minutes. At 6-minute mixing, the agglomerates start to decrease in size from those at 5-minute mixing times, as shown in Figure 25. The agglomerates continue to grow as long as adequate liquid, capillary force and rolling action is available during agglomeration. The agglomerates eventually reach their maximum size and then start to deteriorate as the rolling action introduces rubbing and impact force between the agglomerates, causing them to break apart. These forces now are greater than the capillary force, so the agglomerate sizes decrease.

Since agglomeration is often used to control the amount of fines, mixing time had minimal effect with the wt% -1.7 mm by <1% for all times. This indicates that shorter mixing times for this ore may be effective for agglomeration. A short mixing time would result in a shorter agglomeration drum in practice and reduce the necessary capital.

Electrical Conductivity

Electrical conductivity of agglomerates produced from copper ore can be affected by several factors, such as the nature of samples, moisture content, solution volume, the compaction of the samples and acid concentration (Velarde 2005).

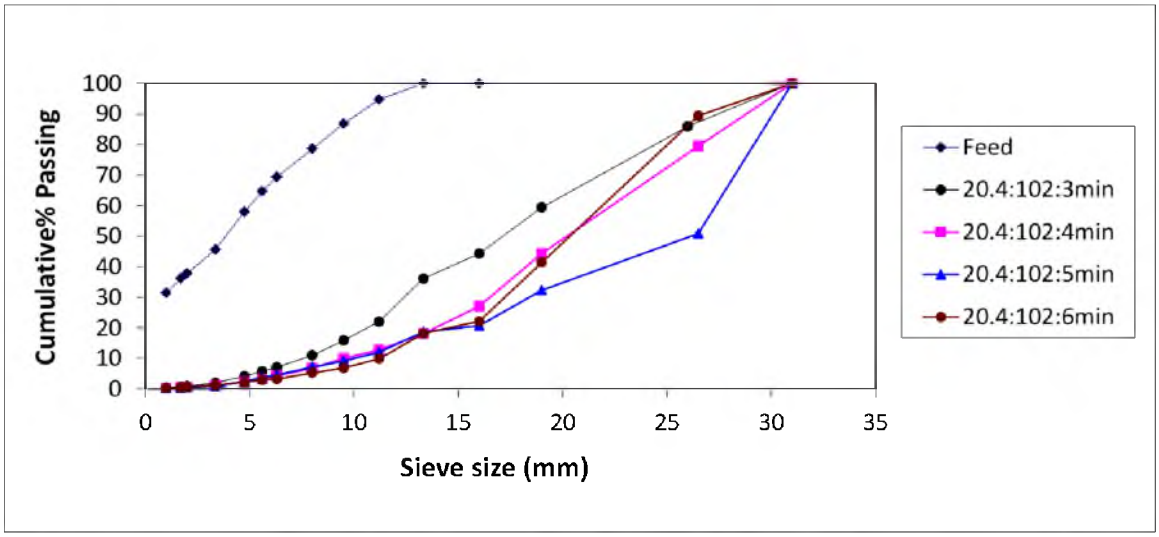

Figure 25. ASDs of agglomerates produced with different mixing times at 20.4% moisture, 102 g/L H_2SO_4 and 31.5% NC.

Table 10. Fine particles, D_{10} and D_{50} of agglomerates at different retention times.

Mixing Time (minute)	Fine particles less than 1.7 mm (%)	D_{10} (mm)	D_{50} (mm)
3	0.77	7.55	17.12
4	0.56	9.46	20.20
5	0.48	9.98	26.15
6	0.53	11.22	20.34

In this study, moisture content, solution volume, acid concentration and the compaction of sample effects on electrical conductivity of nickel laterite agglomerates were investigated.

Electrical conductivity was measured for agglomerates produced with various moisture contents and acid strength. Each condition was measured three times (e.g., one measurement per four kg batch, three batches per condition). The means, standard deviations and coefficient of variation for the measured electrical conductivity values are given in Table 11 along with agglomeration conditions. The coefficient of variation is the ratio of standard deviation and mean for a data set. These dimensionless numbers are useful to compare data sets with different units or means. Most of the coefficients of variation for the conductivity values at 20.4 kg applied load are smaller than those at no load applied. The median percent standard deviation for the conductivity measurements with no load and under a mechanical load were 11% and 6%, respectively. This indicates that electrical conductivity measured under a mechanical load provides a more precise measurement.

In the work of Velarde (2005), it was found that the electrical conductivity (electrical current) values form an exponential curve. Prior to the film formation around copper ore particles (during absorption), increasing moisture content does not increase electrical conductivity (electrical current) values significantly since there are no electrical passages provided by liquid film around the particles.

Velarde (2005) also indicated that proper moisture content for agglomeration can be observed via electrical conductivity (electrical current) values of the agglomerate body.

Table 11. The mean, standard deviation and coefficient of variation of electrical conductivity of agglomerates at different moisture contents and acid concentrations.

Moisture content (%)	Acid concentration (g/L)	Mean conductivity (S/m)		Standard deviation		Coefficient of variation	
		No load	20.4 kg load	No load	20.4 kg load	No load	20.4 kg load
15.3	102	0.01254	0.03281	0.00045	0.00316	0.03554	0.09621
15.7	259	0.02199	0.06623	0.00646	0.01578	0.29374	0.23826
16.0	532	0.02235	0.05728	0.00184	0.00252	0.08239	0.04391
16.1	972	0.01183	0.04142	0.00223	0.00275	0.18830	0.06634
20.4	102	0.02437	0.10350	0.00511	0.02620	0.20960	0.25318
21.0	259	0.03558	0.11336	0.00255	0.00575	0.07157	0.05068
21.5	532	0.05272	0.15239	0.00202	0.00134	0.03838	0.00882
21.7	972	0.02228	0.07432	0.00309	0.00299	0.13881	0.04023
25.6	102	0.02235	0.05728	0.00184	0.00252	0.08239	0.04391
26.3	259	0.26523	0.81840	0.22310	0.38291	0.84115	0.46788
27.0	532	0.11032	0.34597	0.00309	0.01955	0.02801	0.05650
27.2	972	0.03371	0.09697	0.00573	0.01248	0.17000	0.12870

The electrical conductivity (electrical current) values change abruptly with the liquid film present around the agglomerates. This change identifies the proper moisture content for agglomeration.

In this investigation, the relationship between the electrical current and moisture content follow a similar trend as in Velarde's work for relatively low acid concentration (up to 532 g/L). At higher acid concentration, the electrical current at the same moisture content ranges does not follow the trend. Figure 26 illustrates the relationship between the electrical current and moisture content of the agglomerate bed. At higher acid concentration, the moisture content ranges in the study were not large enough to cover the transition region. Therefore, the sudden change in electrical current was not observed. The mean electrical conductivity data for beds of packed agglomerates produced using different acid concentrations and grouped by moisture content are displayed in Figure 27.

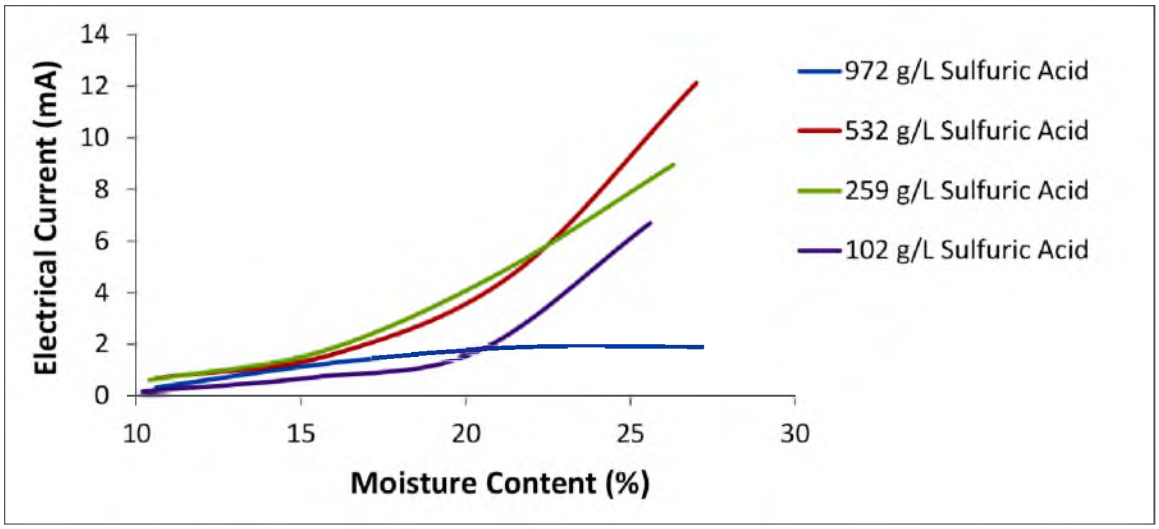

Figure 26. Relationship between moisture content and electrical current of the agglomerates at 20.4 kg load and 2 volt applied.

A maximum in conductivity is observed for each % moisture near acid concentrations of 259 to 532 g/L (21.68-31.71 wt%) These results mirror the values of pure sulfuric acid conductivity values. The conductivity of sulfuric acid also varies with the concentration and it has its maximum value at about 30 wt% at $25\,^{o}C$.

Increasing the moisture content leads to increases in conductivity values. Increasing the solution volume in the agglomeration system creates more liquid paths and thus, current can flow more easily, resulting in larger conductivity values. There appears to be a relationship between the moisture content and electrical conductivity, as shown in Figure 28. The conductivity values are plotted on logarithm scale to amplify the difference between the values.

In the second part of the scoping experiments, drum rotation speed and mixing time were varied while moisture and acid were fixed at 20.4% and 102 g/L H_2SO_4, respectively.

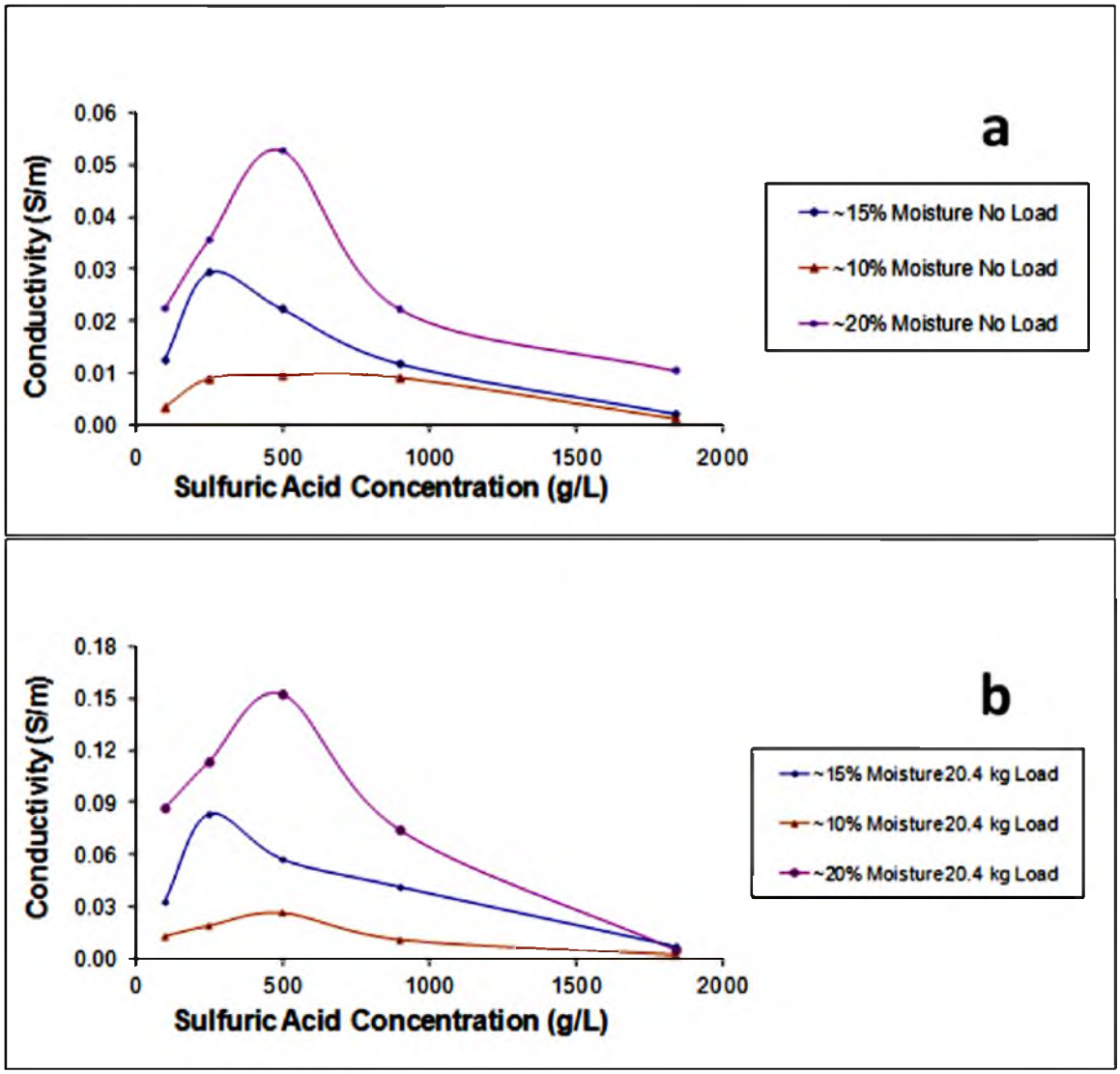

Figure 27. Relationship between acid concentration and electrical conductivity of the agglomerates. a) Conductivity when no mechanical load was applied b) Conductivity when 20.4 kg mechanical load was applied.

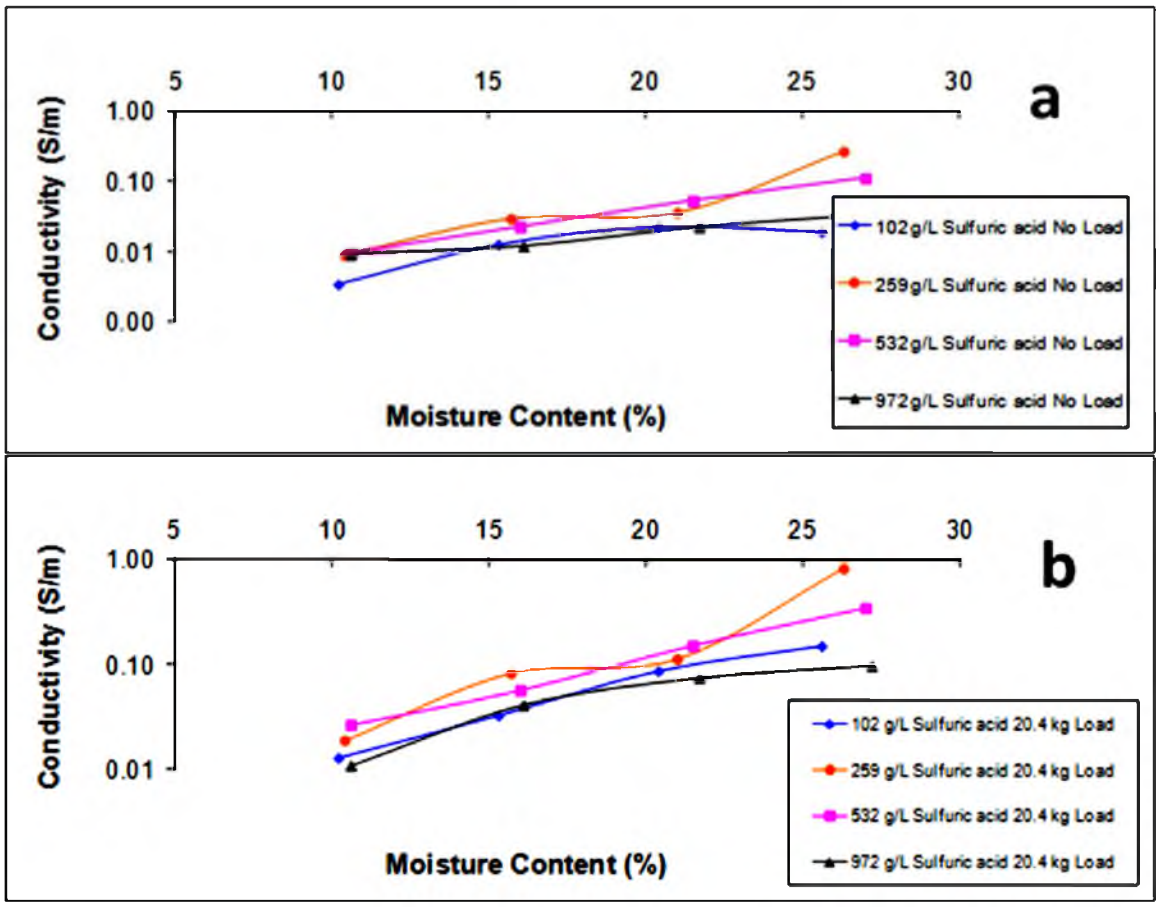

Figure 28. The conductivity values of agglomerates at different acid concentration and moisture contents. a) Conductivity when no mechanical load was applied b) Conductivity when 20.4 kg mechanical load was applied.

Changing mixing time and drum rotation speed during the agglomeration process has no effect on electrical conductivity of agglomerates, as shown in Table 12. The conductivity values of agglomerates were quite constant as the drum rotation speed and retention times change due to the fact that the moisture content and the acid concentration of the solution were fixed. The agglomerate sizes were slightly different during varying mixing time and drum rotation speed; however, the size of agglomerates seems to have no effect on electrical conductivity of the agglomerate bed.

It appears from these scoping tests that electrical conductivity can be used as a moisture content control tool if the acid strength or conductivity of the agglomeration solution is known.

Table 12. The electrical conductivity of agglomerates with 20.4% moisture content and 102 g/L acid concentration at different drum rotation speeds and retention times.

Factors		Conductivity (S/m)		Standard deviation		Coefficient of variation	
		No load	20.4 kg load	No load	20.4 kg load	No load	20.4 kg load
Drum rotation speed (%NC)	15.7	0.02508	0.10575	0.00241	0.01290	0.09826	0.12527
	23.6	0.02768	0.11804				
	31.5	0.02241	0.08681				
	47.1	0.02289	0.10122				
Retention time (minute)	3	0.02241	0.08681	0.00826	0.01269	0.46537	0.14821
	4	0.00764	0.09120				
	5	0.02621	0.09678				
	6	0.01472	0.06757				
Average		0.02113	0.09427				
Standard deviation		0.00669	0.01505				
Coefficient of variation		0.31684	0.15962				

As moisture content controls the formation of agglomeration, its measurement and control is very important to the agglomeration process. Measuring conductivity when the agglomerate bed is subjected to a mechanical load provides a more consistent measurement.

Electrical conductivity exhibits a general trend versus solution volumes. As the added solution increases, the conductivities increase. However, at the largest solution volume added, the conductivities of agglomerates with both no load applied and 20.4 kg of load applied drop significantly.

Since various sulfuric acid concentrations were used in the study, conductivity ratio values were introduced to the investigation to avoid the effect of sulfuric acid conductivity. The conductivity ratio can be calculated by equation (l2).

$$Conductivity\ Ratio = \frac{Measured\ Conductivity}{Conductivity\ of\ Sufuric\ Acid\ Solution} \qquad (12)$$

The relationship between the conductivity ratio and the solution volume indicates an exponential relationship, as shown in Figure 29. Although more solution volume leads to higher conductivities due to the viability of the electron pathways, other factors such as the conductivity of the solution, the natural conductivities of the minerals and the area of void space in the packed bed have contributions to the conductivities. These factors affect the conductivities; therefore, the overall conductivities resulting from these effects produce some scatter in relationship with the solution volume.

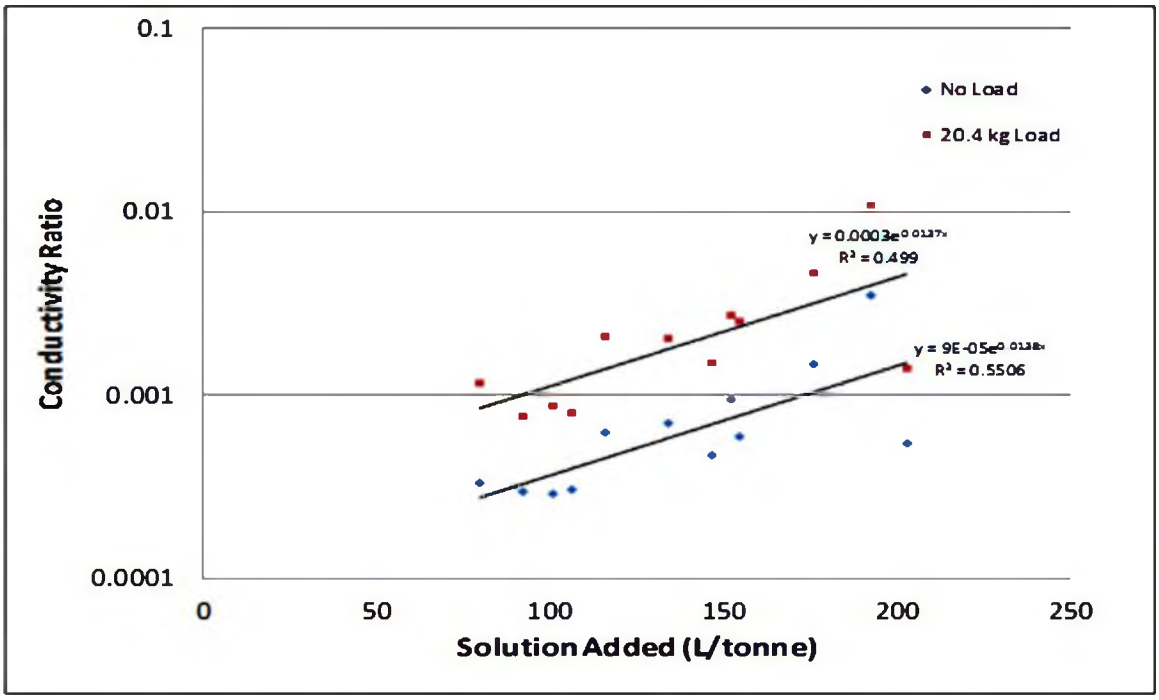

Figure 29. The relationship between the agglomeration solution volume and electrical conductivity ratio.

Permeability

Permeability values for beds of agglomerates as a function of moisture content and acid concentration are shown in Figure 30. In general, permeability increases with increasing moisture at a constant acid strength. Permeability decreases with increasing acid strength at constant moisture. These trends are similar to those observed when examining the effect of the agglomerate size distributions. As the sizes of the agglomerates increase, the void spaces within the packed bed also increase, creating easier pathways for fluids to flow. Easier pathways lead to higher permeability. Eventually, the moisture content can become too high, leading to "mud" formation. This will not cause larger agglomerates to form, thus decreasing the solution paths and

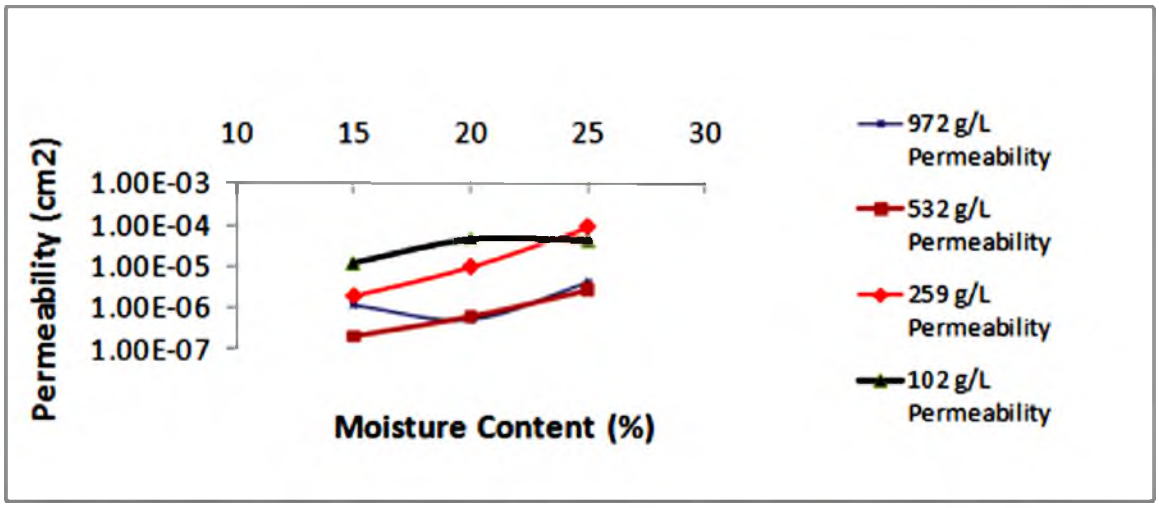

Figure 30. Permeability of agglomerate bed as a function of % moisture and acid strength used during the agglomeration process.

decreasing permeability. This may have happened at 25.6% moisture with 102 g/L H_2SO_4.

Figure 31 shows examples of agglomerates after being subjected to the permeability test. In Figure 31 a), the agglomerates are still attached to each other and they have not slumped (compressed) much during the test. In Figure 31 b), the agglomerates did not hold together and there was a large decrease in bed height during the test. In b), the agglomerates are wet unlike Figure 31 a) which is drier. The permeability value in a) is $9.7x10^{-5} cm^2$ and that in b) is $2.8x10^{-6} cm^2$.

Since permeability and particle size distributions appear to be correlated, the permeability data were plotted versus the volume of solution. Figure 32 illustrates that while scatter in the data exists, an obvious trend is observed that increasing the solution volume over the range examined increases permeability. The agglomerates breaking down during permeability tests are another factor which influences the values of permeability of the agglomerate bed. From observations, higher acid concentrations used

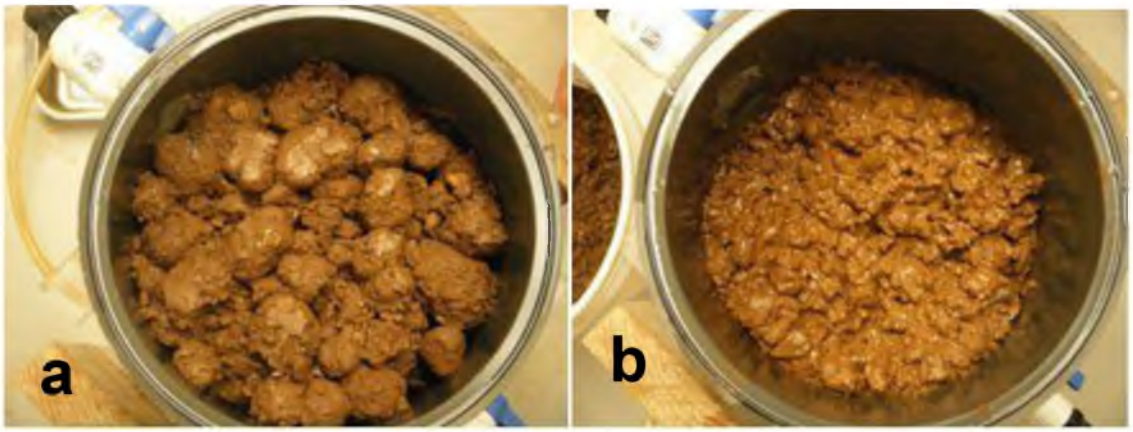

Figure 31. The agglomerates after subjecting to permeability tests; a) agglomerates of 102 g/L acid concentration, 20.4% moisture content and 5 minutes retention time, b) agglomerates of 532g/L acid concentration, 27.0% moisture and 3 minutes retention times.

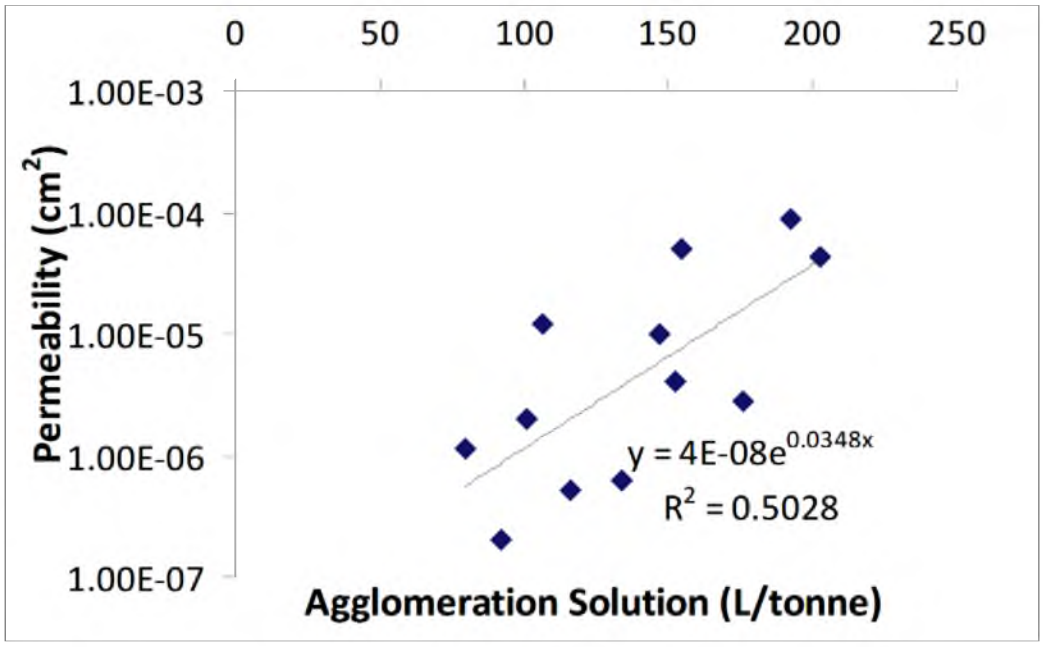

Figure 32. The relationship between agglomeration solution amount and permeability.

during agglomeration produce weaker agglomerates. These agglomerates tend to disintegrate during permeability tests, resulting in lower permeability values.

After the agglomerates break down, the small particles or fines migrate down the column, fill the void spaces within the agglomerate body and decrease the liquid flow paths.

In phase two of the scoping experiments, first the drum rotation speed was varied from 15.7 to 47.1% NC. Figure 33 shows the permeability values of agglomerates as the drum rotation speeds change. From the graph, the permeability values of the agglomerates at different drum rotation speeds are not significantly different and in the range of 1.5 to $4x10^{-5}$ cm^2. Therefore, the drum rotation speed did not have a significant effect on the nickel laterite agglomerate permeability.

Then, the agglomeration times were changed from 3 to 6 minutes. Figure 34 shows that the permeability values of agglomerates produced with different mixing times increased slightly with increasing mixing time. The permeability of agglomerates at different mixing times agrees well with the ASDs of the agglomerates. As the ASDs increase, the permeability also increases.

Table 13 shows the bulk density and porosity values of the agglomerates before and after the permeability experiments. Bulk densities increased and porosities decreased during every permeability test. In general, this was caused by agglomerate degradation caused by the flowing water used in the test. The bulk densities after flooding generally decreased as acid concentration was decreased with constant moisture. The final bulk densities were lowest (e.g., most porosity) with agglomerates produced with 102 g/L H_2SO_4 for every % moisture reported. Thus, examination of agglomerates by examining

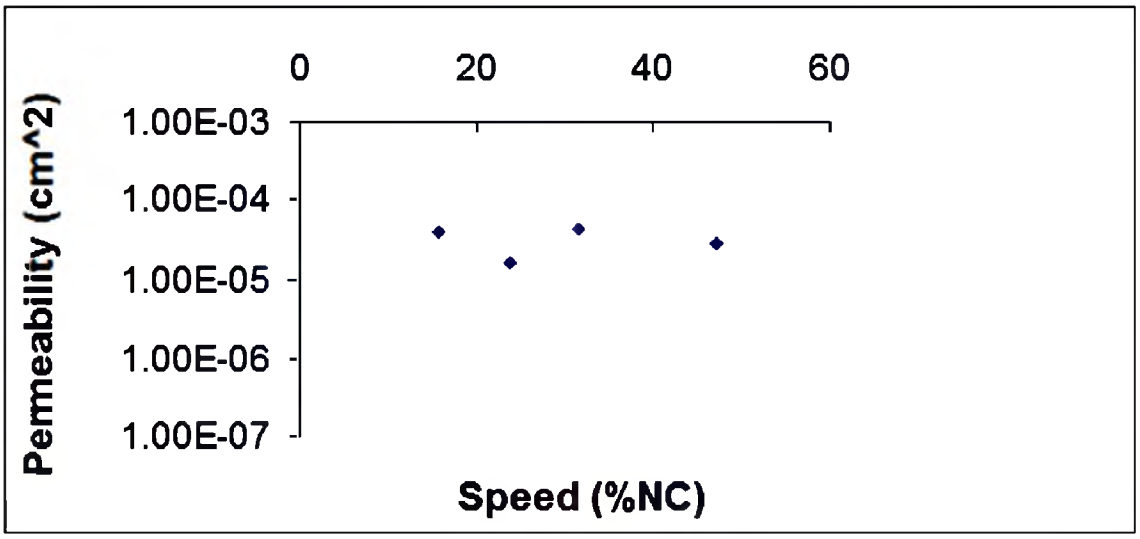

Figure 33. Permeability of the agglomerates of 20.4% moisture content and 102 g/L acid concentration at different drum rotation speeds.

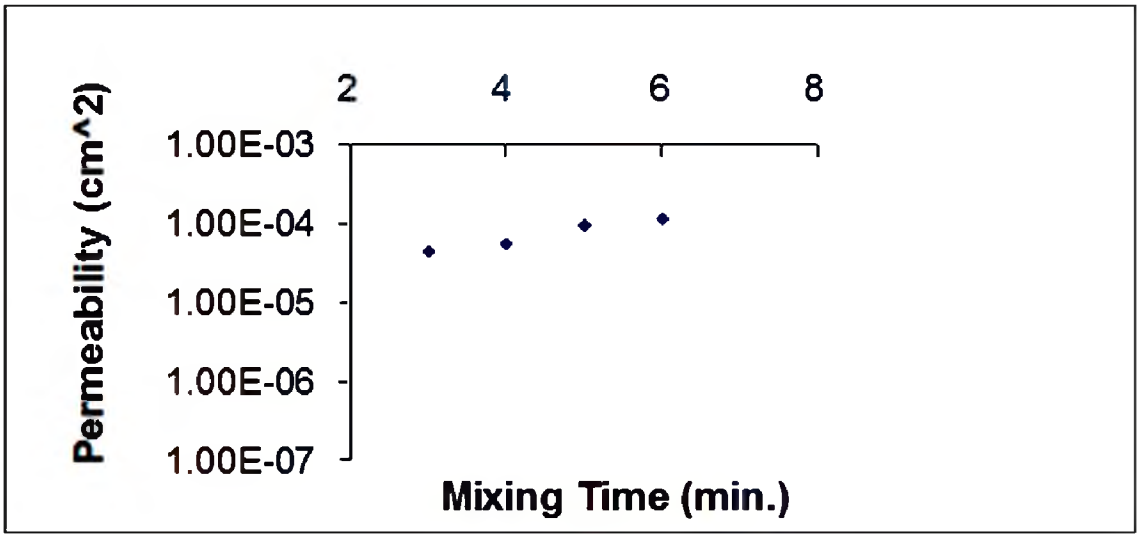

Figure 34. Permeability of the agglomerates of 20.4% moisture content and 102 g/L acid concentration at different retention times.

their bulk density during the permeability test indicates that agglomerates produced with 102 g/L H_2SO_4 provide better porosity and stability within their agglomerate bed, resulting in reasonable permeability value.

Table 13. The bulk density and porosity of agglomerates before and after the permeability tests.

Moisture content (%)	H_2SO_4 (g/L)	Bulk density (g/mL)		Δ Bulk density (%)	Porosity		Porosity change (%)
		Before Perm. Test	After Perm. Test		Before Perm. Test	After Perm. Test	
16.1	972	1.40	1.64	14.29	0.37	0.27	27.85
16.0	532	1.34	1.59	15.79	0.40	0.29	27.71
15.7	259	1.25	1.47	14.81	0.44	0.35	21.85
15.3	102	1.22	1.40	12.96	0.46	0.38	17.73
21.7	972	1.42	1.63	12.96	0.37	0.27	25.54
21.5	532	1.27	1.63	21.82	0.43	0.27	36.65
21.0	259	1.26	1.60	21.43	0.44	0.29	34.92
20.4	102	1.21	1.38	12.28	0.46	0.38	16.46
27.2	972	1.37	1.68	18.18	0.39	0.25	34.98
27.0	532	1.41	1.78	20.75	0.37	0.20	44.60
26.3	259	1.44	1.55	7.41	0.36	0.31	14.25
25.6	102	1.26	1.53	17.86	0.44	0.32	27.74

CHAPTER 5

COLUMN LEACHING

Heap leaching is commonly used in gold and copper extraction due to its low capital and operating costs. However, the low recovery, acid waste and long times are the disadvantages of the heap leaching process (Robertson & Van Staden 2009). The diminution of high-grade nickel sulfide ore deposits and high capital costs for smelting processes stimulate research and development in nickel laterite heap leaching technology. High acid consumption, potential breakdown of the aggregated mineral structures, the pure selectivity of nickel over iron and magnesium and high swelling clay content are the primary issues hindering nickel laterite heap leaching development (McDonald & Whittington 2008a). Column leach experiments are normally conducted to evaluate the possibility of copper and gold heap leaching and can be adapted to evaluate the possibility of nickel laterite heap leaching as well.

Two batches of 25 kg nickel ores were agglomerated in the 30 gallon drum with four 0.5 cm height lifters. The agglomerates were then loaded into a 20.3 cm column. The agglomerates were cured for three days prior to leaching to allow acid to react with the minerals. 65 g/L sulfuric acid solution was then applied at the rate of 4.2 to 6.4 mL/min. Pregnant leaching solution (PLS) was collected for later analysis throughout the experiments.

The moisture content, acid concentration and acid addition values used in agglomeration were varied to examine their effects on leaching performance. The agglomeration conditions employed are summarized in Table 14.

Agglomerate Size Distributions

Leach Feed

Images of agglomerates produced at each condition are shown in Figure 35. The agglomerates vary from dry (13:972) to quite wet (19:313). The agglomerate size distributions produced for column leaching are displayed in Figure 36. As expected, the agglomerate sizes increased as the volume of solution added during the agglomeration process increased. The size of agglomerates decreased as the acid concentration used during agglomeration increases when the moisture content is fixed, although at 13% moisture content, the difference due to the acid concentration was small. The ASDs of the replicated samples show small variation, indicating good experiment reproducibility. The ASDs are summarized in Table 15 in term of D_{50}, D_{10} and percent fines (-1.7 mm).

Table 14. The moisture content, acid concentration and acid addition used during agglomeration for the column leaching experiments.

Moisture Content (%)	Acid Concentration (g/L)	Acid Addition (kg/tonne)
19.6	972	100.5
19.1	313	41.6
16.3*	642	60.2
13.0	972	61.3
12.6	313	25.4

(*) Three columns were produced with these agglomeration conditions to determine experimental error.

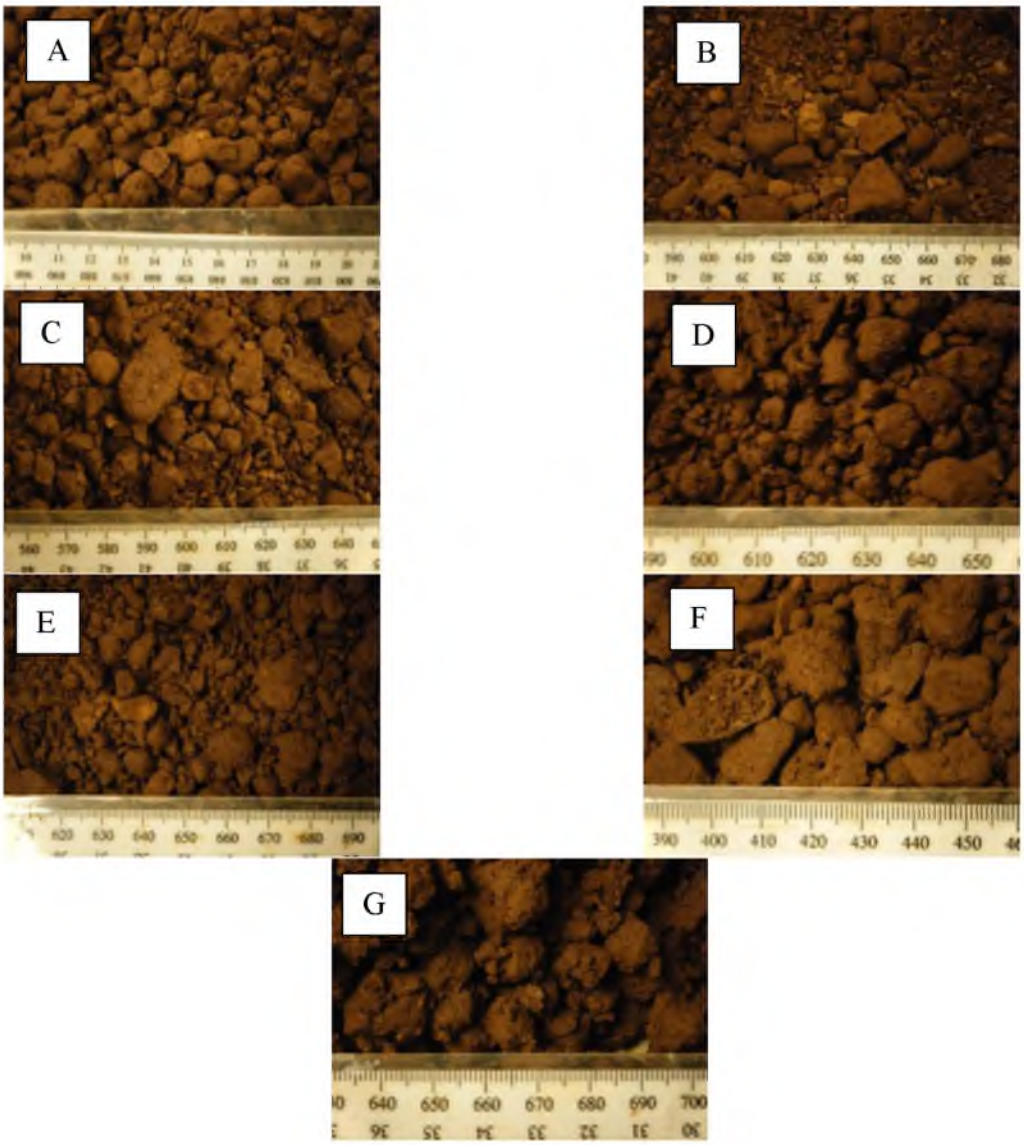

Figure 35. The images of agglomerates at different agglomeration conditions that were loaded into the leaching column: (A) 19:972, (B) 13:972, (C) 16:642_1, (D) 16:642_2, (E) 16:642_3, (F) 13:313, (G) 19:313. Sample ID nomenclature – moisture: acid concentration.

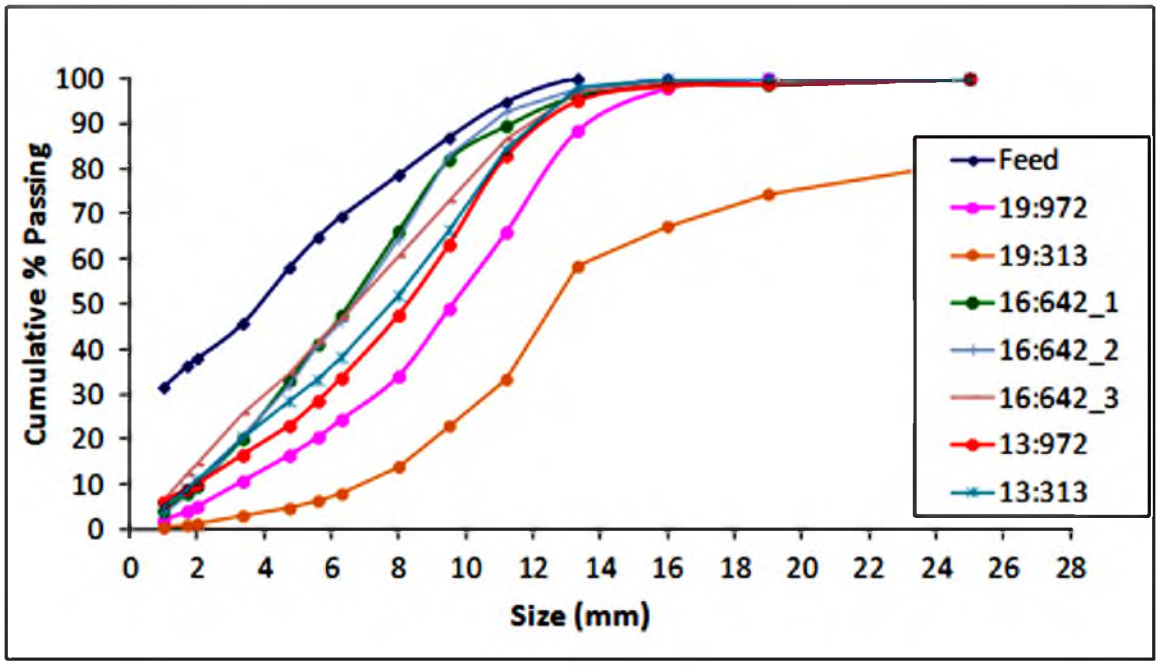

Figure 36. The particle size distribution of agglomerates at different agglomeration conditions during column leaching experiments. Sample ID nomenclature – moisture: acid concentration_ replication experiment.

Table 15. The D_{10}, D_{50} and percent fines of agglomerates at different agglomeration conditions during the column leaching experiments.

Moisture Content (%)	Acid Concentration (g/L)	D_{10} (mm)	D_{50} (mm)	Percent of Fines (-1.7 mm)
19	972	3.20	9.61	3.97
19	313	6.89	12.62	0.93
16	642	2.06	6.53	7.88
16	642	2.08	6.65	7.60
16	642	1.43	6.68	12.24
13	972	2.01	8.24	8.87
13	313	1.86	7.77	9.00

The D_{10} and D_{50} of agglomerates of nickel laterite ores in the column experiments tend to increase as the amount of the agglomeration solution increases. These results continue the trend observed with the previous scoping experiment results, as shown in Figure 37. As indicated in the legend in Figure 37, three different sets of experiments (received ore, crushed ore and column) exhibit similar size vs. liquid addition trends. The crushed ore and column experiments used the same feed material while the received ore was slightly different (see Chapter 6 for details). A correlation between D_{10} and D_{50} and solution volume addition appears to exist. The D_{10} and D_{50} of agglomerates did not significantly changed at lower dosage of solution addition. After about 100 L/tonne, the size of D_{10} and D_{50} of agglomerates increased as the solution volume increases.

Liquid bridges are important in the formation of crushed ore agglomerates. There are four states of liquid bridges: pendular, funicular, capillary and slurry, suspension or droplet (Mitarai & Nori 2006; Agrawal & Naveen 2011). In a pendular state, the liquid bridges are formed at the contacting point between the particles. As the liquid volume increases and some pores are filled with liquid, the liquid bridges occur around the contacting points. This is a funicular state. In capillary state, almost all the pores are filled with liquid, and the liquid surfaces are drawn back to the pore under capillary action. As the liquid volume further increases, the particles are completely surrounded by the liquid and the droplet state is reached (Mitarai & Nori 2006).

At lower dosage of solution addition, the liquid bridges start to form at the contacting points (pendular state) and the cohesive forces are not strong enough to produce coarser agglomerates. As the solution volume increases and the saturation state reaches funicular state, the cohesive forces are increased; therefore, the agglomerate sizes

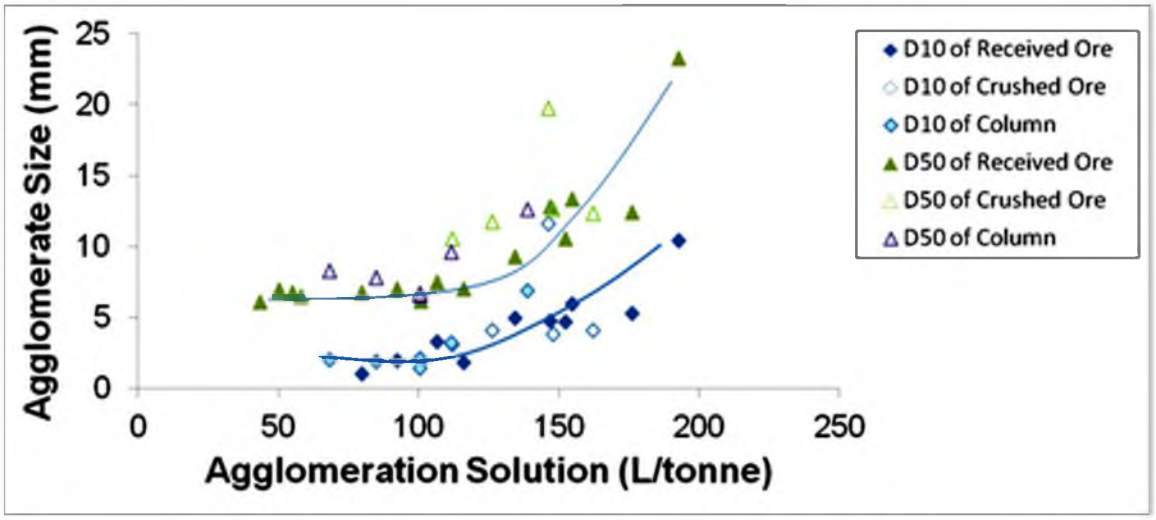

Figure 37. Correlation of D_{10} and D_{50} agglomerates with solution volume addition.

begin to increase. The agglomerate sizes continuous to increase through the capillary state. If the saturation state is beyond the capillary state, then mud-like particles are formed.

The acid solution used during agglomeration has different acid concentrations and therefore, the density and viscosity of the solution are different. As the acid concentration of the solution increases, the density and viscosity of the acid solution also increase. The correlation between the D_{10} and D_{50} of agglomeration at different acid solution density is illustrated in Figure 38. Since lower viscosity solution can travel and cover more surface area around the particles and provides necessary capillary forces which enhanced the agglomeration, using lower acid concentration solution during agglomeration tends to produce coarser agglomerates than using higher acid concentration solution.

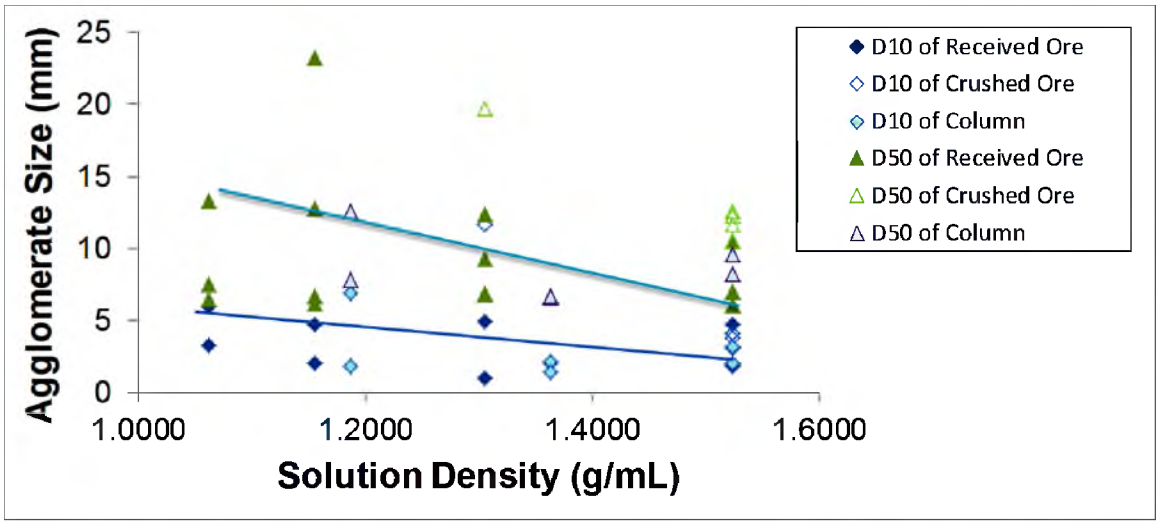

Figure 38. Correlation of D_{10} and D_{50} agglomerates with density of agglomeration solution.

Leach Residuals

Following a 90 day leach cycle, the ASDs of the leach residuals were examined. The ASDs of the agglomerates from the top, center and bottom of each column were examined. An example of plotted ASDs is shown in Figure 39 along with the ASD from the leach feed agglomerates for comparison purposes. The ASDs of the agglomerates from the other columns are shown in Appendix A. The legends in each figure have forms of A:B:C:D and A:B:No.:C:D. A represents the moisture content, B represents the acid concentration, C represents the sample collecting time (B: before leaching and A: after leaching), D represents the position of samples being collected (T: top of the column, C: center of the column and B: bottom of the column) and the number between B and C represents the replicate sample.

It is obvious from the ASDs that the sizes of agglomerates after leaching experiments are smaller than those before leaching experiments. Particle sizes after

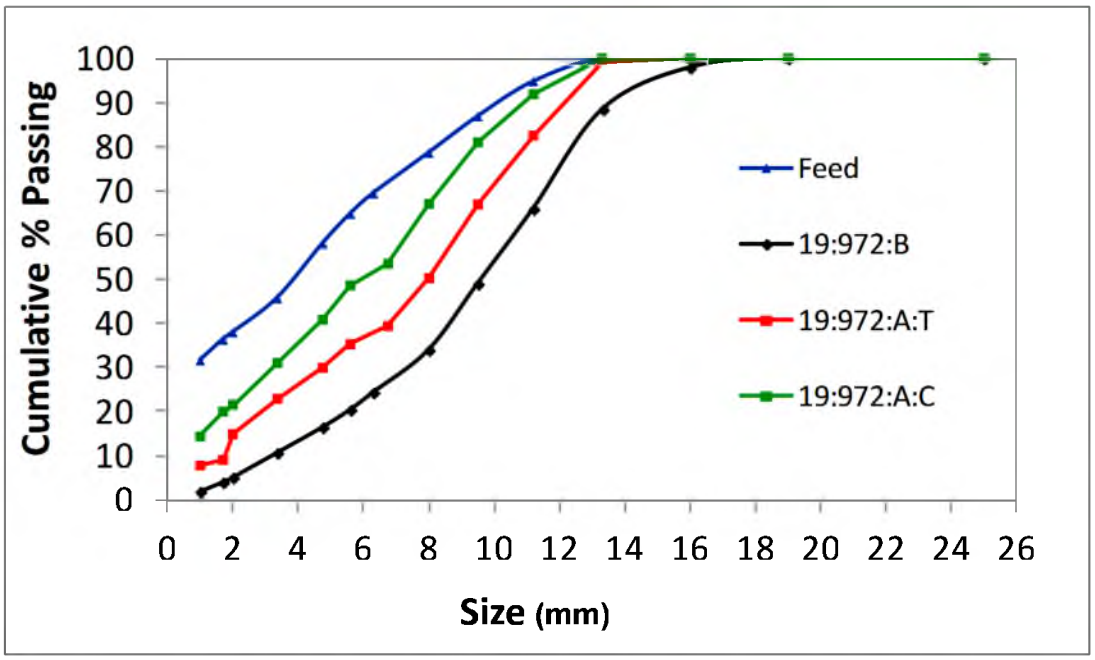

Figure 39. The agglomerate size distributions of the agglomerates at 19% moisture content and 972 g/L acid concentration condition after column leaching experiments were completed are compared with the agglomerate size distributions prior to leaching and the ore feed distribution prior to agglomeration.

leaching are still larger than the feed size. The amount of fines in the leach residuals are higher than the agglomerates. The agglomerates are obviously degraded during the leaching experiments, resulting in a decrease in agglomerate and/or particle sizes and an increase in the presence of fines. The leaching solution may dissolve and destroy the agglomeration bonding within the agglomerates; therefore, the agglomerates disintegrate and release the insoluble fines into the liquid flow system.

The fines and smaller agglomerates result from the breakage of coarser agglomerates. The comparison between the percent of fines (less than 1.7 mm) before and after leaching experiments of each agglomeration condition and at different positions are in Table 16. The amount of fines at the bottom position of 19 % and 13% moisture content and 972 g/L acid concentration could not be obtained.

Table 16. Comparison between the percent of fines before and after column leaching experiments of agglomerates at different agglomeration condition and at different position of the columns.

Moisture content (%)	Acid concentration (g/L)	Acid addition (kg/tone)	Percent of fines (-1.7 mm) (%)				
			Feed	Before leaching	After leaching		
					Top of column	Center of column	Bottom of column
19	972	100.5	36.3	4.0	9.8	20.0	-
19	313	61.3		0.9	9.5	10.6	8.3
16	642	60.2		7.9	17.6	23.4	13.2
16	642	60.2		7.6	28.2	21.5	16.3
16	642	60.2		12.2	13.2	23.3	13.5
13	972	41.6		8.9	19.0	12.3	-
13	313	25.4		9.0	17.9	28.3	20.3

In these columns, the bottom was filled with mud, making agglomerate sizing impossible. Interestingly, there was no percolation problem observed during the experiments. Regardless, the formation of mud indicates the agglomerates would have poor heap stability. Thus, 972 g/L acid concentration is too concentrated to be used during agglomeration for this ore.

The fines after column leaching are higher than those before leaching. This indicates that the agglomerates are falling apart during the leaching period. After the agglomerates break, the fines are expected to migrate down the column along with the raffinate. However, the amount of fines remaining in the leach residuals of each column at different positions shows vast variation, and contradicts the expectation. The breakage of agglomerates, the migration of fines and the dissolution of particles during column leaching experiments are complicated. Additional experiments are required for understanding these mechanisms on the observed results.

Table 17 presents the D_{10} and D_{50} of both agglomerates and leach residuals at different agglomeration conditions and positions. The only agglomeration condition at which D_{10} can be obtained from the leach residual at all positions is 313g/L acid concentration and 19 % moisture content. D_{10} cannot be obtained from all positions of the leach residuals of the other agglomeration conditions due to the value being smaller than the smallest sieve used. The D_{50} can be obtained from every leach residual with different agglomeration conditions except at the bottom of the 972 g/L acid column. Graphs illustrating the relationship between moisture content and acid concentration with D_{50} in the leach residual are displayed in Figures 38 and 39, respectively.

As presented in Figure 40 and 41, the D_{50} of leach residuals may increase slightly as the moisture content increased during agglomeration. The D_{50} of agglomerates prior to leaching also increases as the moisture content increases. At high moisture content conditions, the agglomerate sizes are bigger than those at low moisture contents at the beginning of the leach experiment. The percent size change of leach residual size is presented in Table 18.

As illustrated in Table 18, the percent change values for D_{50} for leach residuals are less negative at low moisture content than at high moisture content. However, the correlation between acid concentration and the percent change of D_{50} for the leach residuals is scattered. Since the agglomerate sizes at high moisture content are coarser than those at low moisture content, the degradation of the agglomerates at high moisture content tends to be bigger than those at low moisture content.

Table 17. Comparison between the D_{10} and D_{50} of leach residuals before and after column leaching experiments at different agglomeration condition and at different position of the columns.

Agglomeration conditions		D_{10} (mm)				D_{50} (mm)			
		Before leaching	After leaching			Before leaching	After leaching		
Moisture content (%)	Acid concentration (g/L)		Top	Center	Bottom		Top	Center	Bottom
Feed	Feed	<1.0	-	-	-	3.9	-	-	-
19	972	3.2	1.8	<1.0	-	9.6	8.0	5.9	-
19	313	6.9	1.8	1.6	2.0	12.6	8.5	7.9	8.5
16	642	2.1	1.1	<1.0	1.2	6.5	4.9	4.0	6.0
16	642	2.1	<1.0	<1.0	<1.0	6.7	3.7	5.0	5.2
16	642	1.4	1.3	<1.0	1.2	6.7	7.5	5.0	7.2
13	972	2.0	<1.0	1.3	-	8.2	5.8	7.0	-
13	313	1.9	1.0	<1.0	<1.0	7.8	6.9	4.3	6.8

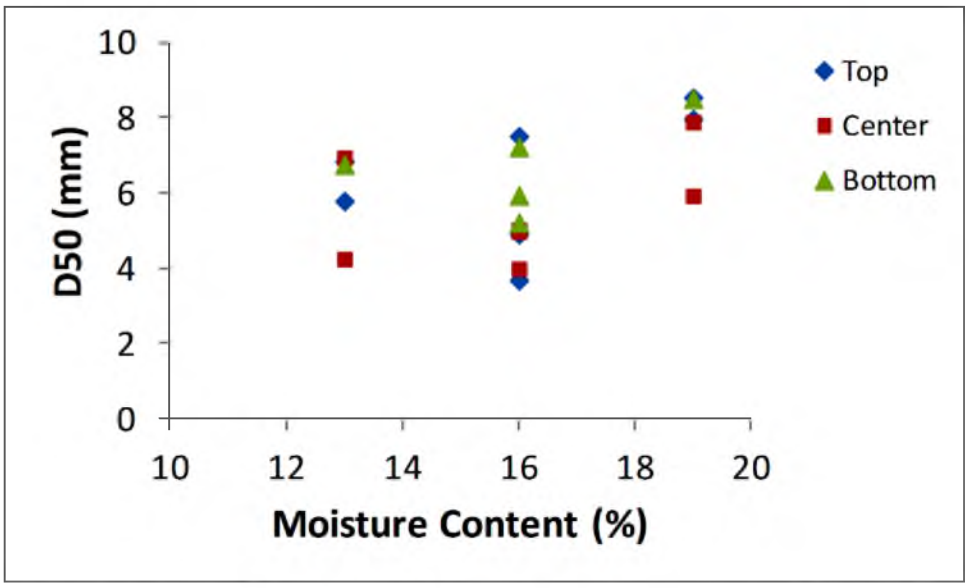

Figure 40. The relationship between moisture content and D_{50} of leach residuals at different column positions.

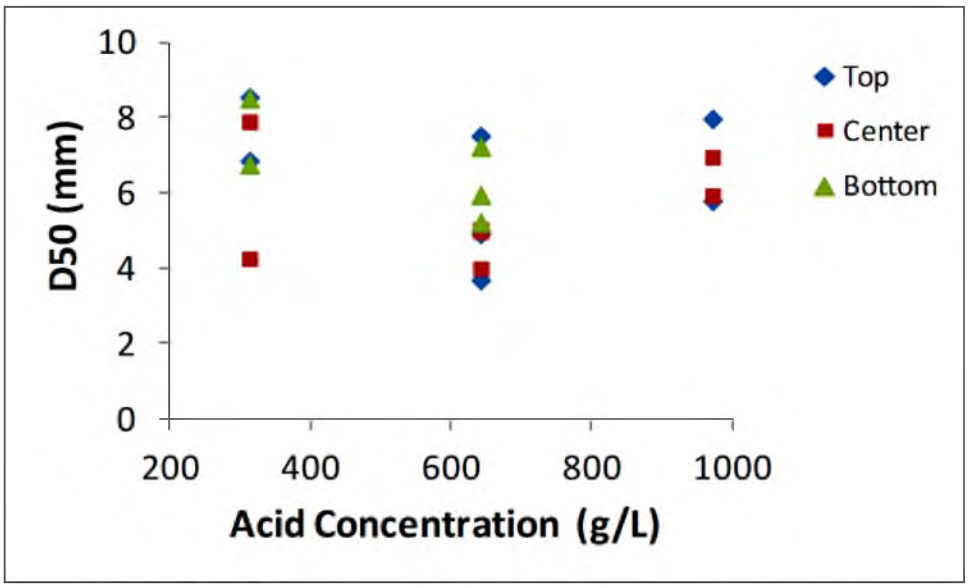

Figure 41. The relationship between acid concentration and D_{50} of leach residuals at different column positions.

Table 18. The D_{50} of leach residual changing at different agglomeration conditions.

Moisture content (%)	Acid concentration (g/L)	D_{50} (mm)				Average Leach residual size changing (%)
		Before leaching	After leaching			
			Top	Center	Bottom	
19	972	9.61	7.97	5.93	-	-27.67
19	313	12.62	8.54	7.89	8.51	-34.10
16	642	6.53	4.91	4.00	5.95	-31.78
16	642	6.65	3.69	5.03	5.22	-34.47
16	642	6.68	7.51	4.99	7.23	-6.44
13	972	8.24	5.79	6.95	-	-22.69
13	313	7.77	6.85	4.25	6.76	-23.31

The types of agglomerates are important. There are two types of agglomerates in wet agglomeration: coalescence and layering (Capes 1980). The agglomerate nuclei form when the liquid phase is introduced to the agglomeration system. After this nucleation phase, the agglomerates can grow by layering on the coarser particles or continue growing by themselves. The coalescence agglomerates can totally break and dissolve unlike layering agglomerates. The cores of layering agglomerates can or cannot be dissolved or destroyed by raffinate and compaction. This will add some variation to the percent degradation of the leach residuals. From the results, the strength of the agglomerates cannot be determined by these leaching experiments. Many factors, such as beginning agglomerate size, types of agglomerates, level of compaction and the mineralogy of the samples affect the strength of the agglomerates during column leaching experiments. Therefore, more experiments have to be performed in order to investigate the strength of the agglomerates.

Electrical Conductivity

The electrical conductivities of agglomerates produced for column leaching are given in Table 19. As expected, at the same moisture content, the conductivities of agglomerates at 313 g/L acid concentration were higher than that of 972 g/L acid concentration due to the effects of sulfuric acid conductivity. Conductivity also increased as the moisture content of the agglomerates increased. The conductivity of samples when no mechanical load was applied was lower than when a 20.45 kg load was applied. More compaction provides more direct electrical pathways as the agglomerate particles are forced to contact each other.

Increasing solution in the agglomeration process leads to more connected liquid paths which the electricity can travel easily; therefore, the electrical conductivity values also increase.

Figure 42 illustrates the relationship between conductivity ratio and agglomeration solution addition. The conductivity ratio values were used to avoid the

Table 19. The electrical conductivity of agglomerates at different agglomeration conditions.

Moisture Content (%)	Acid Concentration (g/L)	Electrical Conductivity (mS/m)		Conductivity Ratio	
		No Load	20.45 kg Load	No Load	20.45 kg Load
19	972	12.28	60.33	0.00034	0.00169
19	313	66.79	303.10	0.00083	0.00378
16	642	53.86	115.16	0.00082	0.00175
16	642	38.62	95.62	0.00059	0.00146
16	642	88.46	232.38	0.00135	0.00354
13	972	9.64	26.06	0.00027	0.00073
13	313	32.38	66.86	0.00040	0.00083

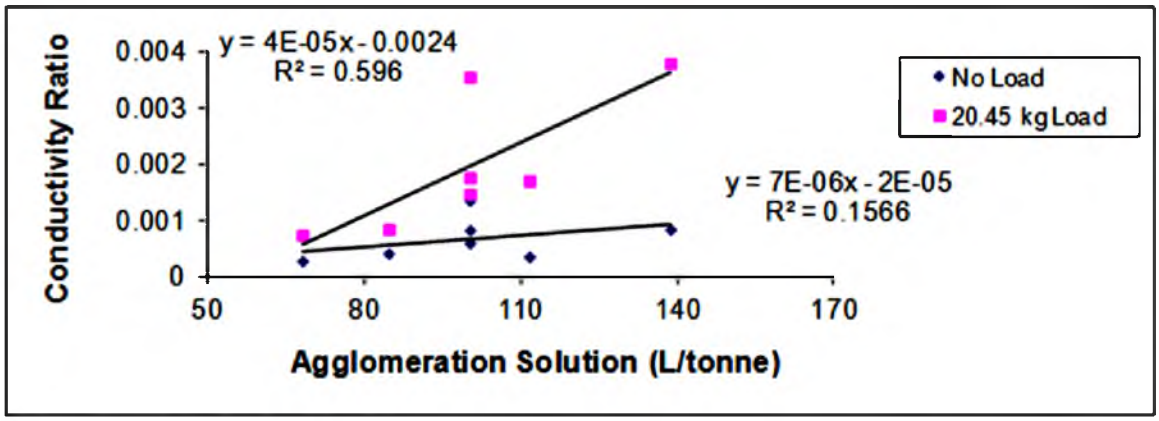

Figure 42. The relationship between agglomeration solution amount and conductivity ratio for agglomerates used in column leaching experiment.

effect of conductivity of sulfuric acid. These results are correlated with the scoping experiment results, as illustrated in Figure 43. The slightly higher conductivity in the column experiments may be due to the slightly different mineralogy of the ores used in each experiment. The nickel laterite ore was adjusted to use in the column leaching experiment due to the depletion of the specific size fraction. This adjustment changes the mineral composition of the ore. Therefore, the electrical conductivity values may be affected by the change.

As the agglomeration condition is determined, the conductivity of the obtained agglomerates is quite constant. Therefore, the conductivity can be used as a quick control tool for the agglomeration process.

Permeability

The saturated hydraulic conductivities of agglomerates for column leaching experiments are given in Table 20. The values increase as the solution addition increases, as shown in Figure 44. The hydraulic conductivity of replicate samples exhibited some

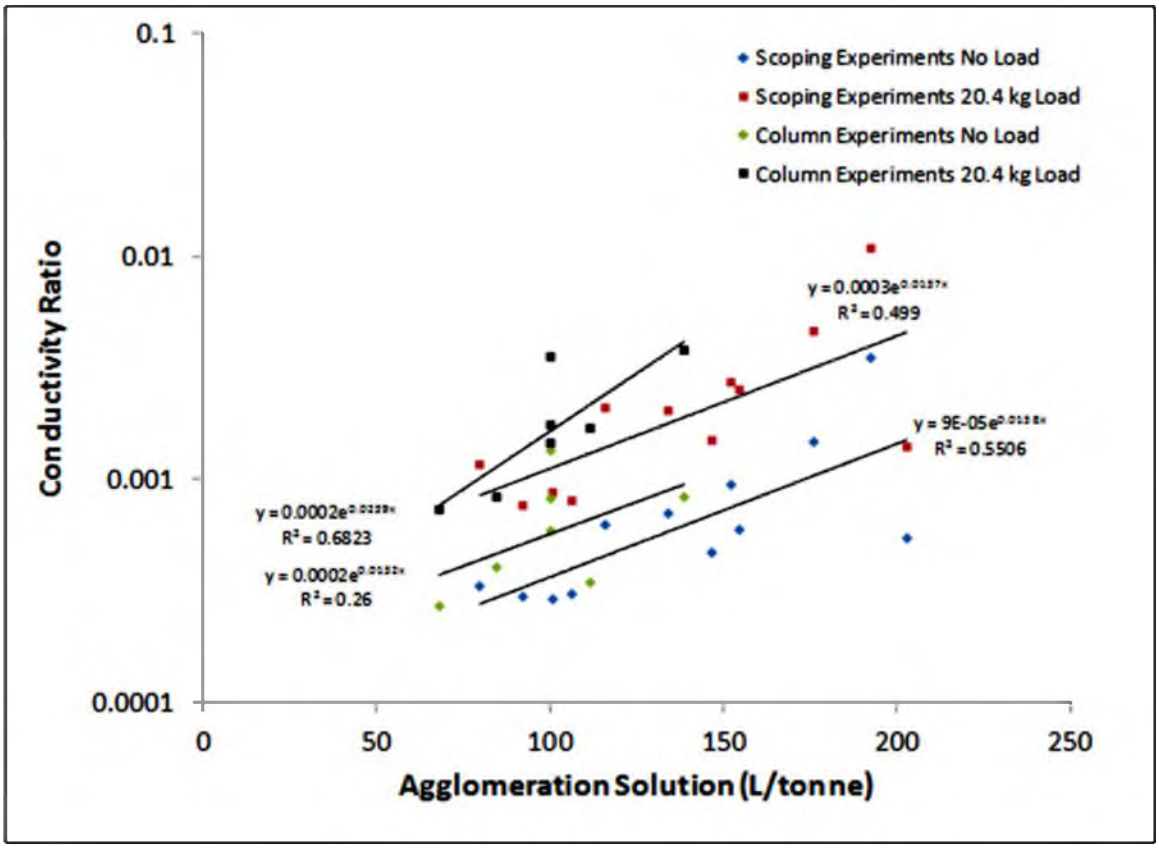

Figure 43. The relationship between agglomeration solution amount and conductivity ratio of agglomerates during scoping and column leaching experiments.

variability, indicating experimental and measurement error. The saturated hydraulic conductivity of agglomerates at 313 g/L acid concentration is higher than that at 972 g/L acid concentration at 19% moisture content. The saturated hydraulic conductivity of 13 % moisture content is lower than that of 19 % moisture content at the same acid concentration. These results show the same trend as the scoping experiment results, as shown in Figure 45. However, the hydraulic conductivity of agglomerates for the column leaching experiment is lower than those in scoping experiments. This may due to the different mineralogy of the nickel laterite used in both experiments.

Table 20. The permeability values of agglomerates at different agglomeration conditions.

Moisture Content (%)	Acid Concentration (g/L)	Saturated Hydraulic Conductivity (cm/s)	Break Through Times (Hrs)	Drain Down Times (Hrs)	24 hours Drain Down Volume (mL)
19	972	$2.9x10^{-2}$	10	38	987
19	313	$1.3x10^{-1}$	5	40	697
16	642	$2.0x10^{-2}$	8	48	1120
16	642	$7.4x10^{-3}$	6	49	1161
16	642	$3.8x10^{-3}$	10	38	1123
13	972	$1.7x10^{-2}$	16	39	1153
13	313	$2.2x10^{-3}$	11	30	965

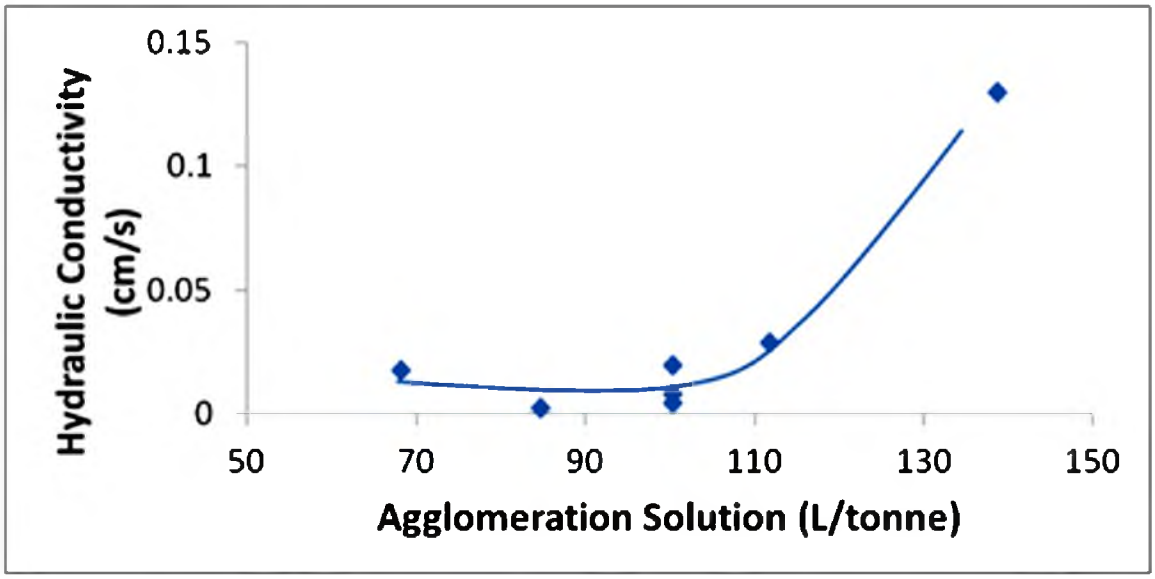

Figure 44. The relationship between agglomeration solution amount and permeability.

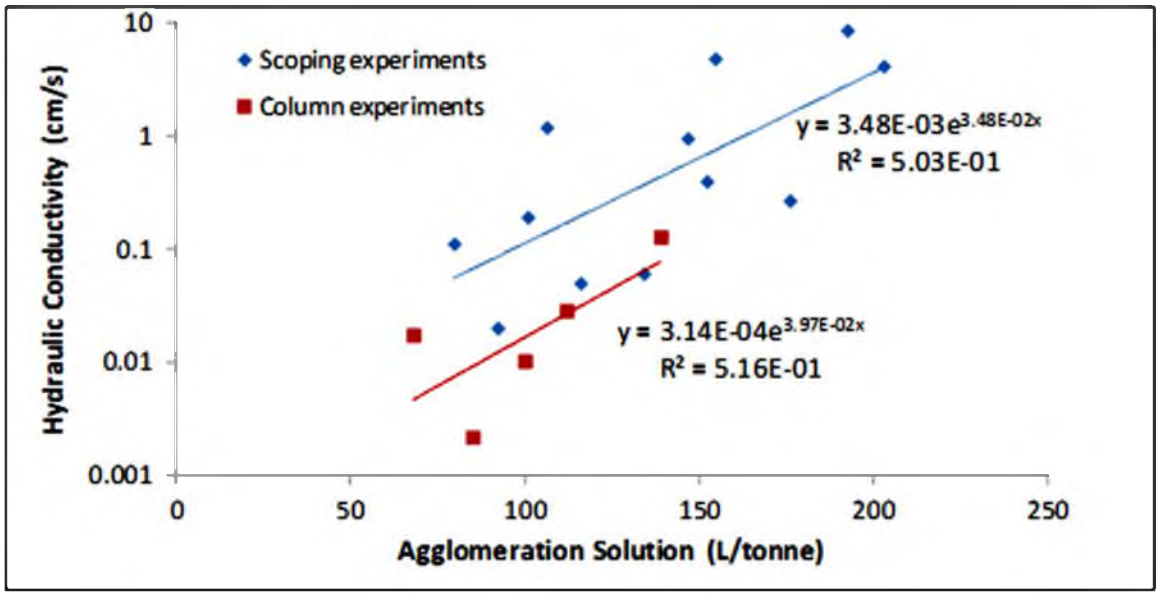

Figure 45. The hydraulic conductivity of agglomerates at different condition during scoping and column leaching experiments.

When more solution is applied during agglomeration, more capillary forces can be generated which enhance agglomeration. Therefore, the size of agglomerates is coarser and creates more void space within the ore body, leading to higher hydraulic conductivity values. However, the strength of the agglomerates also plays a role in the hydraulic conductivity values. Strong agglomerates do not break easily, resulting in high hydraulic conductivity values.

As illustrated in Figure 44, the saturated hydraulic conductivity of agglomerates starts increasing at about 100 L/tonne of solution addition. This value also correlates with the D_{10} and D_{50} of the agglomerates which also start increasing around 100 L/tonne. 100 L/tonne of solution appears adequate to agglomerate this particular nickel laterite ore. Since the agglomerate sizes increase, the hydraulic conductivity also increases.

After the raffinate was applied on top of each column, the solution flowed through the agglomerates and then came out at the bottom of the column. The time from

application of liquid at the top to release of liquid at the bottom is called the breakthrough time. The breakthrough time can be used as an indicator of the permeability of the experimental columns. Figure 46 shows the relationship between the breakthrough times and the agglomeration solution addition rate. As expected, the breakthrough times decrease as the agglomeration solution increases. The higher agglomeration solution volume fills the agglomerate pores and produces coarser agglomerates which provide better solution pathways within the agglomerate body. Therefore, the breakthrough time of high solution addition agglomerates is lower than that of low solution addition agglomerates.

After the leaching experiments were completed, solution drain down times and volumes were recorded. The example of the drain down curve of leaching experiments is given in Figure 47. As seen in Table 20 and Figures 48, the solution drain down times seem to be independent of the agglomeration solution. The solution drain down volumes within the first 24 hours of each column exhibited minimal variation except for 313 g/L acid concentration and 19% moisture content. The lack of variation in the drain down times and volumes indicate the degradation of the agglomerates described previously. The coarser particles broke into smaller particles and these transformations changed the hydraulic conductivity within the column. This effected the drain down times and volumes in the experiments. However, due to the mineralogy of the nickel laterite, the complex mechanism of the agglomerate break down and the migration of fines within the column, a consistent trend of the drain down times is not observed. The solution drain down volume of 313 g/L acid concentration and 19% moisture content are lower than the

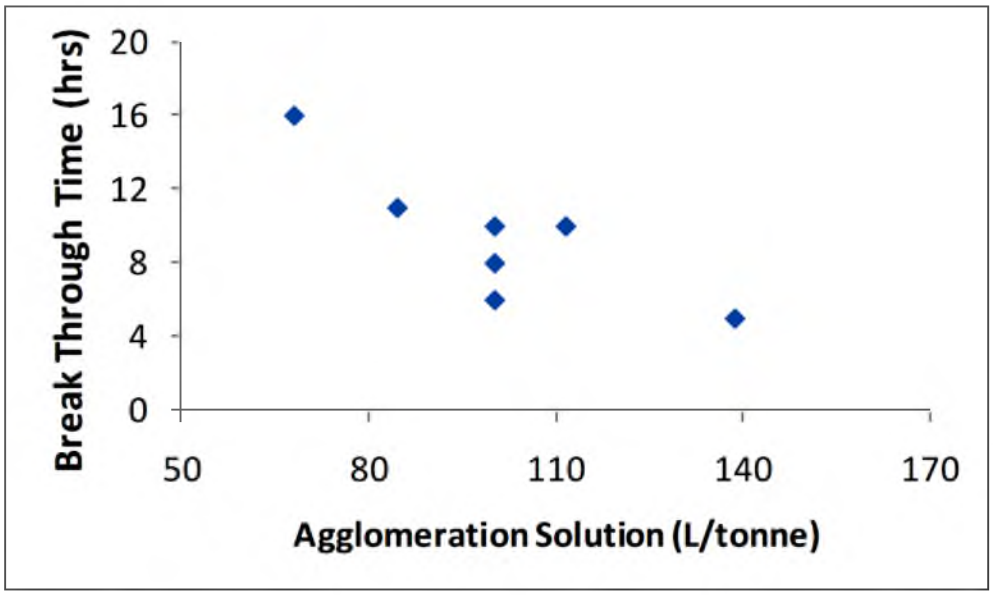

Figure 46. The relationship between agglomeration solution amount and breakthrough times.

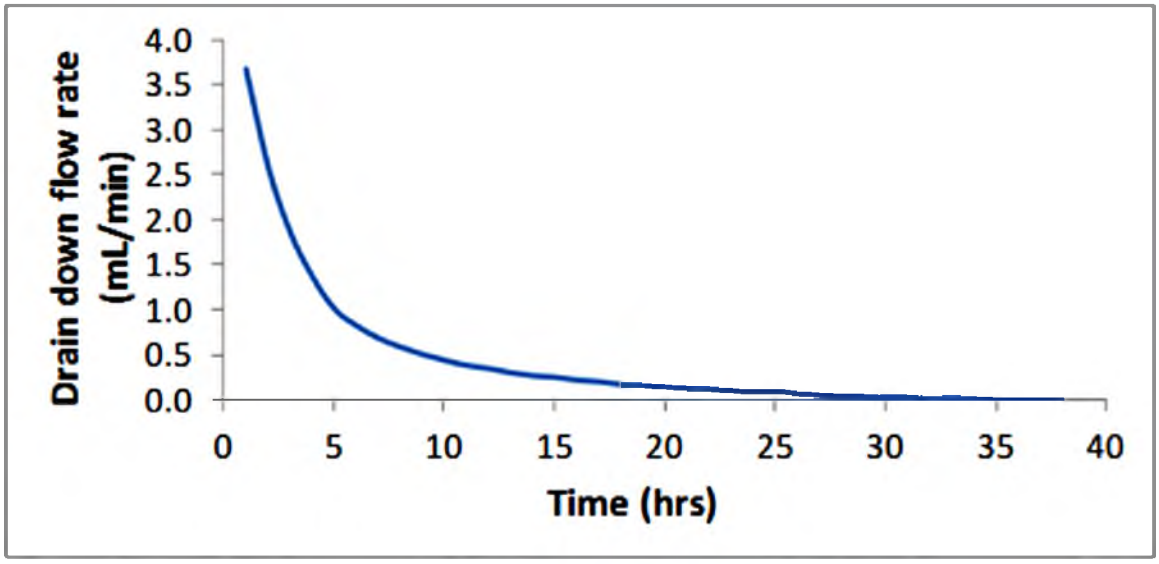

Figure 47. The drain down curve of leaching experiment at 972 g/L acid concentration and 19% moisture content agglomeration condition.

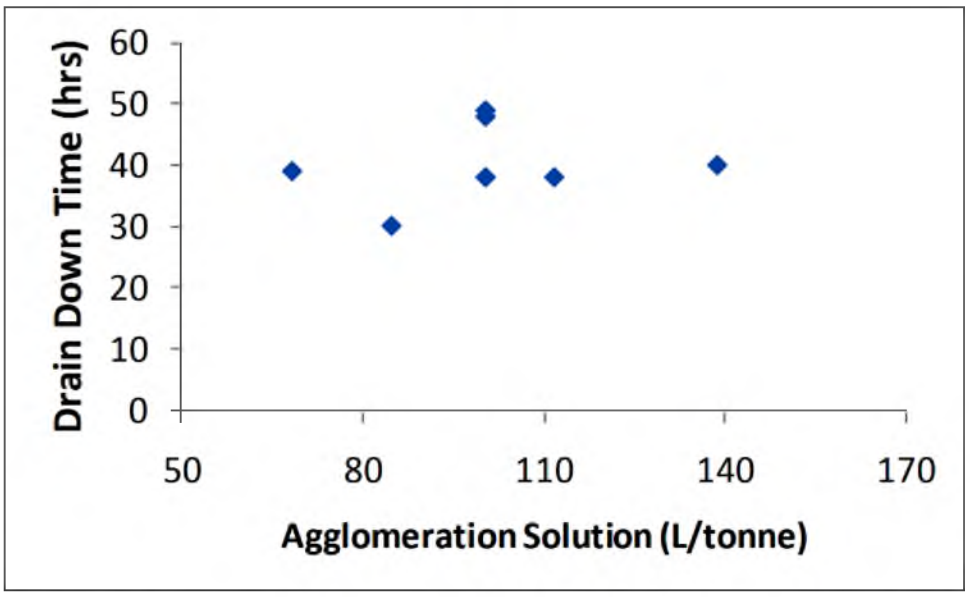

Figure 48. The relationship between agglomeration solution amount and solution drain down times.

other agglomeration condition agglomerates, possibly due to the fact that the solution was still trapped in the column. Longer times may need to drain all the solution out.

Column Leaching Results

Seven columns of 20.3 cm were filled with approximately 50 kg of agglomerates, as discussing previously. Another column was filled with unagglomerated ores (feed). The leaching solution could not flow through the feed column easily, causing flooding with solution leaking from the top of the column at the flow rate employed.

The solution could flow through all of the columns filled with agglomerates. The agglomeration process increased the ore particle size and decreased the amount of fines in the ore body. Therefore, the permeability of the ore body rises and reduces solution blockage.

Bulk Density and Slumping

Agglomerate bulk density can be used as a compaction indicator within the column. The higher the bulk density is, the more compact the agglomerate bed is. The bulk densities produced at different agglomeration conditions are summarized in Table 21. The bulk density values of agglomerates are significantly lower than that of feed sample, as expected. The bulk density of the agglomerates has small variation except at 19% moisture content and 313 g/L acid concentration condition. Since the agglomerates at 19% moisture content and 313 g/L acid concentration are coarser, they have less bulk density and more porosity.

Robertson et al. (2010) indicate that heaps can slump up to 20% within the first week of leaching. Therefore, slump or height decrease during the column leaching can also be used to examine agglomerates strength. The slump of each column after leaching 90 days is also provided in Table 21. The columns that contained agglomerates with the high acid concentration slump more than the columns filled with agglomerates with the low acid concentration. Higher acid used during agglomeration promoted the dissolution of minerals and created mud at the bottom of the columns, resulting in more slump of the column. Thus, it would appear that agglomerates produced with lower acid concentration slumped less.

Leachate Density, pH and ORP

The pregnant leaching solution (PLS) was collected throughout the leaching experiments, as discuss in the experimental section. The PLS samples were weighted, measured for pH, ORP and volume.

Table 21. The bulk density of the agglomerates at different agglomeration conditions and the slump after column leaching experiment.

Moisture Content (%)	Acid Concentration (g/L)	Initial Bulk Density (g/mL)	Slump After Column Leaching (cm)
Feed	-	1.67	-
19	972	1.24	24.1
19	313	1.15	8.5
16	642	1.26 (+/- 0.04)	10.2 (+/-2.0)
13	972	1.25	19.0
13	313	1.27	6.5

The PLS densities from each column versus time are shown in Figure 49. The solution density is highest on the first day and decreases as leaching time increases and becomes essentially constant after the first week of leaching. This may be due to the mineral elements at the boundaries of the agglomerates that were leached easily on the first several days of leaching. As the leaching times increase, the leaching solution has to diffuse toward the center of the agglomerates in order to dissolve leachable mineral elements. Therefore, fewer mineral elements were leached out compared to the first several days of leaching. The PLS solution density tended to equal the feed leach solution (also known as raffinate) density of 1.04 g/L near the end of the leaching test. The PLS solution density of the three replicated samples are almost identical, as shown in Figure 50.

Another factor that may affect the PLS densities is the concentration of acid used during agglomeration. The densities of agglomeration solution are in the range of 1.19 to 1.53 g/mL and the highest PLS densities of each column vary from 1.19 to 1.43 g/mL. The PLS density is mixed with the agglomeration solution densities; however, the correlation between the two is not obvious. These two factors, mineral dissolving and

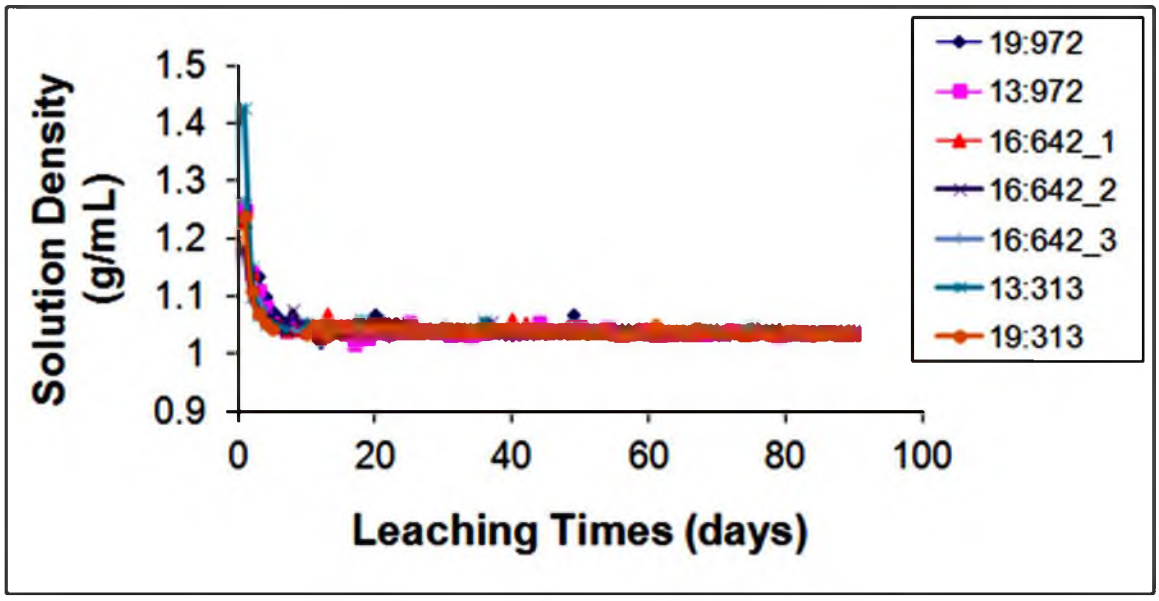

Figure 49. The relationship between the leaching times and solution density of different agglomeration conditions.

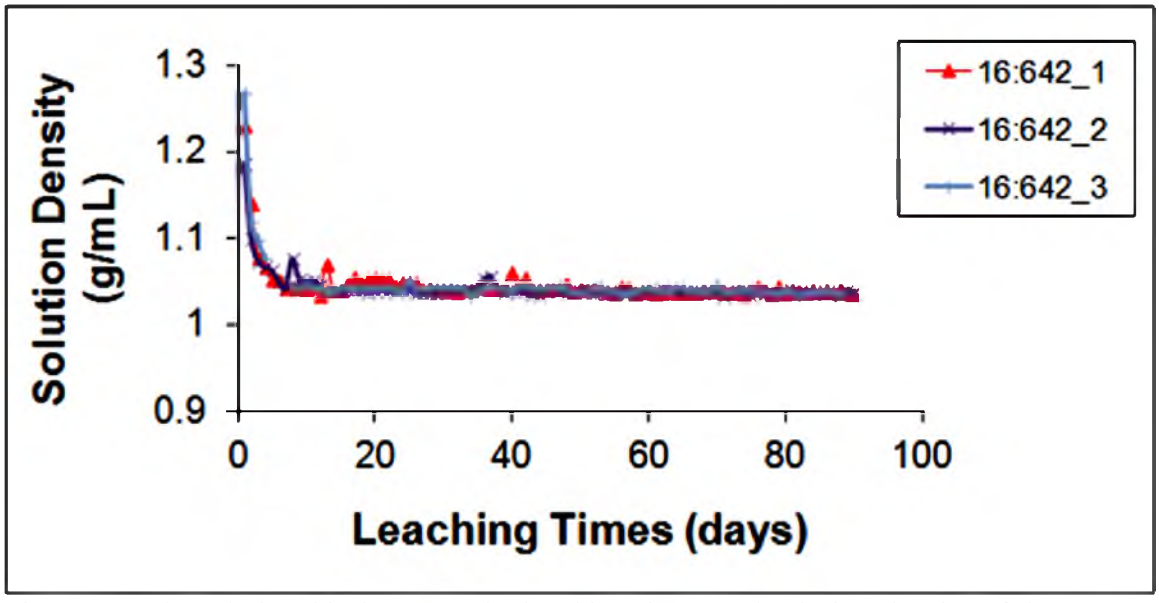

Figure 50. The relationship between the leaching times and solution density of three replicated agglomeration conditions.

agglomeration solution densities, contribute to the high PLS densities of each column within the first several days of leaching.

The pH and ORP of PLS samples were also measured. The pH of the PLS increased as the leaching time increased and then slowly decreased toward the pH of the leach solution after one week of leaching, as shown in Figures 51 and 52. The extremely low pH at the beginning of leaching was due to the high concentration of sulfuric acid that was used during the agglomeration process.

As the leaching time increased, the pH increased and reached a value which is close to the pH of the raffinate used in the experiment. The pH of the raffinate used in the column leaching experiment was 0.36. The pH of three replicated samples exhibited little variation.

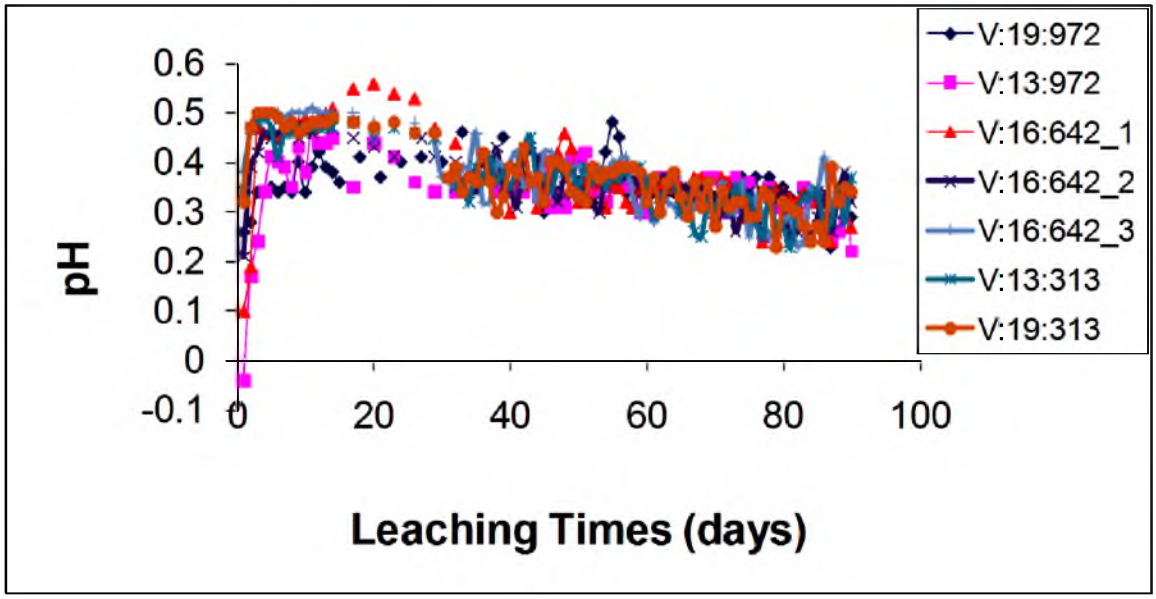

Figure 51. The relationship between the leaching times and pH of different agglomeration conditions.

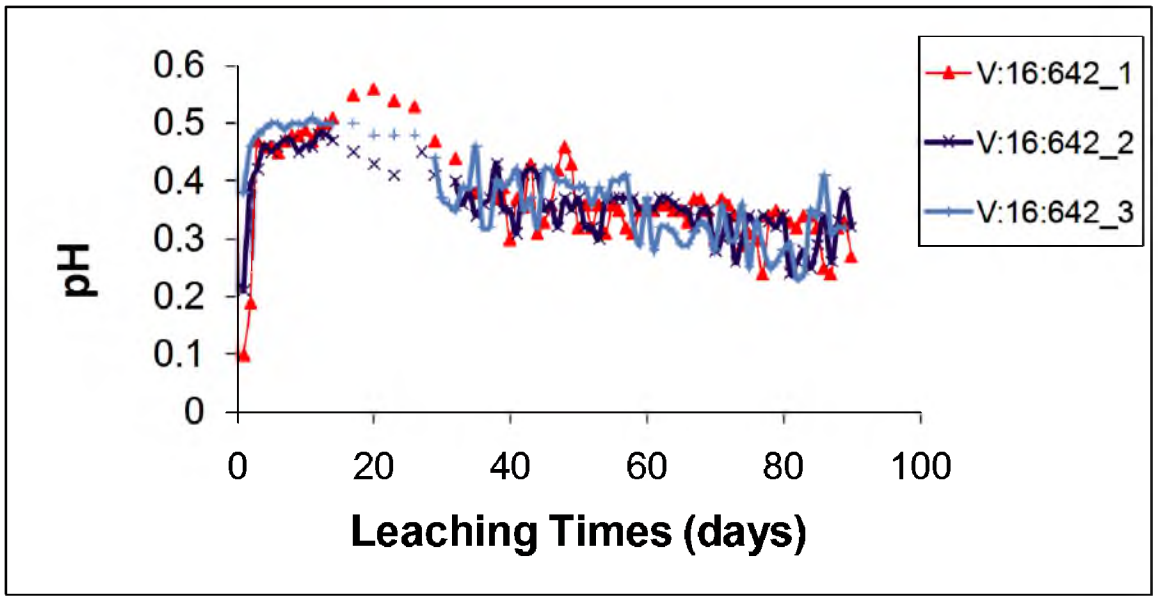

Figure 52. The relationship between the leaching times and pH of three replicated agglomeration conditions.

The ORP values decrease slightly within the first week of leaching and then reach a stable plateau. The ORP of the solution is affected by several reactions; however, the ferric to ferrous redox reaction seems to predominate since the ORP value is close to the standard reduction potential of 0.770 V, as shown in Figures 53 and 54. The values are high at the beginning of the test due to the fact that a high amount of ferric iron is dissolved into the raffinate solution. As the leaching time increases, the amount of iron in the solution decreases and the ORP of the solution also decreases. The studied nickel laterite ore contained high iron content (≈ 15%) (Castro & Pereira 2009). The main iron containing minerals are silico-ferruginous plasma, and iron oxi-hydroxides.

Metal Extractions

The extraction of nickel, cobalt, iron, aluminum, manganese and magnesium obtained by leaching was determined by ICP-OES. An example of leaching results from

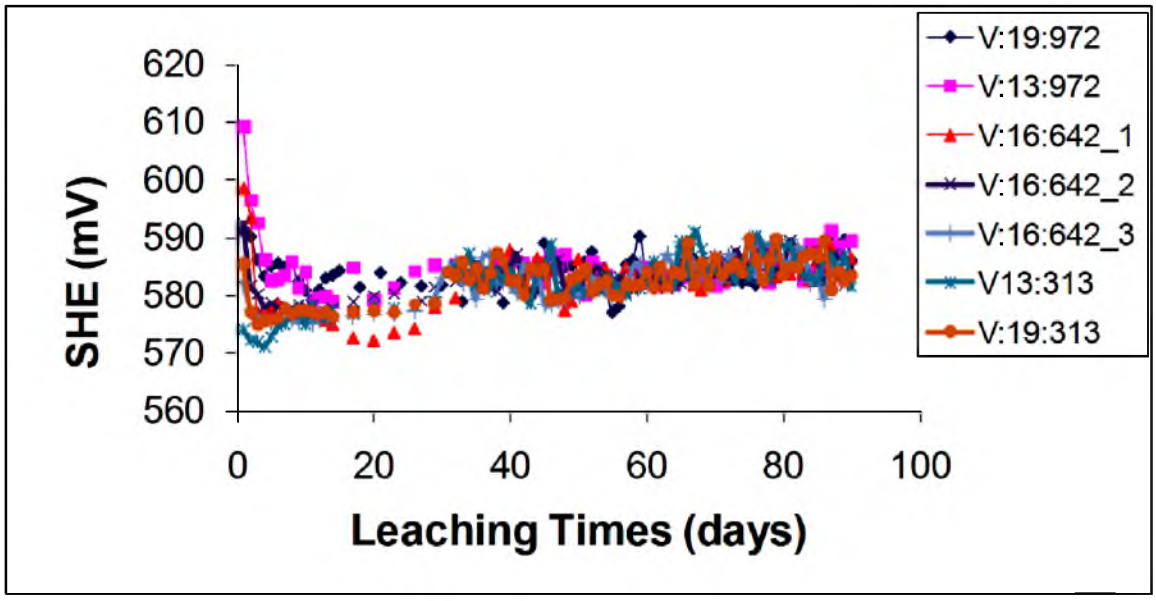

Figure 53. The relationship between the leaching times and ORP of different agglomeration conditions.

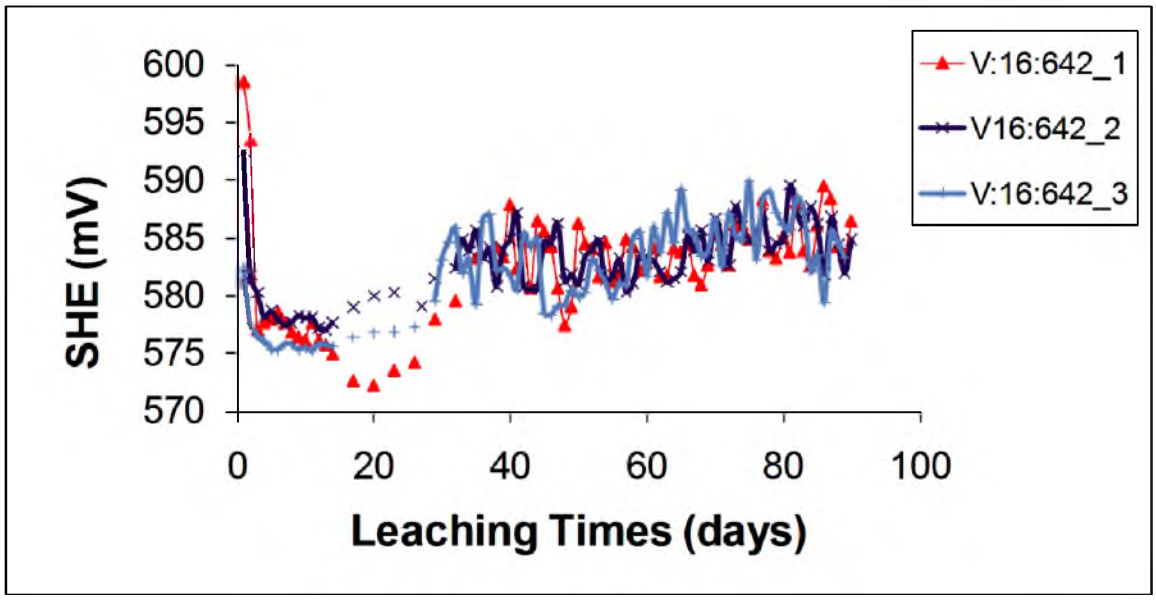

Figure 54. The relationship between the leaching times and ORP of three replicated agglomeration conditions.

one of the columns is shown in Figure 55. The remainder of the leaching results for each column is displayed in Appendix B. Table 22 summarizes the percent extractions after 90 days of leaching as a function of the different agglomeration conditions. As expected, high acid concentration during the agglomeration process produces higher extraction rates of metal.

A 58% extraction of nickel was achieved after 90 days of leaching when the high acid strength and lowest moisture content were employed during agglomeration. 30% nickel extraction can be reached within 7 days of leaching. After one week, the extraction of nickel was gradually increased. Higher extraction of metals can be expected if the leaching time is increased.

The extraction of cobalt in these experiments cannot be fully determined. After approximately 30 days of leaching, the concentration of cobalt in the PLS was extremely low and below the detection limit of ICP-OES. The extractions of metals from the replicate columns are shown in Figures 56 and 57. They show minor variation with the extraction of magnesium.

The magnesium extraction variation may be due to the uncertainty of the magnesium amount in the nickel laterite themselves. This indicates that the extraction results of most metals are fairly reproducible.

A linear regression was used to analyze the relationship between the metal extraction rates and the effects of moisture content and acid concentration used during agglomeration. Table 23 illustrates the linear regression analyzed results. The significant level was 0.05. The relationship between metal extraction rates and acid concentration used during agglomeration is quite linear. Moisture content is statistically insignificant at

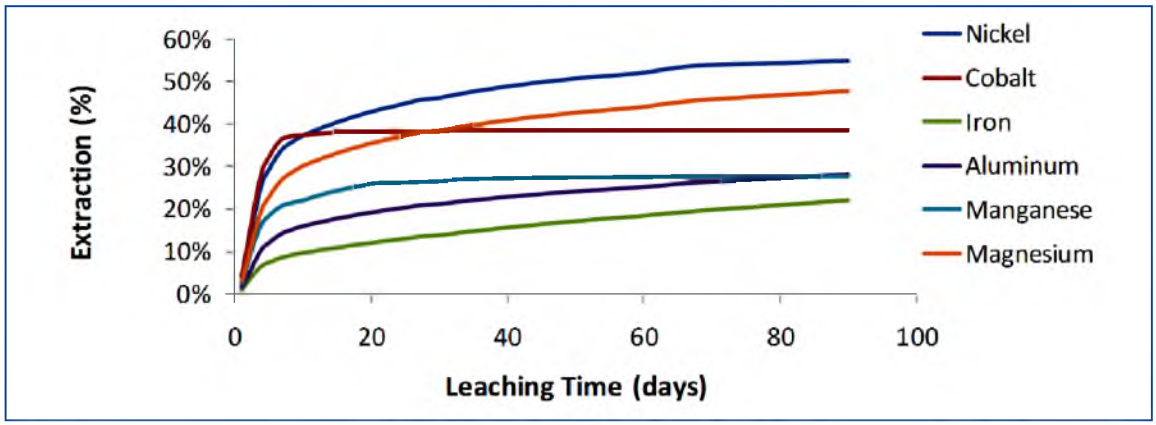

Figure 55. The extraction of analyzed elements of 972 g/L acid concentration and 19% moisture content.

Table 22. Interested element extraction rates after 90 days at different agglomeration conditions.

Moisture Content (%)	Acid Conc. (g/L)	Nickel Ext. (%)	Cobalt Ext. (%)	Iron Ext. (%)	Aluminum Ext. (%)	Magnesium Ext. (%)	Manganese Ext. (%)
19	972	54.8	38.7	22.0	28.1	47.9	27.9
19	313	48.2	20.9	17.0	26.1	42.4	18.4
16	642	51.0	33.1	18.9	26.3	31.7	22.0
16	642	49.2	28.5	18.7	26.5	43.2	19.7
16	642	51.4	26.8	18.7	27.3	42.5	20.3
13	972	58.7	36.8	21.6	28.0	36.6	26.4
13	313	48.9	22.0	17.4	25.8	42.5	17.5

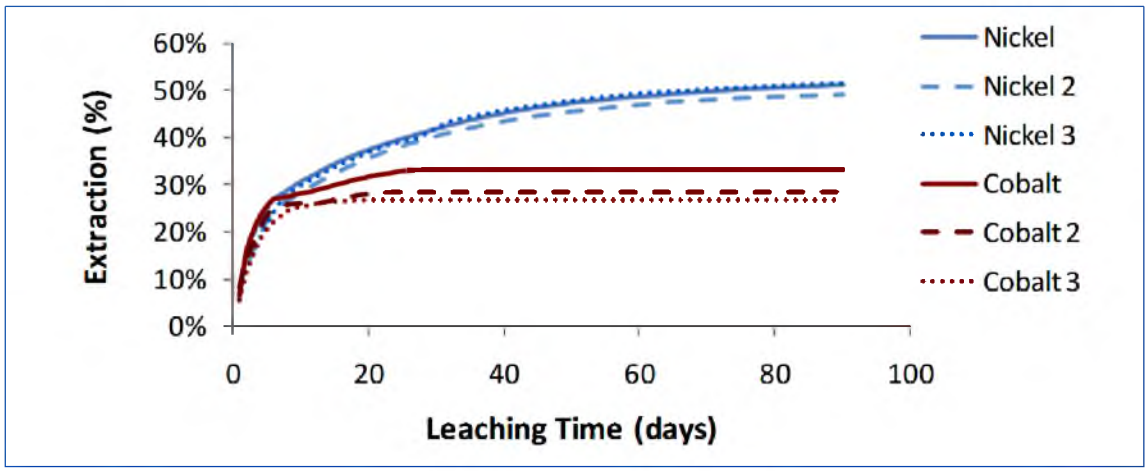

Figure 56. The extraction of nickel and cobalt of 642 g/L acid concentration and 16% moisture content.

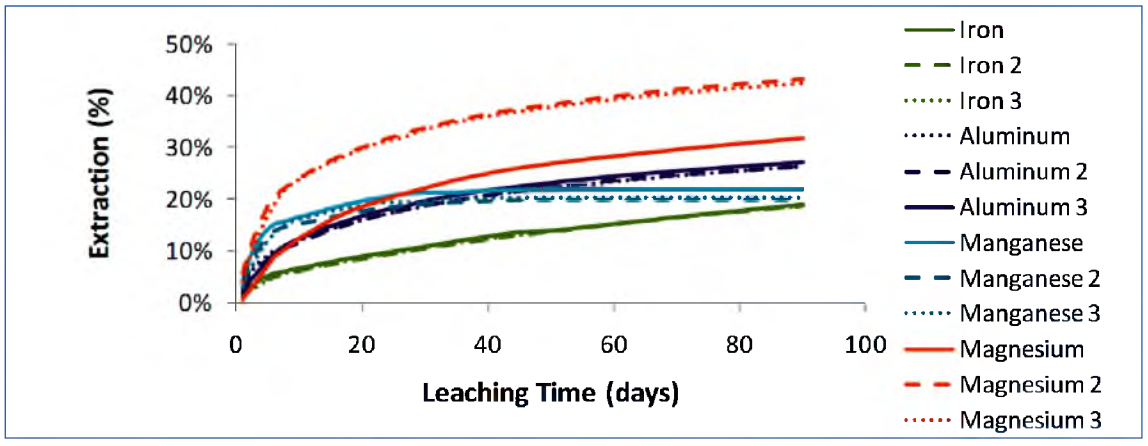

Figure 57. The extraction of iron, aluminum, manganese and magnesium of 642 g/L acid concentration and 16% moisture content.

Table 23. The linear regression analyzed results.

Metals	R^2	P Value		Coefficient		
		Moisture	Acid Conc.	Intercept	Moisture	Acid Conc.
Nickel	0.85	0.27	0.01	49.93	-0.38	0.01
Cobalt	0.92	0.89	0.002	12.64	0.06	0.02
Iron	0.95	0.92	0.0009	14.83	-0.009	0.007
Aluminum	0.86	0.59	0.008	24.10	0.04	0.003
Manganese	0.90	0.49	0.004	9.70	0.19	0.014
Magnesium	0.19	0.39	0.98	26.15	0.93	-0.0002

the significant level of 0.05. Acid concentration is statistically significant at significant level of 0.05 for all metal extractions except for magnesium.

Nickel

The different acid additions during the agglomeration process affect the extraction of the elements of interest. As seen in an example in Figure 58, the extraction of the nickel increases as the acid concentration during agglomeration increased.

The effects are profound during the first week of column leaching experiments. Figure 59 illustrates the extraction rate of nickel within 7 days. In the first week of leaching, the effect of sulfuric acid added during agglomeration is still strong. The more acid added to the agglomerates, the more minerals were exposed to the acid. Therefore, the extraction of nickel within the first week of leaching of each column was varied depending on the acid amount added during agglomeration. The strong acid addition during agglomeration may dissolve the elements of interest at the boundary of the coarser

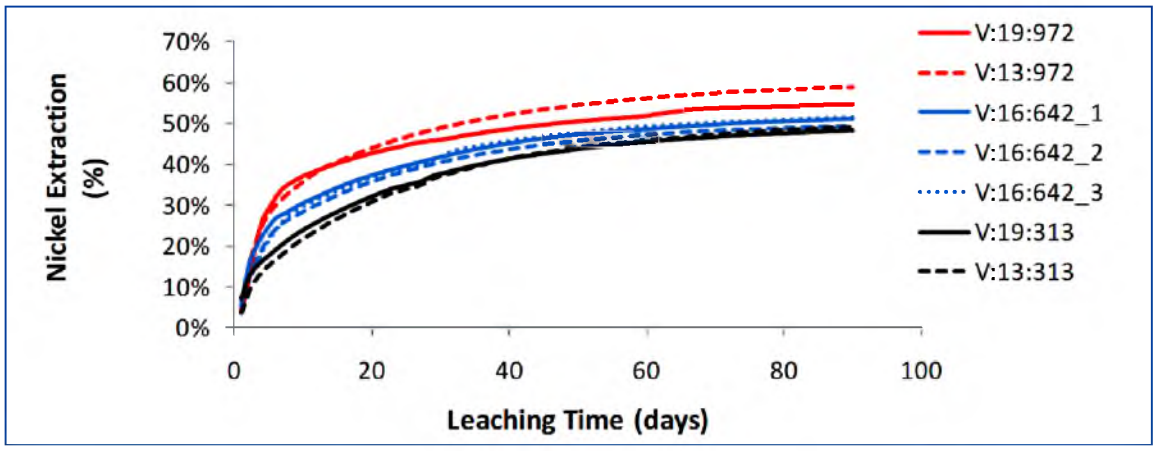

Figure 58. The extraction of nickel at different agglomeration conditions.

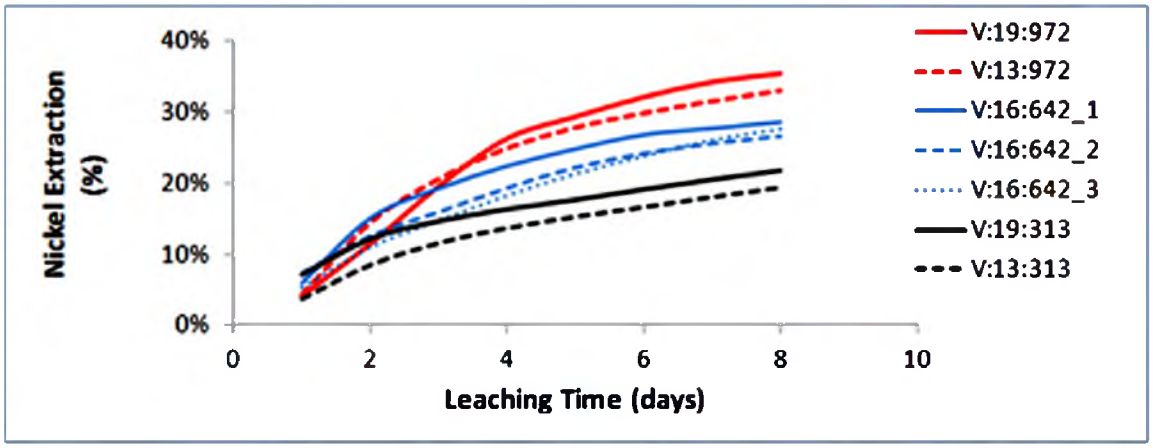

Figure 59. The extraction of nickel at different agglomeration condition within 7 days of leaching.

particles, dissolve fine particles and create new phases which are easily leached by the raffinate. Therefore, the extraction of the elements of interest is higher as the acid addition increases.

The extraction rate of nickel as a function of acid concentration and times is illustrated in Figure 60. The extraction rate of nickel increases constantly in the first 20 days of leaching; however, the extraction rate for 90 days of leaching does not increase as

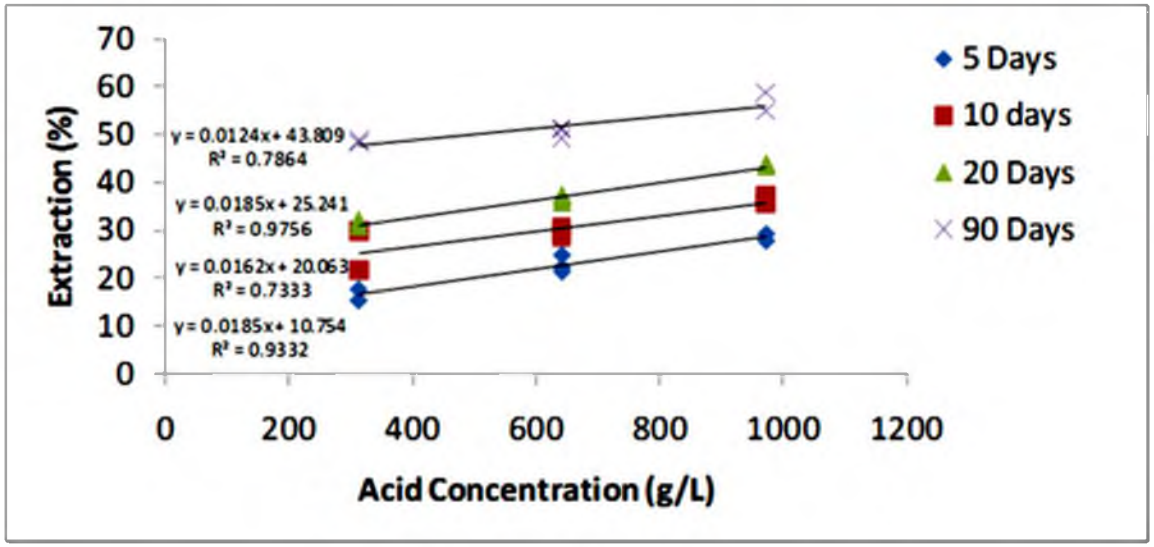

Figure 60. The relationship between acid concentration and nickel extraction rate at different leaching times.

fast as the first 20 days of leaching. The main nickel-bearing minerals are clay minerals and silico-ferruginous plasma. Clays are mostly fine and easy to dissolve by sulfuric acid. This contributes to the fast nickel extraction rate within the first 20 days.

As the leaching times increase, the nickel in the clay phases is depleted and the solution has to percolate through the internal voids of the coarser particles to leach the nickel out. Furthermore, the other nickel-containing mineral phases may possibly be harder to dissolve with the acid strength used in this study. Therefore, the extraction of nickel after 20 days of leaching was slower.

Cobalt

The extraction rate of cobalt as a function of time and acid strength is shown in Figure 61. The extraction rate of cobalt increases rapidly in the first 10 days and then, the rate is slightly lower as the leaching times reach 20 days. Beyond 20 days of leaching, the

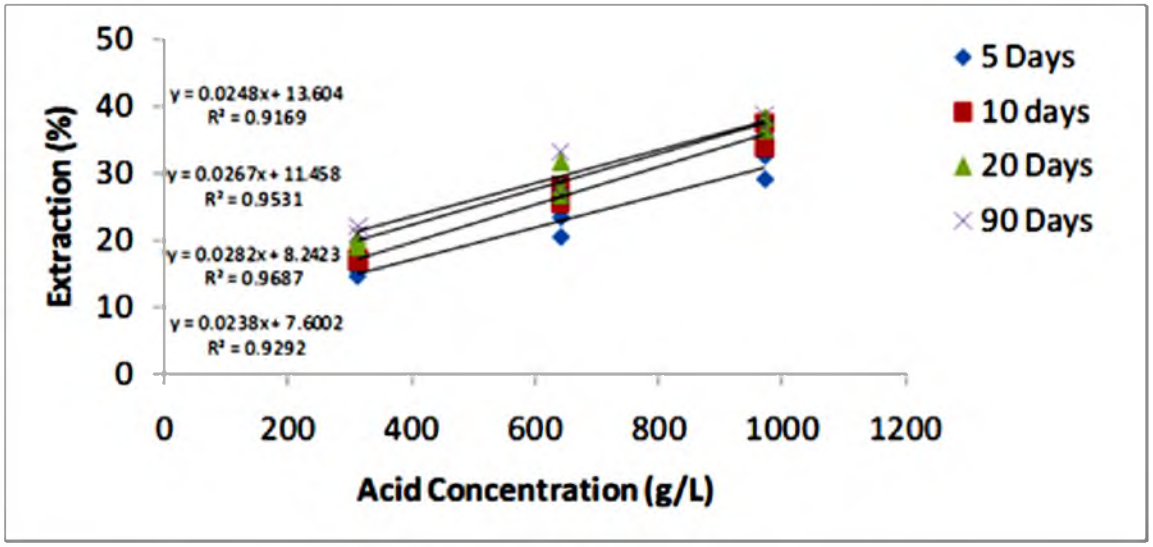

Figure 61. The relationship between acid concentration and cobalt extraction rate at different leaching times.

amount of cobalt is very small and below the detection limit of the ICP OES used in this study. The cobalt in the study ore is small and associated with clays. Since clays dissolve easily, the cobalt is also released easily and fast in the beginning of leaching. However, as the leaching times increase, the cobalt is diminished and the extraction rate slows down.

Iron and aluminum

The extraction rate of iron and aluminum as functions of leaching times and acid concentration are illustrated in Figures 62 and 63, respectively. The extraction of iron and aluminum double from 5 to 10 days and from 10 to 20 days of leaching. The extraction rates of iron and aluminum at 90 days of leaching are triple and double, respectively, the extractions at 20 days of leaching. The availability of iron in this nickel laterite ore is high; however, it associates with slightly harder to dissolve phases. Therefore, the total extraction is quite low. The extraction rate is continuously increased due to the huge

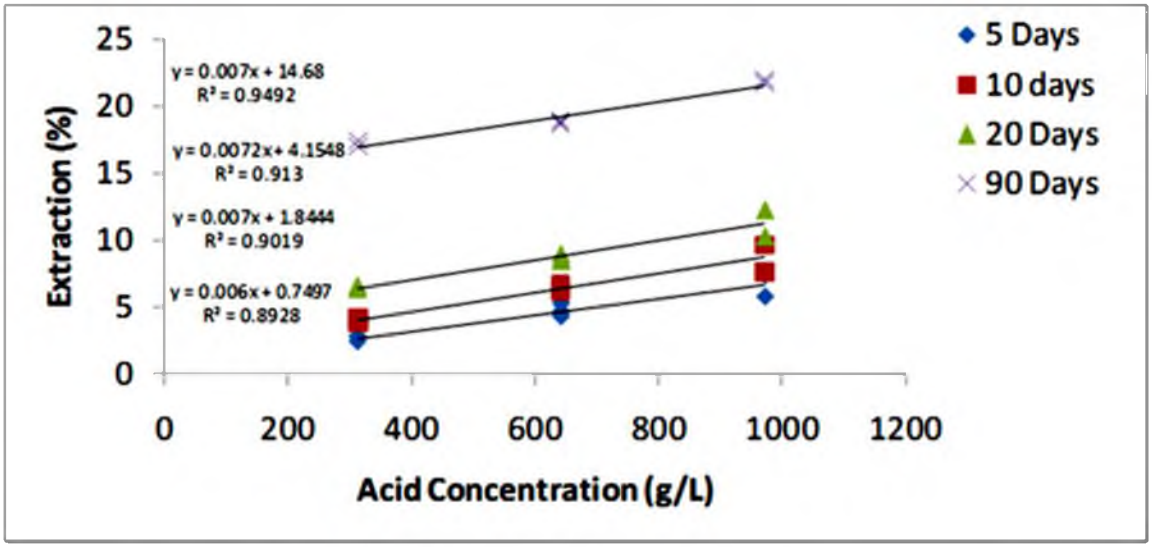

Figure 62. The relationship between acid concentration and iron extraction rate at different leaching times.

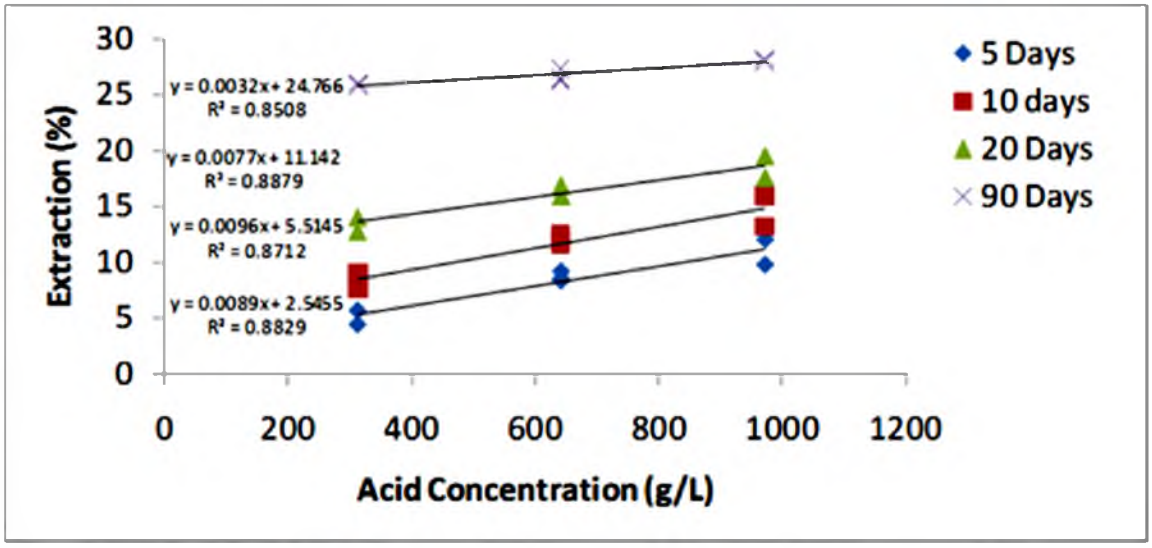

Figure 63. The relationship between acid concentration and aluminum extraction rate at different leaching times.

viability of the iron in the ore. The extraction rate of aluminum increases rapidly in the first 20 days of leaching due to its association with clay minerals. However, as the leaching times increase, to 90 days of leaching, the availability of aluminum is diminished so the extraction rate is dropped.

Manganese and magnesium

The extraction of manganese and magnesium as functions of leaching times and acid strength are displayed in Figures 64 and 65, respectively. The extraction of manganese increases steadily in the first 20 days of leaching. From 20 days to 90 days of leaching, the extraction rate of manganese drops significantly. Since manganese content and the distribution in coarser particles are low in the nickel laterite used in this study, the extraction rate of manganese decreases drastically after 20 days of leaching. The manganese content is below the detection limit of the ICP-OES used in this analysis toward the end of 90 days of leaching.

The extraction of magnesium also increases constantly during the first 20 days of leaching regardless of the variation in the replicate columns. The extraction rate increases slowly as the leaching time extends beyond 20 days. The magnesium deposits in the fines are leaching out first; therefore, the extraction rate during the first 20 days increases constantly.

Effect of agglomeration moisture

The moisture content of agglomerates has an insignificant effect on the extraction of elements of interest. The extraction of analyzed elements at the lowest and highest moisture contents but the same acid concentration is practically identical.

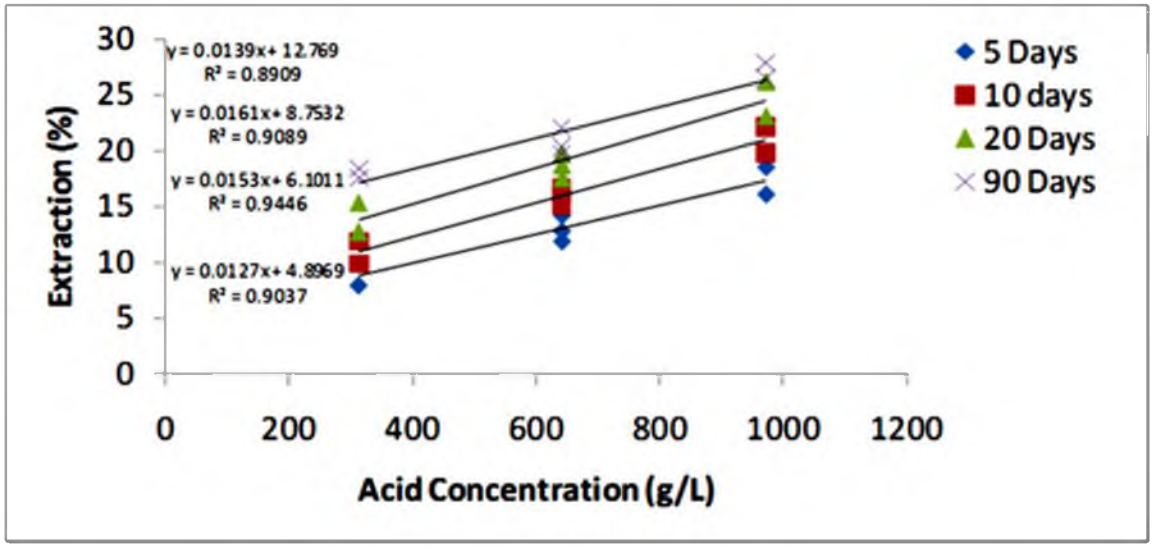

Figure 64. The relationship between acid concentration and manganese extraction rate at different leaching times.

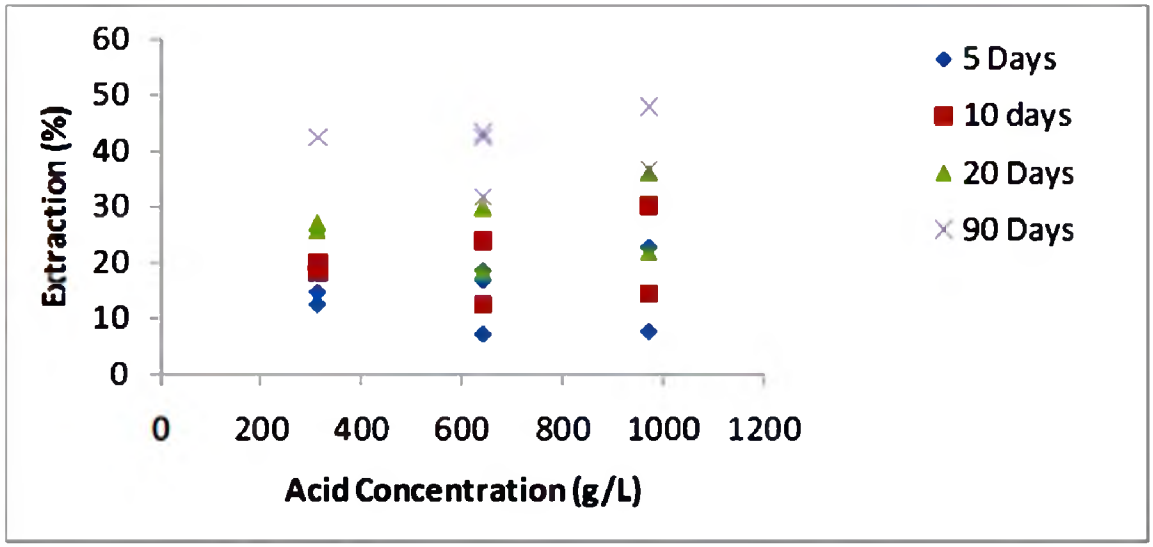

Figure 65. The relationship between acid concentration and magnesium extraction rate at different leaching times.

The water addition amount during agglomeration seems to decrease the extraction of the elements of interest except magnesium. Figures 66-67 show the relationship between water addition amount and recoveries of nickel and magnesium. Adding more water during agglomeration leads to coarser agglomerates. The solution requires more time to diffuse into the core of these agglomerates and dissolve the elements of interest.

The voids between the coarser agglomerates are wider than that of finer agglomerates. The solution flows more rapidly through porous material than it diffuses into the particles. These may lead to a lower extraction rate for coarser agglomerates and high water addition than finer agglomerates and lesser water addition. However, the water addition and agglomerate size seem to have small effects on magnesium extraction.

Leaching selectivity

The leaching selectivity of nickel to other elements is important for postleaching processing. The selectivity of nickel to iron, nickel to aluminum and nickel to magnesium can be observed from the Ni:Fe, Ni:Al and Ni:Mg ratios. These ratios can be calculated by comparing the amount of other metals in weight % to the amount of nickel in weight %. The ratios are calculated from both feed material and the metal extractions at 90 days of leaching.

The Ni:Fe, Ni:Al and Ni:Mg ratios of the column experiment liquor are given in Table 24. The Ni:Fe ratio in the leach liquor is between 5:1 and 6:1, for nickel extraction of about 40 to 56%, compared to 15:1 in the nickel laterite ores from the industrial sponsor. The nickel in this laterite ore is easier to dissolve by the leach solution used in this study than iron. The Ni:Al and Ni:Mg ratios in the nickel laterite ore are 2.4:1 and

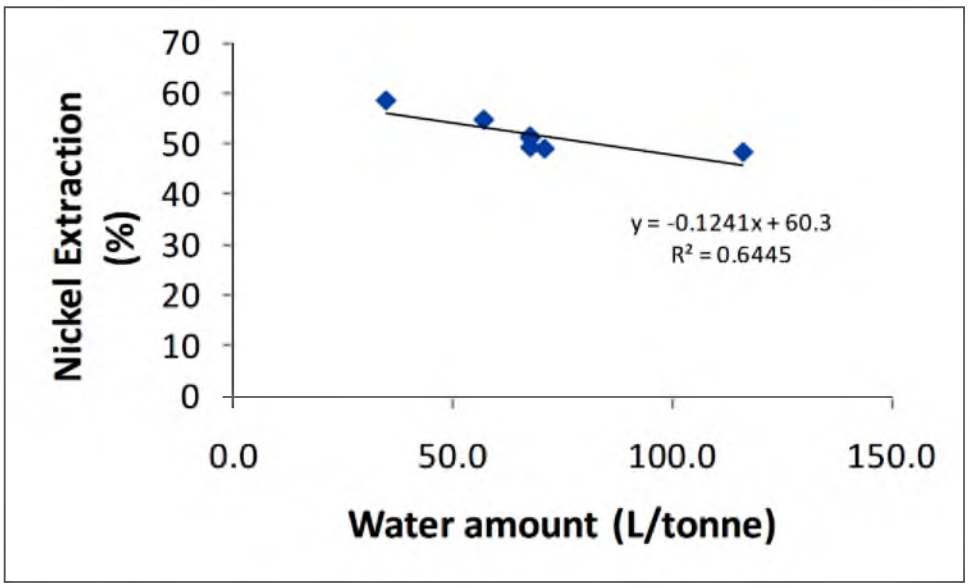

Figure 66. The relationship between water amount addition during agglomeration and nickel extraction.

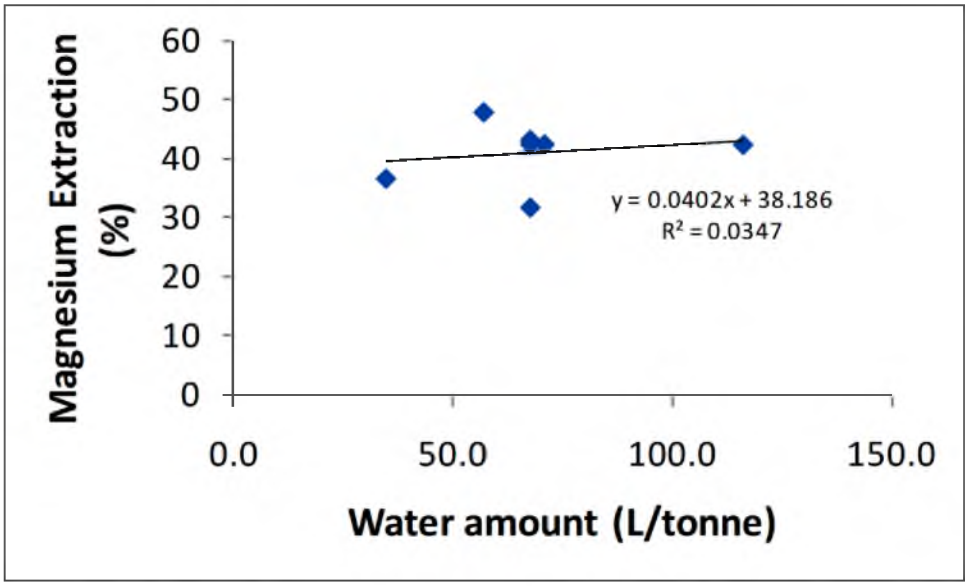

Figure 67. The relationship between water amount addition during agglomeration and magnesium extraction.

Table 24. The Ni:Fe, Ni:Al and Ni:Mg ratios of the column experiment PLS at different agglomeration conditions.

Moisture Content (%)	Acid Concentration (g/L)	Ni:Fe Ratio	Ni:Al Ratio	Ni:Mg Ratio
19	972	1/6.1	1/1.2	1/2.2
19	313	1/5.6	1/1.1	1/1.5
16	642	1/5.6	1/1.2	1/1.5
16	642	1/5.8	1/1.3	1/2.2
16	642	1/5.5	1/1.3	1/1.2
13	972	1/5.4	1/1.3	1/2.0
13	313	1/5.4	1/1.3	1/2.1

Note: Ore ratios; Ni:Fe = 1:15, Ni:Al = 1:2.4 and Ni:Mg = 1:2.5

2.5:1, respectively. From the leach solution results, the Ni:Al ratio is between 1.1 and 1.3 and the Ni:Mg ratio ranges from 1.5 to 2.2.

The Ni:Al ratio decreases about 50%; however, the Ni:Mg ratio is slightly decreased. The magnesium and nickel was leached out of the ore body at almost the same amount in 90 days of leaching. The aluminum to nickel ratios for each column varies. It varies from almost equal leaching selectivity to nickel to about half of leaching selectivity of nickel.

The main iron-bearing minerals are silico-ferruginous plasma and iron oxy-hydroxide. These two phases may not dissolve well in the acid solution used in this study; therefore, the iron content in the leach liquor is low. The magnesium and aluminum are associated with the clay minerals and can also be found in silico-ferruginous plasma. Since nickel is also found mostly in clay minerals and silico-ferruginous plasma, in order to leach nickel out, the aluminum and magnesium are also leached out. Hence, the Ni:Mg ratio of the PLS is not significantly different from the feed materials. Aluminum is often also fixed in the silico-ferruginous plasma phase more than in the clays minerals;

therefore, the Ni:Al ratio of leaching liquor decreases but not as much as iron. The detailed mineralogy analysis by QEMSCAN is presented in Chapter 6.

Leaching kinetics

Several kinetic models have been used to investigate the leaching reaction, including the shrinking core model, homogeneous model, uniform pore model, random pore model and grain model (Georgiou & Papangelakis 1998).

In heap leaching, a shrinking core model has been used to study reaction kinetics of particles (Miller 2006; Robertson et al. 2010). In a large-scale heap, the kinetics of reaction between acid and spherical particles is controlled by diffusion of acid and product species. Assuming that the dissolution reaction at the interface is rapid, all the acid is consumed at the interface of the unleached core and no diffusion of acid beyond the interface (Robertson et al. 2010). Miller (2006) analyzes the data collected from more than 50 commercial and laboratory copper heap leach tests. Most of the minerals are oxide and secondary sulfide ores. He found that the leaching rate of oxide and secondary sulfide copper ores is diffusion controlled throughout the entire process. The schematic image of the shrinking core model for the oxide ores is given in Figure 68.

The diffusion rate of reagent through the porous layer can be described by Fick's law, given in equation (13).

$$\frac{dn_{acid}}{dt} = -AD_{eff}\left(\frac{dC_{acid}}{dr}\right) = -4\pi r_c D_{eff}\left(\frac{dC_{acid}}{dr}\right) \qquad (13)$$

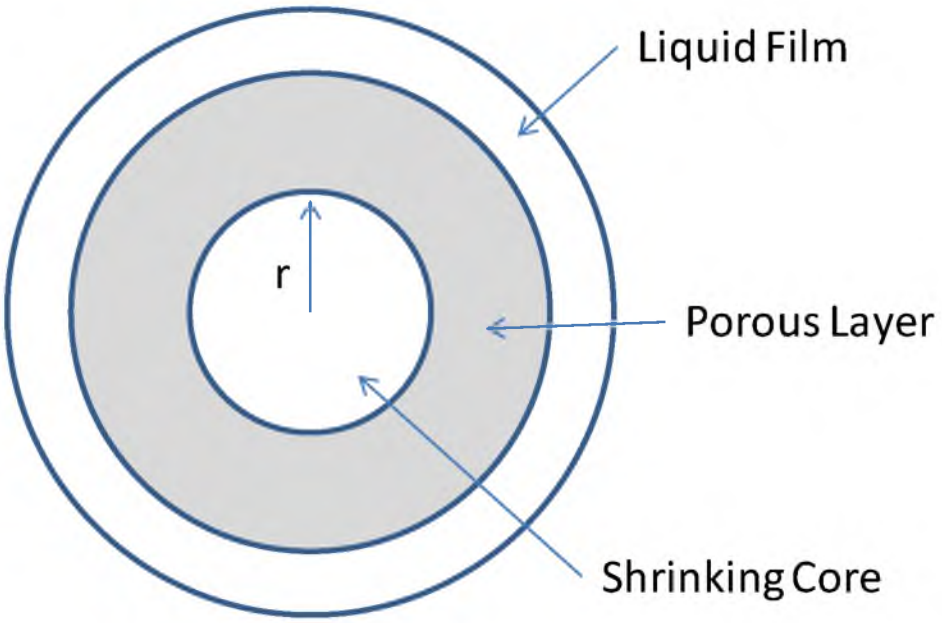

Figure 68. The shrinking core model of oxide ore particle. Adapted from Robertson et al. 2010.

Equation (13) can then be integrated between the limits of r_o/C_o and r_c/C_c and the result is given in equation (14).

$$\frac{dn_{acid}}{dt} = 4\pi D_{eff}\left(\frac{r_o r_c}{r_o - r_c}\right)(C_c - C_o) = B\frac{dn_{Ni}}{dt} \tag{14}$$

where D_{eff} = Effective diffusion coefficient = $D_{\text{int}}\varepsilon/T$

D_{int} = Intrinsic diffusion coefficient

ε = Particle voidage

T = Void tortuosity

A = Area of shrinking core

r = Radius of particles

C = Acid concentration in solution phase

B = Stoichiometric factor, mole of acid consumed per mole of oxide mineral extracted

The fractional conversion of the oxide species, α, for a sphere is given in equation (15).

$$\alpha = 1 - \left(\frac{r_c}{r_o}\right)^3 \text{ therefore } \frac{d\alpha}{dt} = -\left(\frac{3r_c^3}{r_o^3}\right)\frac{dr}{dt} \tag{15}$$

The reaction occurs only at the surface of the shrinking core so the number of moles of species remaining in the shrinking core can be described as in equation (16).

$$n_{Ni} = \frac{4}{3}\pi r_c^3 \frac{\rho}{M} \text{ therefore} \frac{dn_{Ni}}{dt} = 4\pi \frac{\rho}{M} r_c^2 \frac{dr}{dt} \tag{16}$$

where ρ = Density of the reaction portion of the particles

M = Molecular weight of the reaction portion of the particles

The shrinking core model for diffusion control given in equation (17) can be obtained by combining and integrating equations (14), (15) and (16) with time.

$$1-\frac{2}{3}\alpha-(1-\alpha)^{\frac{2}{3}}=\left(\frac{2MD_{eff}C_o}{\rho Br_o^2}\right)t \qquad (17)$$

The shrinking core model involved rate control given in equation (18) can be derived via a similar method.

$$1-(1-\alpha)^{\frac{1}{3}}=\left(\frac{kC_o}{\rho r_o}\right)t \qquad (18)$$

where k = Reaction rate

In this study, the leaching kinetics of Ni, Fe, Al and Mg were investigated. Leaching times were plotted against both $1-\frac{2}{3}\alpha-(1-\alpha)^{\frac{2}{3}}$ and $1-(1-\alpha)^{\frac{1}{3}}$. Examples of both plots are illustrated in Figure 69. If the process is reaction controlled, the plot of $1-(1-\alpha)^{\frac{1}{3}}$ versus time should be linear. If the process is diffusion controlled, the plot of $1-\frac{2}{3}\alpha-(1-\alpha)^{\frac{2}{3}}$ versus time should be linear.

As shown in Figure 69, neither shrinking core model fits the leaching kinetic of nickel for the entire 90 days of leaching. The metal leach kinetics of nickel laterite agglomerates are complicated and hard to predict. Agglomerate size distribution changes due to acid dissolving during leaching, affecting the leaching kinetic of metals. The variation of acid leach solution concentration along the depth of column is the other factor influencing the leaching kinetics of interested metals. Other factors such as porosity of agglomerates and agglomerate bed, and liberation of metals have to be studied to understand the leach kinetics of metals in nickel laterite column leaching.

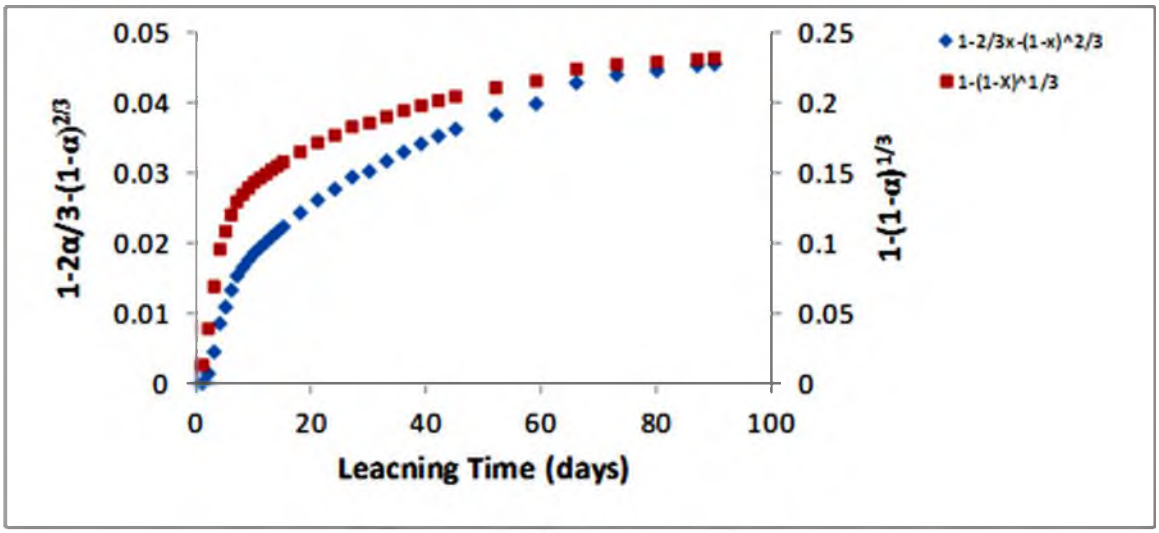

Figure 69. The plots of $1-\frac{2}{3}\alpha-(1-\alpha)^{\frac{2}{3}}$ and $1-(1-\alpha)^{\frac{1}{3}}$ versus leaching time for nickel extraction at 972 g/L acid concentration and 19% moisture content.

CHAPTER 6

PHASE CHARACTERIZATION AND PHASE TRANSFORMATION DURING AGGLOMERATION AND LEACHING

Phase Characterization

Nickel laterite ores consist of several minerals, including quartz, chromite, various clay minerals and amorphous phases. The main nickel-bearing minerals in this nickel laterite ore are chlorite, vermiculite, smectite, manganese oxides and silico-ferruginous plasma (Castro & Pereira 2009). Chlorite, vermiculite and smectite are clay minerals. Silico-ferruginous plasma is an amorphous, quartz-like phase composed of variable amounts of oxygen, silicon and iron and may contain an appreciable amount of nickel. The minerals in the ores can be modified by using high-concentration sulfuric acid during the agglomeration process. The leaching process also affects the minerals. X-ray diffraction, electron microprobe and QEMSCAN are used to analyze the mineralogical and mineral chemistry changes from feed to agglomerate and from agglomerate to leach residuals. The minerals and the methods which were used to analyze those minerals are given in Table 25.

Table 25. The minerals and analytical methods used to characterize the minerals.

Mineral Phases	Analyzing Methods			Abbreviations used in XRD
	XRD	QEMSCAN	EMPA	
Quartz	X	X	X	Q
Silico-ferruginous plasma		X	X	
Chlorite/Smectite/Vermiculite/Serpentine	X	X	X	Chl (chlorite) /Smec (smectite)
Iron oxy-hydroxides		X	X	Fe Ox.
Manganese oxides		X	X	
Kaolinite	X	X	X	Kao
Chromite	X	X	X	Cr
Talc	X	X	X	
Phlogopite		X	X	
"Nickel Phase"		X	X	
Other phases		X	X	
"Sulfate Phase"		X	X	
Epoxy		X		

Nickel-bearing and sulfate-hydroxide phases are of particular interest. To highlight the nickel-bearing phases, the species "Nickel phase" was created. This "Nickel phase" typically contains more than approximately 5 wt% nickel.

"Nickel phase" is not truly a phase; it is an artificial creation to illustrate where the nickel is located in the mineral matrix. In QEMSCAN images, it is illustrated by green color.

A sulfate-hydroxide phase formed when nickel laterite was agglomerated with sulfuric acid and then dried. To highlight the distribution of sulfur, the species "Sulfate phase" was created. It is believed that the "Sulfate phase" is a real phase or phases which contained evelated sulfur from the addition of sulfuric acid. It is illustrated by yellow color in QEMSCAN images.

The sulfate-hydroxide and nickel-bearing phases can contain additional elements; however, they need to have more than ~5% element weight percent of nickel or sulfur to be detected by QEMSCAN.

Nickel-Bearing Phases

A small amount of nickel is present in olivines and pyroxenes which are the main phases in the parent rock of nickel laterite ores. Olivine and pyroxene are easily altered during weathering. The nickel is released and migrates down the laterite profiles to be precipitated as the substituted element in various authigenic mineral phases.

Nickel ions (Ni^{++}) substitute for magnesium ions (Mg^{++}), iron ions (Fe^{+++} and Fe^{++}) and manganese ions (Mn^{++}) in various phases. Nickel occurs mainly in hydrated Mg-Ni silicate (e.g., ganierite), smectite clay, iron oxy-hydroxides, chlorite and manganese oxides (Brand et al. 1998). In this particular nickel laterite, the nickel can also be found in the silico-ferruginous plasma phase. Figures 70, 71 and 72 illustrate the nickel found in the laterite ore samples studied. As illustrated in Figures 70, 71 and 72, nickel pixels appear in the silico-ferruginous plasma, iron oxy-hydroxide, manganese oxides and chlorite particles.

Nickel occurs more commonly in clays than the silico-ferruginous plasma. The clay minerals normally contain magnesium which is more soluble than nickel; therefore, nickel can easily exchange in the magnesium sites during laterization. During weathering, magnesium or nickel are dissolved and migrate from olivine, leaving SiO_2 and some iron, the silico-ferruginous plasma phase. Some nickel remains trapped in this phase.

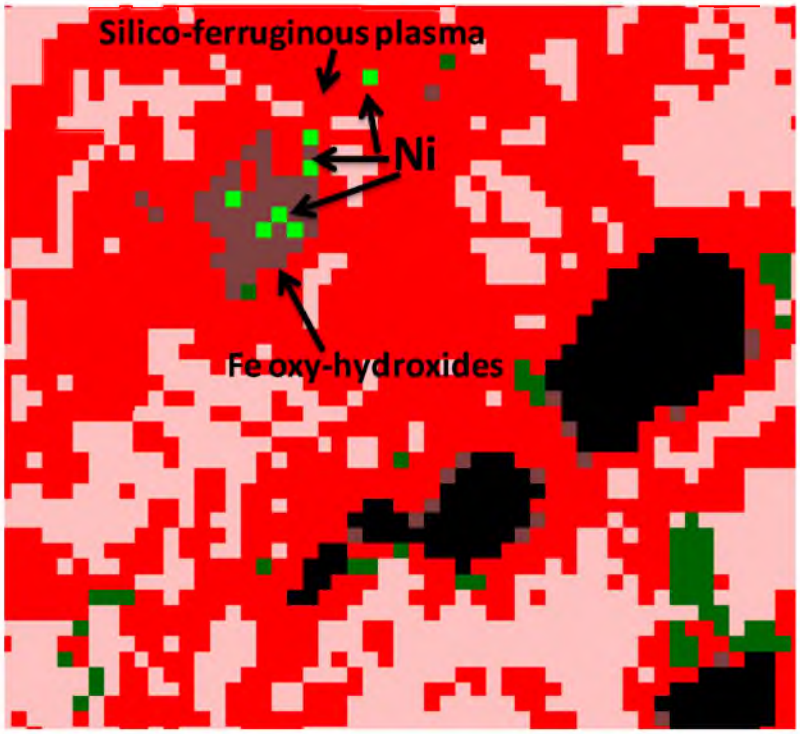

Figure 70. QEMSCAN image of nickel contained in iron oxy-hydroxide and silico-ferruginous plasma phases of the feed.

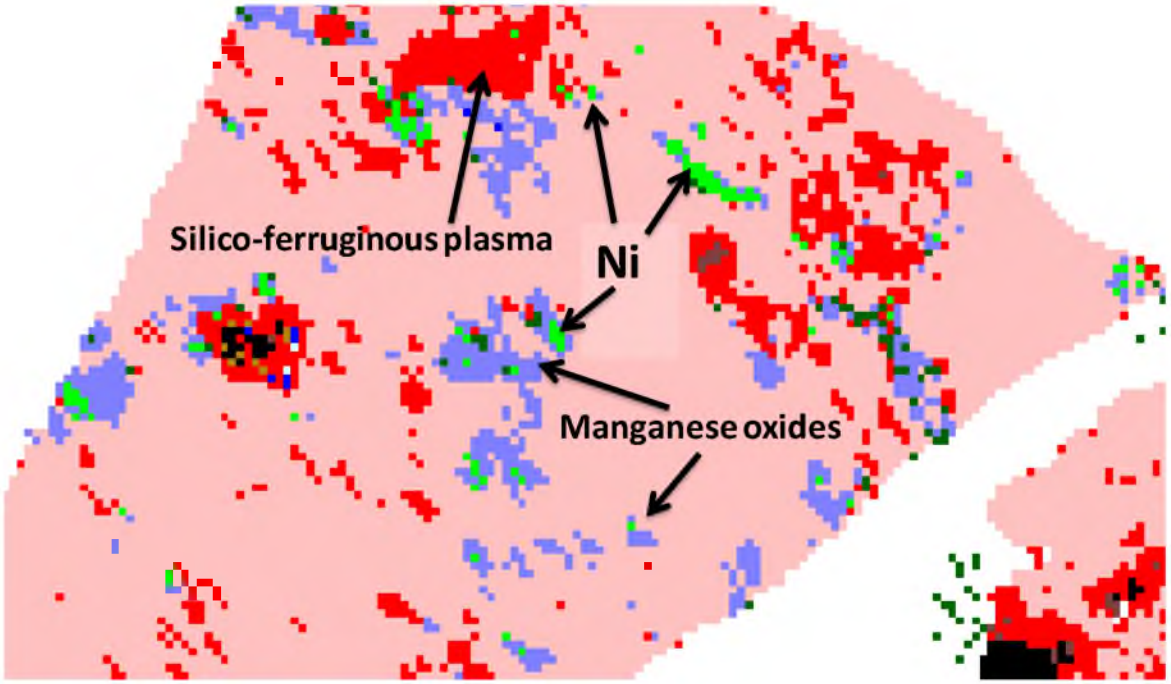

Figure 71. QEMSCAN image of nickel contained in manganese oxide and silico-ferruginous plasma phase of the feed.

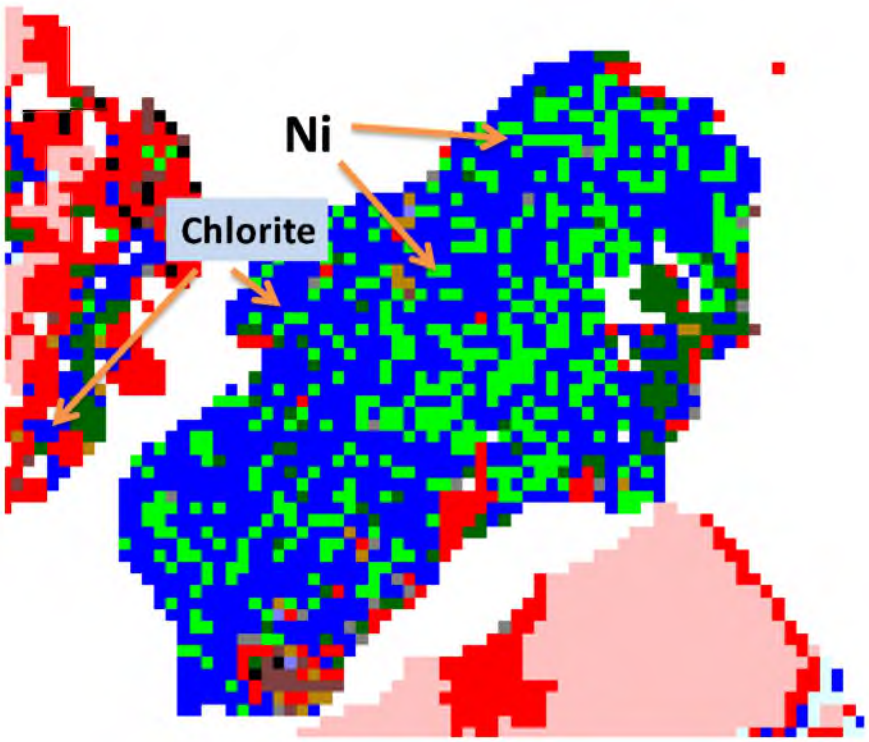

Figure 72. The QEMSCAN image of nickel-bearing chlorite phase in the feed.

Sulfate-Hydroxide Phases

Electron microprobe analysis suggests that the sulfate phase that formed after agglomeration is an intimate mixture of multiple phases, including plasma, Fe-Alunogen ($(Al,Fe)_2(SO_4)_3.nH_2O$) and clays (Table 26).

Since sulfuric acid was used during agglomeration, sulfuric acid likely dissolved some iron and aluminum in the ore which then formed Fe-Alunogen upon drying of the sample or if saturation was achieved in the liquid phase between particles. Clays and plasma react with the sulfuric acid as well. Therefore, Fe-Alunogen, plasma and clays are intimately intergrown.

The sulfate phase can be used to describe the types of agglomerates in nickel laterite agglomeration. There are two types of agglomerates, coalesced and layered

Table 26. Representative electron microprobe analyses of phases in agglomerate samples.

Sample	NiO (%)	CoO (%)	Fe_2O_3 (%)	Al_2O_3 (%)	SiO_2 (%)	MgO (%)	MnO (%)	Cr_2O_3 (%)	SO_3 (%)	Sum (%)	Phases
1	6.98	0.04	11.65	8.59	44.89	13.48	0.12	0.16	8.48	94.39	Sulfate
2	1.14	0.09	34.27	5.78	37.34	2.17	0.45	0.94	7.48	89.65	Sulfate
3	7.91	0.03	9.67	7.54	37.55	16.00	0.14	0.19	15.41	94.43	Sulfate
4	2.84	0.03	35.96	0.70	27.73	2.68	0.61	0.19	8.07	78.80	Sulfate
5	3.21	0.22	37.05	0.73	29.72	3.20	1.74	0.29	12.55	88.71	Sulfate
6	9.03	0.00	3.71	10.06	37.72	19.92	0.11	0.00	3.03	83.59	Sulfate
7	2.85	0.12	26.91	10.22	29.19	3.18	0.24	0.45	7.56	80.72	Sulfate
8	13.07	0.04	11.91	8.47	34.60	13.67	0.16	0.02	4.44	86.40	Sulfate
9	11.82	0.16	20.73	7.56	32.82	10.46	0.24	0.20	3.04	87.02	Sulfate
10	2.34	0.00	22.21	9.65	28.61	10.62	0.18	0.32	3.92	77.84	Sulfate
11	0.40	0.00	8.97	0.52	89.15	0.15	0.04	0.24	0.69	100.15	Plasma
12	0.31	0.00	7.15	0.25	89.09	0.32	0.03	0.12	0.62	97.88	Plasma
13	0.20	0.00	5.76	0.22	90.93	0.21	0.05	0.12	0.60	98.09	Plasma
14	0.16	0.00	5.21	0.36	92.21	0.14	0.07	0.09	0.52	98.76	Plasma
15	0.15	0.04	5.29	2.56	88.73	0.28	0.05	0.19	1.14	98.42	Plasma
16	6.43	0.04	15.61	11.34	31.20	18.11	0.27	0.05	3.22	86.27	Clays
17	7.09	0.11	14.64	11.12	31.06	17.82	0.40	0.00	3.78	86.01	Clays
18	0.33	0.05	11.34	13.36	25.64	27.39	0.00	0.42	0.51	79.04	Clays
19	0.63	0.01	8.09	11.10	30.40	23.95	0.03	1.44	2.28	77.91	Clays
20	6.55	0.09	32.60	10.32	27.83	7.23	0.13	0.80	2.85	88.40	Clays

Note: Analysis 1-5 are from samples of agglomerate treated with 61.3 kg/tonne of sulfuric acid addition rate; analyses 6-10 are from samples of agglomerate treated with 25.4 kg/tonne of sulfuric acid addition rate

(Figures 73 and 74). Figure 73 shows layered agglomerates. The ores contain quartz and silico-ferruginous plasma phases in host particles. Fines are attached to the host particles with the sulfate phase, clay mineral, fragments of quartz and silico-ferruginous plasma. The acid amount used during agglomeration does not appear to transform the clay minerals into the sulfate phase.

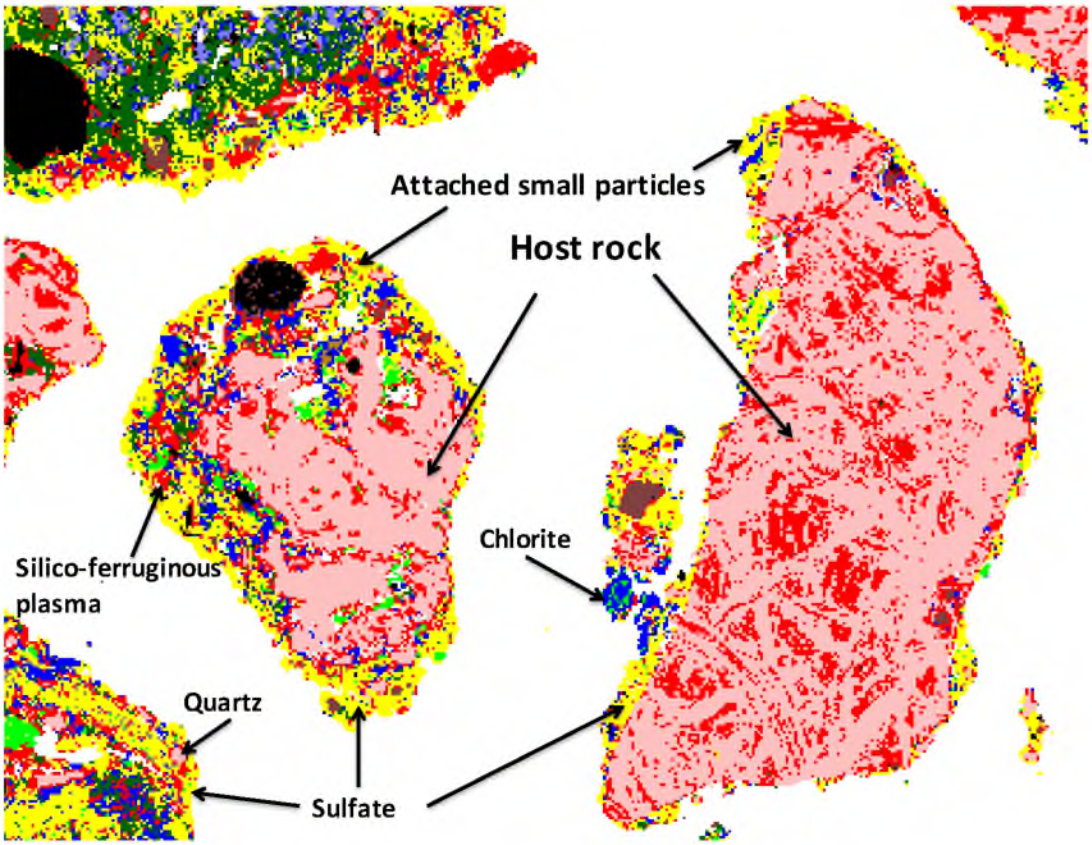

Figure 73. QEMSCAN image of layered agglomerates.

The nickel-containing phases (green color) can be present in both host particle pores and in layered regions in the agglomerates. The nickel-bearing phases evidently react with sulfuric acid and are associated with the sulfate phase. Since nickel is present in silico-ferruginous plasma, smectite, chlorite, vermiculite and serpentine, these phases potentially react with sulfuric acid and release nickel along with other elements into the sulfate phase. Some nickel is still trapped inside the host particle and does not dissolve with sulfuric acid added during the agglomeration process.

Figure 74 illustrates coalesced agglomerates. The agglomerates in Figure 74 do not have recognizable host particles. They are composed of small particles attached

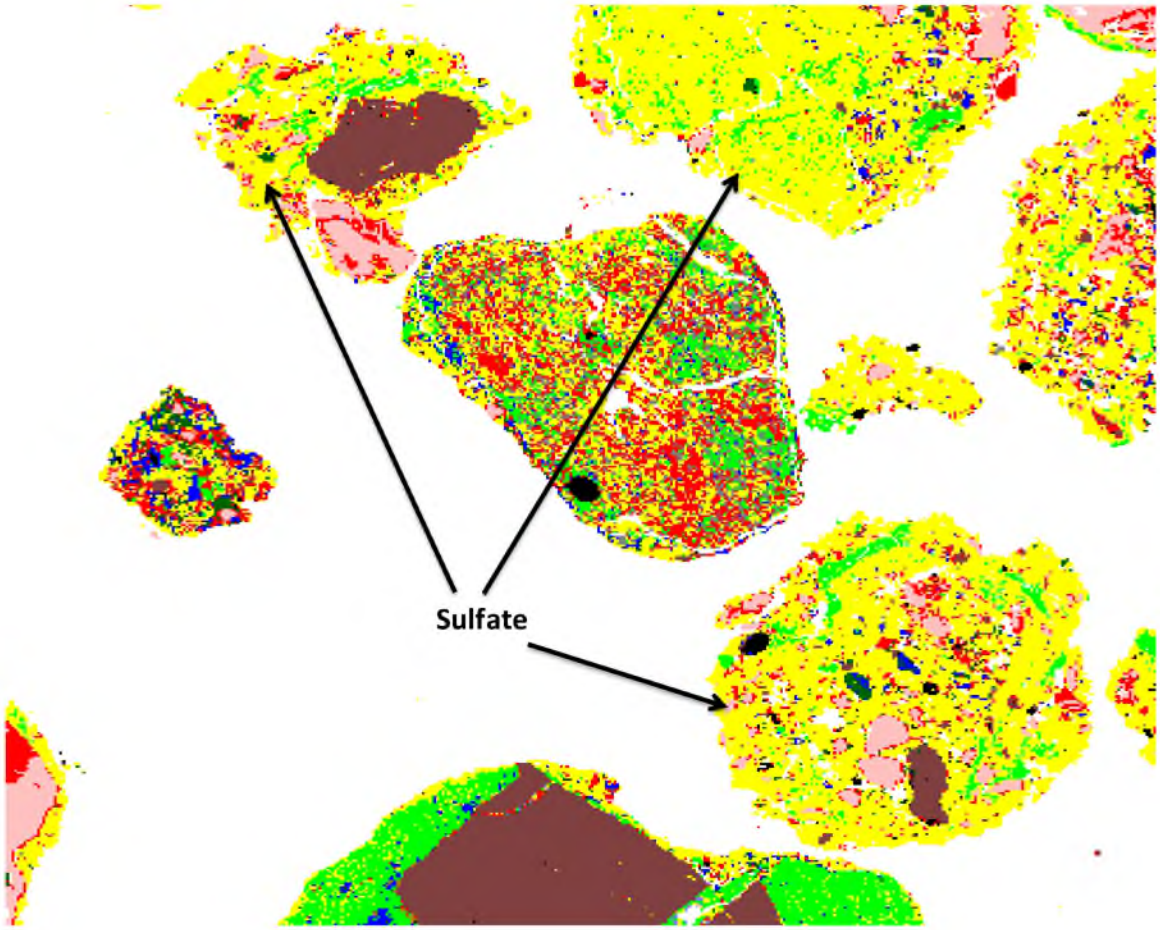

Figure 74. QEMSCAN image of coalescent agglomerates.

together. Quartz, silio-ferruginous plasma and iron oxy-hydroxide coarser particles are present in the agglomerates; however, they are not large enough to be host particles. The agglomerates contain mostly sulfate phase, quartz, silico-ferruginous plasma, iron oxy-hydroxide and clay minerals. Since the sulfate phase represents the transformed nickel-bearing phases, and the agglomerates are mostly composed of sulfate phase, the nickel is then distributed throughout the agglomerate.

Silico-Ferruginous Plasma

The plasma phase is subdivided into quartz and silico-ferruginous plasma on the basis of whether iron is present in QEMSCAN analysis SIP (sponsored SIP). Even though the silico-ferruginous plasma is a quartz-like phase, it can be distinguished by QEMSCAN. The quartz SIP entry includes the minerals or phases which contain high silicon which may contain small amounts of chloride, calcium or phosphorus and may not contain iron, aluminum, magnesium, manganese or other heavy metals. The silico-ferruginous plasma contains any amount of silicon, iron and/or magnesium. Other elements such as aluminum, nickel, and cobalt are allowed to be present in the silico-ferruginous plasma.

Some plasma is categorized as quartz by QEMSCAN due to the relatively high iron detection limit of QEMSCAN (~5%). Electron microprobe analysis shows that all plasma contains substantial concentrations of nickel (0.00-0.28%), iron (0.20-5.24), Al (0.00-0.05) and/or magnesium (0.00-0.43). This finding indicates that either no quartz is present in the samples or that plasma contains micron-scale inclusions of silicate minerals. Nevertheless, XRD indicates that a quartz-like phase is present in the samples. Maturation of plasma may result in domains with large enough dimensions having the quartz structure.

The quartz and silico-ferruginous plasma ratio (Q/SFP) can be used to monitor the proportions of these two phases during agglomeration and leaching processes. After agglomeration, the Q/SFP ratio slightly decreases, as shown in Table 27. However, after 90 days of leaching, the Q/SFP ratio decreases significantly.

Table 27. The quartz/silicoferruginous plasma ratio of feed, agglomerates and leached residual sample.

Samples	Acid Addition (kg/tonne)	NiO (%)	Quartz/Silico-ferruginous plasma ratio
Feed		0.00-0.28	2.8/1.0
Agglomerate	25.4	0.15-0.40	1.8/1.0
	41.6		2.5/1.0
	60.2		2.5/1.0
	61.3		1.7/1.0
	100.5		1.3/1.0
Leached Residual	25.4	0.06-0.28	1.1/1.0
	41.6		1.0/2.6
	60.2		1.1/1.0
	61.3		1.0/1.3
	100.5		1.0/1.0

Sulfuric acid appears to react with the mineral phases, leading to the formation of quartz-like minerals such as plasma. Silico-ferruginous plasma seems to be formed more than quartz.

Nickel accompanies iron in plasma at levels below the detection limit of QEMSCAN, leading to an underestimate of nickel content in plasma and overestimate of total quartz in the samples.

Clay Minerals

Smectite is identified by comparing diffraction patterns of air-dried and ethylene glycol saturated samples, as shown in Figure 75. A 001 reflection of an air-dried sample is at about 6^{o} 2θ (15Å). After treated by ethylene glycol, a 001 reflection shifts to about 5.2^{o} 2θ (16.9Å) (Moore & Reynolds, Jr., 1989). The 001 reflection of the air-dried received ore sample is at about 6^{o} 2θ and it shifts back to about 5.2^{o} 2θ after the samples were saturated with ethylene glycol.

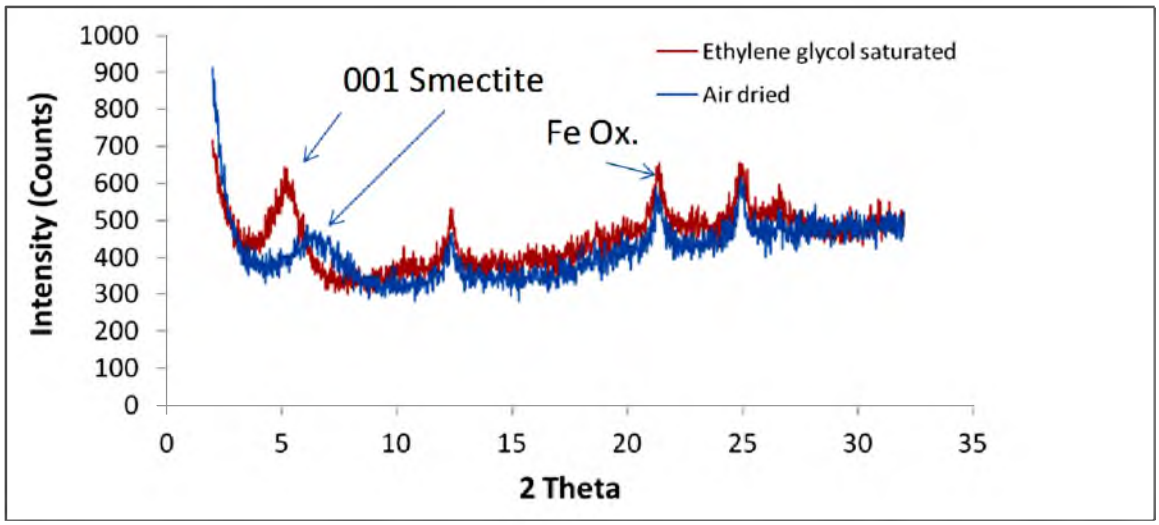

Figure 75. Smectite peak in the ethylene glycol-saturated and air-dried state of received ore sample (clay mineral separated).

Chlorite and kaolinite can be distinguished by XRD. The 001 reflection peak of kaolinite and 002 reflection peak of chlorite are at about 12.5° 2θ. The 002 reflection peak of kaolinite and 004 reflection peak of chlorite are at about 25° 2θ (Moore & Reynolds, Jr. 1989). However, the 001 and 003 peaks of chlorite are at about 6.2 and 18.8° 2θ and are used to identify the presence of chlorite.

Unfortunately, in the diffraction pattern of the received ore sample, the 001 and 003 reflection peak of chlorite is weak due to high iron content in the minerals (Moore & Reynolds, Jr. 1989). The data are consistent with the presence of both chlorite and kaolinite in the samples. The QEMSCAN is also used to identify mineral phases in both crushed and received ore samples.

Phase Characterization of Feed

Feed material used in this study was previously investigated by the industrial sponsor. The mineralogical composition of the nickel laterite ore by size is given in Table

28. The nickel distribution within the nickel-bearing phases is presented in Table 29. The methods used to determine the mineral compositions are undisclosed by the industrial sponsor. Nickel occurs mainly in silico-ferruginous plasma, clay minerals and manganese oxides.

The mineralogy of the feed ore is also shown as a function of particle size. It can be seen that the clay minerals (chlorite and smectite), as expected, are found in the smaller particle size classes. Quartz, on the other hand, is more predominant in the largest size class.

X-ray diffraction was used to analyze feed samples to confirm the presence of clay minerals. Since the largest feed size fraction received from sponsored industry was consumed, oversized feed was crushed and used to create the size fraction (-12.5 +3.17 mm). All size fractions were analyzed by x-ray, microprobe and QEMSCAN to compare their mineralogy. The XRD results of both samples are illustrated in Figures 76 and 77.

The received ore and crushed ore samples show some differences in mineralogy. The main mineral in both samples is quartz. Kaolinite, chromite and iron oxides are also present in both samples. However, the received ore sample has more clay minerals, especially chlorite and smectite.

The smectite peak can be identified only when the samples are saturated by ethylene glycol (Figure 77). From the industrial sponsor results, the received ore is evenly composed of quartz, silico-ferruginous plasma and smectite/chlorite/vermiculite. The XRD pattern of the received ore samples shows the presence of smectite and chlorite. This result confirms the presence of clay minerals within the feed samples. Interestingly, talc is not present in this XRD pattern. The 001 reflection of talc is 9.3 ^{o} 2θ.

Table 28. The mineralogical composition of nickel laterite by size fraction (Castro & Pereira 2009).

Phases	Global	+ 50 mm	- 50 mm + 12.5 mm	- 12.5 mm + 3.17 mm	- 3.17 mm + 0.5 mm	- 0.5 mm
Quartz/Chalcedony	29.72	57.04	48.42	27.23	15.81	7.17
Silico-Ferruginous Plasma	29.33	24.70	33.19	32.02	25.33	28.56
Chlorite/Smectite/Vermiculite	18.75	2.71	2.92	22.52	30.47	25.59
Talc	0.54	0.62	0.90	0.59	0.34	0.11
Serpentine	3.89	3.77	5.20	5.57	2.95	2.71
Phlogopite	1.42	0.48	0.61	1.57	2.08	2.40
Kaolinite	0.5	0.79	0.44	0.44	0.57	0.64
Iron-oxy hydroxides	5.29	4.95	3.87	3.76	6.77	9.78
Manganese oxides	0.76	0.15	0.28	0.65	1.44	1.37
Chromites	3.03	2.49	2.40	1.94	3.48	6.24
Titanium-Iron oxides	1.30	0.09	0.04	0.53	2.66	0.85
Pyroxenes	0.48	0.12	0.25	0.63	0.76	0.80
Kaolinite/Fe Ox./Quartz aggregates	4.81	1.55	0.87	2.27	7.17	13.55
Other phases	0.16	0.56	0.60	0.29	0.17	0.24

Table 29. Nickel distribution among nickel-bearing phases separated by sizes in weight percent (Castro & Pereira 2009).

Phases	Global	+ 50 mm	- 50 mm + 12.5 mm	- 12.5 mm + 3.17 mm	- 3.17 mm + 0.5 mm	- 0.5 mm
Silico-Ferruginous Plasma	30%	54%	60%	26%	25%	36%
Chlorite/Smectite/Vermiculite	54%	21%	19%	64%	61%	43%
Serpentine	1%	2%	3%	1%	1%	1%
Phlogopite	2%	3%	3%	2%	2%	2%
Kaolinite	0%	1%	1%	0%	0%	0%
Iron-oxy hydroxides	3%	6%	6%	2%	2%	3%
Manganese oxides	7%	7%	6%	3%	6%	8%
Kaolinite/Fe Ox./Quartz aggregates	4%	6%	3%	2%	4%	7%
Other phases	0%	0%	0%	0%	0%	0%
Total	100%	100%	100%	100%	100%	100%

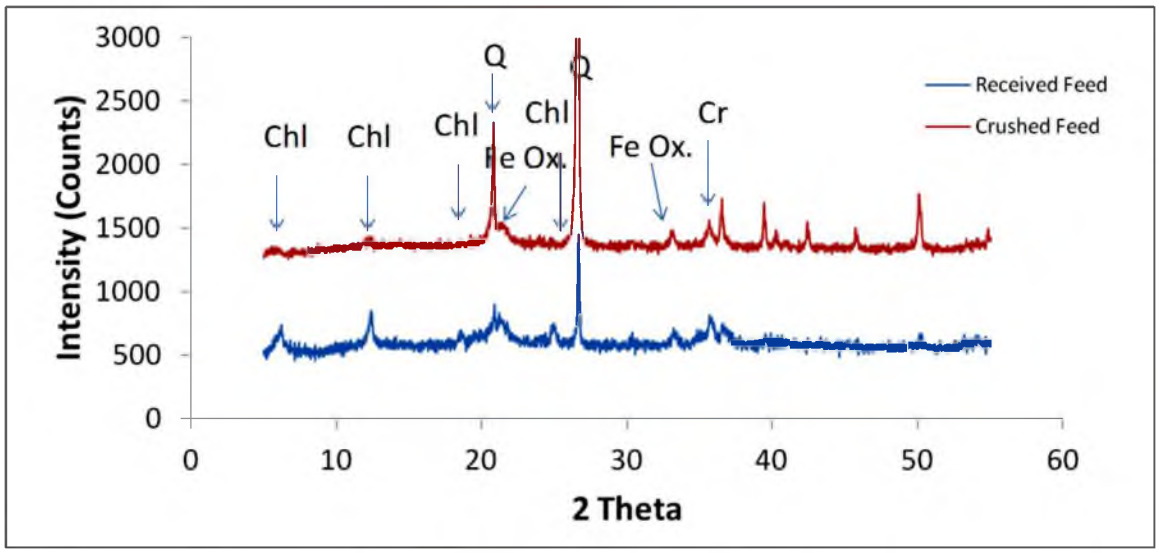

Figure 76. X-ray diffraction pattern of feed samples.

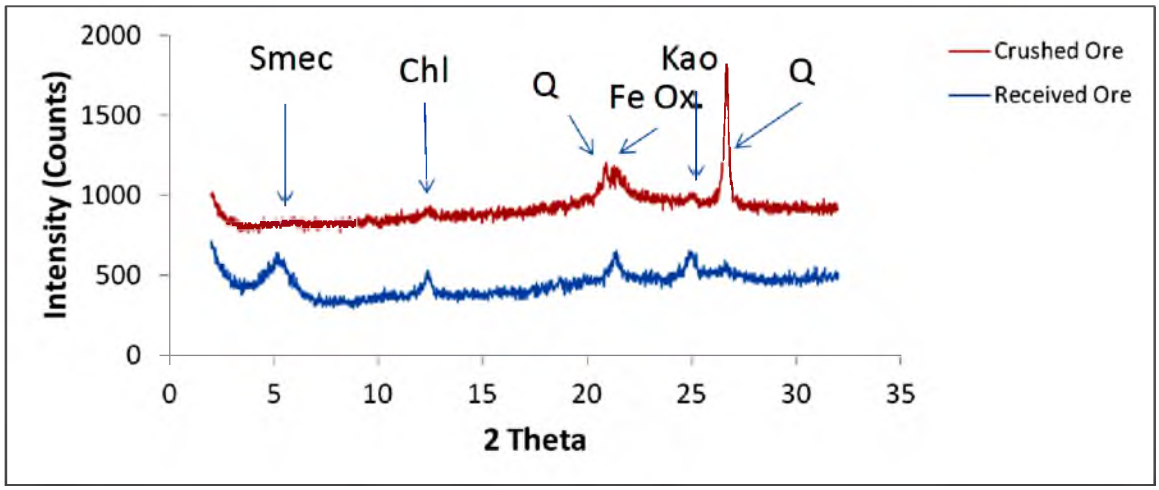

Figure 77. X-ray diffraction pattern of feed samples after coarser particles were removed and saturated with ethylene glycol to show the presence of smectite.

Samples for QEMSCAN analysis were separated from two size fractions, -2.0 +0.9 mm and -0.5 +0.3 mm, and corresponded exactly to the size fractions studied by sponsor: -2.0 +0.9 mm is in -3.17 +0.5 mm size fraction and -0.5 +0.3 mm is in -0.5 mm size fraction. The area percents of phases for the feed samples are given in Table 30.

The QEMSCAN images of feed samples are shown in Figure 78. A different color has been assigned to represent each phase in the samples (Table 31). The species identification protocol (SIP) used to classify the minerals in this study was nearly identical to the SIP of the sponsor. However, minor adjustments were made to improve its robustness.

Table 30. Area percent of phases in the feed samples.

Mineral phases	Area percent (%)			
	Received ore		Crushed ore	
	-2.0 +0.9 mm	-0.5 +0.3 mm	-2.0 +0.9 mm	-0.5 +0.3 mm
Quartz	28.0	8.5	69.8	54.1
Silico-ferruginous plasma	35.3	45.6	24.8	28.7
Chlorite/Smectite/Vermiculite/Serpentine	12.8	18.1	1.0	3.4
Iron oxy-hydroxides	10.3	8.1	1.0	5.8
Manganese oxides	0.2	0.3	0.2	0.9
Kaolinite	0.3	1.0	0.1	0.5
Chromite	2.3	5.8	1.3	3.0
Talc	0.2	0.1	1.3	1.5
Phlogopite	0.6	1.9	0.3	0.7
Nickel	8.7	8.8	0.1	1.0
Other phases	1.4	1.8	0.1	0.3

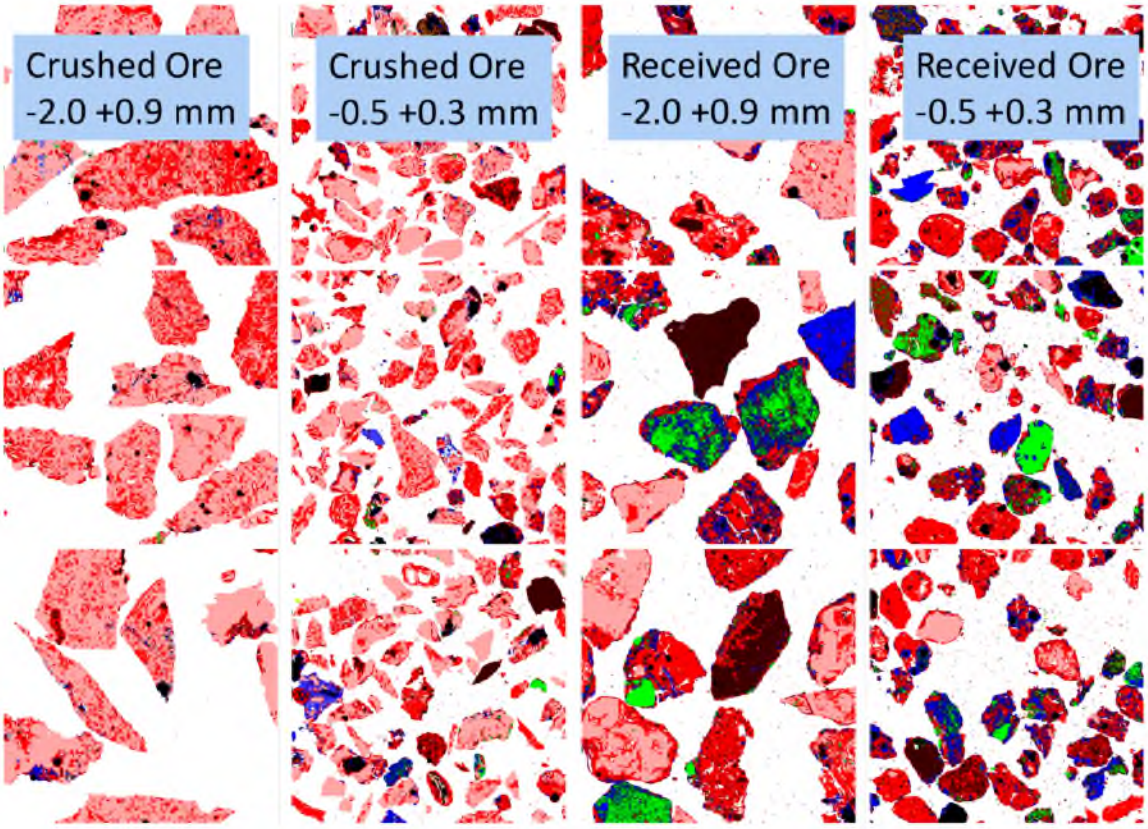

Figure 78. QEMSCAN image of feed samples. Key to phases is given in Table 26.

Table 31. Colors assigned to represent each mineral.

Mineral	Color
Quartz	
Silico-ferruginous plasma	
Chlorite/Smectite/Vermiculite/Serpentine	
Iron oxy-hydroxides	
Manganese oxides	
Kaolinite	
Chromite	
Talc	
Phlogopite	
Nickel	
Other phases	
Sulfur	
Epoxy	

As expected, the crushed ore samples are high in quartz and silico-ferruginous plasma and low in clay minerals. Since the coarse particles prior to crushing contain high quartz and silico-ferruginous plasma and low clay minerals, the crushed sample then shows high amounts of quartz and silico-ferruginous plasma. Nickel content in the coarse particles prior to crushing is also low; therefore, the nickel content in the crushed ore sample is lower than the received sample.

The received ore sample contains less quartz and silico-ferruginous plasma than the crushed ore sample. The clay mineral amount is higher than in the crushed sample. Since the clay mineral content is greater, the nickel content is also expected to be higher. Normally, the clay minerals increase as the size fraction of the ore particles decrease. From the electron microprobe (EMP) data (Table 32), silico-ferruginous plasma and clays can contain nickel and cobalt.

The amount of nickel and cobalt in clays is higher than silico-ferruginous plasma. Quartz contains only silicon and a very small amount of iron. This may be the quartz-like phase which results from weathering of olivine or pyroxene. The silico-ferruginous plasma can contain iron, magnesium and small amounts of nickel, cobalt and manganese.

Phase Transformation during Agglomeration

In agglomeration, sulfuric acid and water were added to the nickel laterite ore. Agglomerates form by liquid bridging between particles. When nickel laterite is subjected to water and sulfuric acid, some phases were dissolved and some new phases formed. The agglomerates were air dried for several days prior to the leaching experiment. The most abundant new phase was a sulfate that contained some iron, magnesium manganese, aluminum and nickel.

Table 32. Representative electron microprobe analyses of various phases in feeds.

Sample	NiO (%)	CoO (%)	Fe_2O_3 (%)	Al_2O_3 (%)	SiO_2 (%)	MgO (%)	MnO (%)	Cr_2O_3 (%)	Sum (%)	Phases
1	0.0	0.0	0.54	0.0	100.08	0.0	0.0	0.0	100.62	Quartz
2	0.0	0.0	1.02	0.0	99.51	0.0	0.0	0.0	100.53	Quartz
3	0.0	0.0	0.81	0.0	100.60	0.0	0.0	0.0	101.41	Quartz
4	0.0	0.0	0.20	0.0	100.15	0.0	0.0	0.0	100.35	Quartz
5	0.0	0.0	0.55	0.0	99.54	0.0	0.0	0.0	100.09	Quartz
6	0.28	0.02	2.68	0.01	95.72	0.23	0.04	0.00	98.99	Plasma
7	0.28	0.06	3.49	0.01	96.65	0.23	0.00	0.09	100.80	Plasma
8	0.23	0.02	3.80	0.05	95.69	0.43	0.05	0.00	100.27	Plasma
9	0.21	0.02	5.15	0.00	94.43	0.14	0.03	0.00	99.97	Plasma
10	0.18	0.01	5.24	0.05	85.34	0.02	0.06	0.11	91.00	Plasma
11	0.42	0.06	47.82	0.79	30.72	1.72	1.43	1.96	84.93	Clays
12	22.36	0.27	19.14	0.19	30.63	5.96	0.10	0.00	78.65	Clays
13	1.93	0.07	16.53	12.64	30.49	25.94	0.03	0.93	88.56	Clays
14	4.45	0.13	0.00	11.36	26.09	27.55	0.01	0.23	69.82	Clays

The moisture content used during agglomeration was varied from 13 to 19% on a dry basis (Figures 79 and 80). The main phases contained in the feed samples are still contained in the agglomerates. Clay minerals such as chlorite, kaolinite and smectite still remained in the agglomerates after treatment with the sulfuric acid and water. The sulfate phase is not observed in the XRD pattern and appears to be x-ray amorphous. Table 33 illustrates the QEMSCAN results of agglomerates at different solution addition rates.

Quartz, silico-ferruginous plasma and chromite are stable as solution addition to the agglomeration varied. These two phases are very stable and less likely to dissolve. There is no distinctive relationship between solution addition and how the phases change during agglomeration. The area percents of the other mineral vary as the solution addition during agglomeration increases.

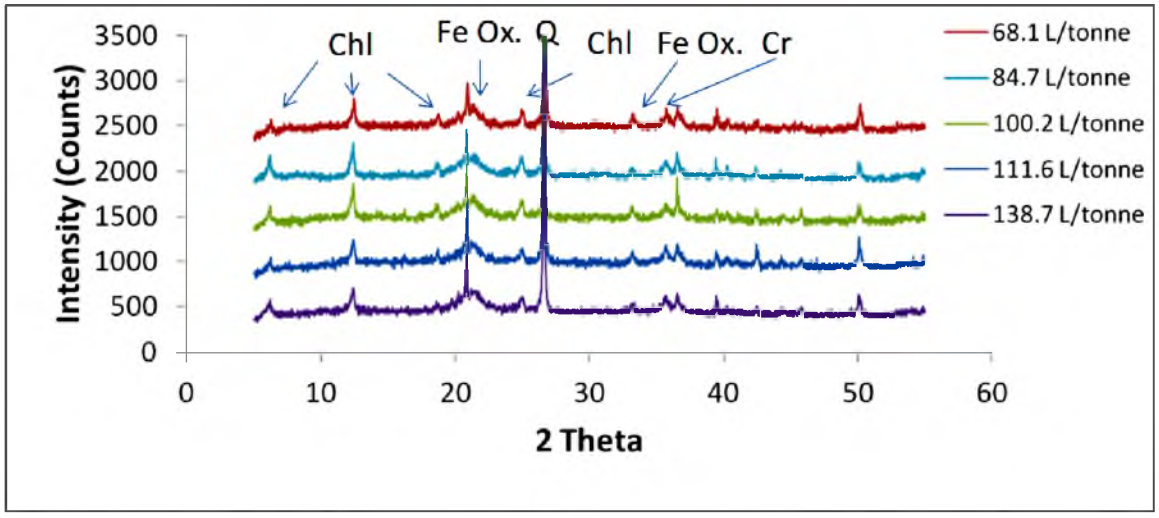

Figure 79. X-ray diffraction pattern of agglomerate samples at different solution addition rates.

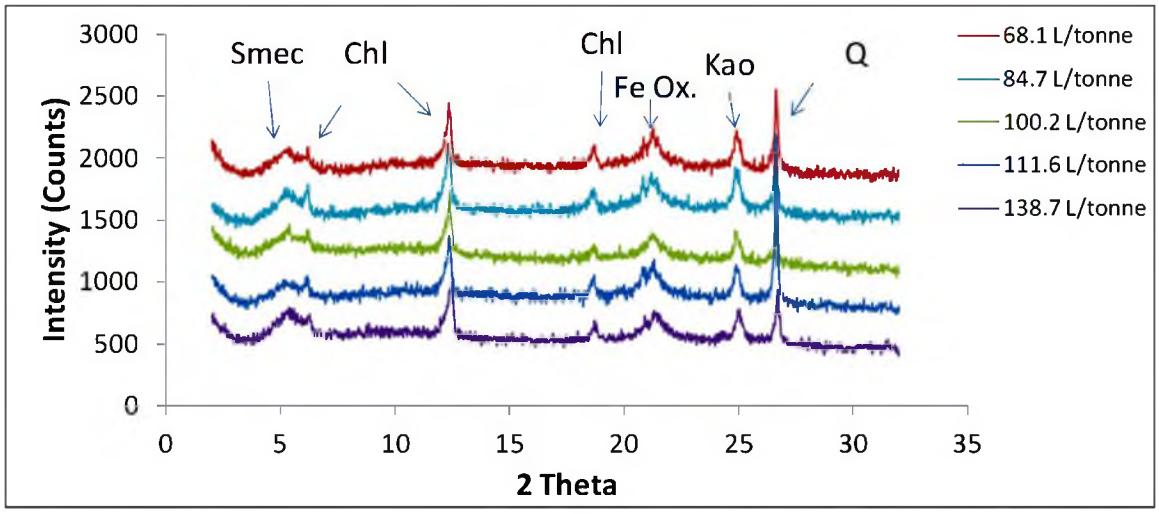

Figure 80. X-ray diffraction pattern of agglomerate samples at different solution addition rates after coarser particles were removed and samples were saturated with ethylene glycol.

Table 33. The area percent of phases in agglomerates at different solution addition rates.

Phases	Area Percent (%)									
	Solution Addition (L/tonne)									
	68.1		84.7		100.2		111.6		138.7	
	1	2	1	2	1	2	1	2	1	2
Sulfate phase	32.6	52.1	13.0	35.9	43.0	46.2	33.2	52.0	22.9	48.0
Quartz	28.4	12.0	42.2	12.9	32.0	15.5	27.6	15.9	30.7	17.6
Silico-ferruginous plasma	16.9	15.4	23.0	27.4	13.0	20.9	20.9	13.6	12.1	9.7
Chlorite/Smectite/Vermiculite/Serpentine	8.0	6.3	4.9	11.0	2.5	4.7	5.1	2.9	9.5	3.5
Iron oxy-hydroxides	3.0	4.3	1.3	2.4	1.4	3.4	1.4	3.3	3.5	8.3
Manganese oxides	0.3	0.0	0.3	0.0	0.0	0.0	1.4	0.0	0.1	0.2
Kaolinite	0.2	0.5	0.8	1.5	1.8	1.0	4.1	0.3	0.2	0.8
Chromite	3.0	3.0	2.7	3.4	2.6	3.2	2.2	2.8	1.7	3.9
Talc	1.0	0.2	1.2	0.2	0.1	0.2	0.2	0.3	0.4	0.4
Phlogopite	2.0	0.3	0.5	0.6	0.3	0.5	0.5	0.5	0.5	0.5
Nickel	4.7	5.4	9.8	4.1	3.2	3.9	3.3	8.0	11.5	7.1
Other phases	0.3	0.4	0.3	0.6	0.2	0.3	0.2	0.4	0.9	0.1

1 is -2.0 +0.9 mm size fraction and 2 is -0.5 +0.3 size fraction. Nickel can be any mineral with more than ~ 5% nickel

The area percent of mineral phases for agglomerates at different acid addition are given in Table 34. The relation between the acid addition and area percent of the sulfate phase is illustrated in Figure 81. The sulfate phase increases as the acid addition increases, as expected. More sulfuric acid addition provides more sulfur in the system and sulfur can react with other minerals to form a sulfate phase.

The effect of acid addition on the silico-ferruginous plasma phase changing during the agglomeration process is not discernible. The clay phase tends to decrease as the rates of acid addition during agglomeration increases in the smaller size fraction studied (Figure 82). The clay minerals easily dissolve in acid solution. Therefore, increasing acid addition during agglomeration leads to a decrease in the clay mineral amount.

The electron microprobe results of agglomerates are shown previously in Table 26. Sulfur elements can be identified in the agglomerates due to the sulfuric acid addition during the agglomeration process. Nickel, magnesium and manganese amounts in the agglomerates (sulfate phase) are higher than the feed. The iron, cobalt and aluminum amount in the agglomerates are slightly higher than the feed. The solubility of each element in the ores contributes to the element contents in the agglomerates. High solubility elements are dissolved by the sulfuric acid and re-precipitated as the sulfate phase, while the low solubility elements remain in the host particles. The amount of sulfur in the agglomerates varied from 0.23 to nearly 10%. The sulfuric acid dissolved clay minerals, silico-ferruginous plasma and other phases and formed a sulfate phase which is an amorphous phase. The silico-ferruginous plasma and clays can still be identified by the electron microprobe.

Table 34. The area percent of phases in agglomerates at different acid addition rates

Phases	Area Percent (%)									
	Acid Addition (kg/tonne)									
	25.4		41.6		60.2		61.3		100.5	
	1	2	1	2	1	2	1	2	1	2
Sulfate phase	13.0	35.9	22.9	48.0	43.0	46.2	32.6	52.1	33.2	52.0
Quartz	42.2	12.9	30.7	17.6	32.0	15.5	28.4	12.0	27.6	15.9
Silico-ferruginous plasma	23.0	27.4	12.1	9.7	13.0	20.9	16.9	15.4	20.9	13.6
Chlorite/Smectite/Vermiculite/Serpentine	4.9	11.0	9.5	3.5	2.5	4.7	8.0	6.3	5.1	2.9
Iron oxy-hydroxides	1.3	2.4	3.5	8.3	1.4	3.4	3.0	4.3	1.4	3.3
Manganese oxides	0.3	0.0	0.1	0.2	0.0	0.0	0.3	0.0	1.4	0.0
Kaolinite	0.8	1.5	0.2	0.8	1.8	1.0	0.2	0.5	4.1	0.3
Chromite	2.7	3.4	1.7	3.9	2.6	3.2	3.0	3.0	2.2	2.8
Talc	1.2	0.2	0.4	0.4	0.1	0.2	1.0	0.2	0.2	0.3
Phlogopite	0.5	0.6	0.5	0.5	0.3	0.5	2.0	0.3	0.5	0.5
Nickel	9.8	4.1	11.5	7.1	3.2	3.9	4.7	5.4	3.3	8.0
Other phases	0.3	0.6	0.9	0.1	0.2	0.3	0.3	0.4	0.2	0.4

1 is -2.0 +0.9 mm size fraction and 2 is -0.5 +0.3 size fraction. Nickel can be any mineral with more than ~ 5% nickel

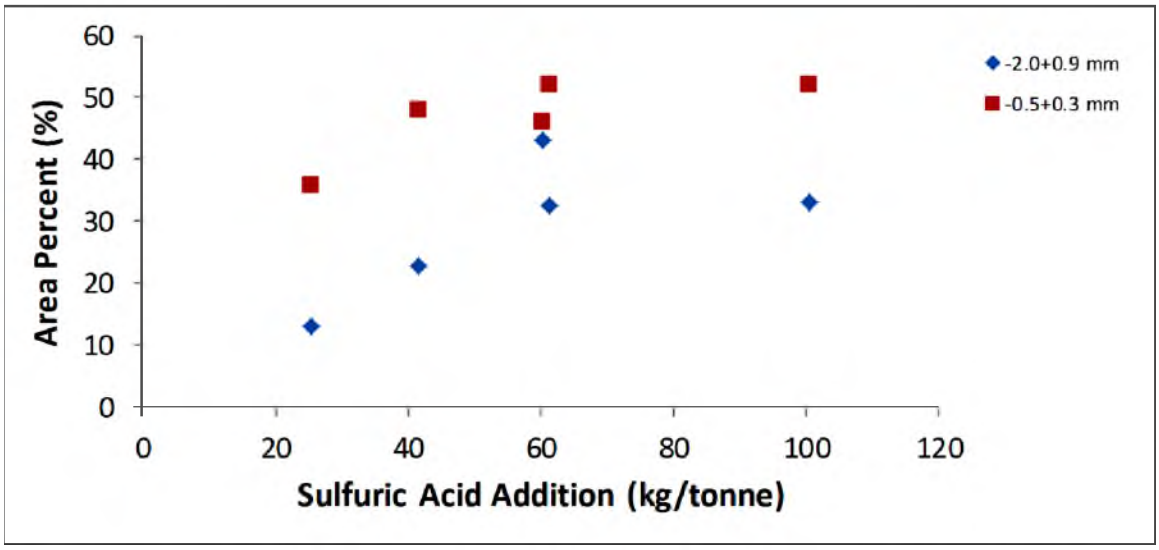

Figure 81. The relationship between acid addition and area percent of sulfate phase.

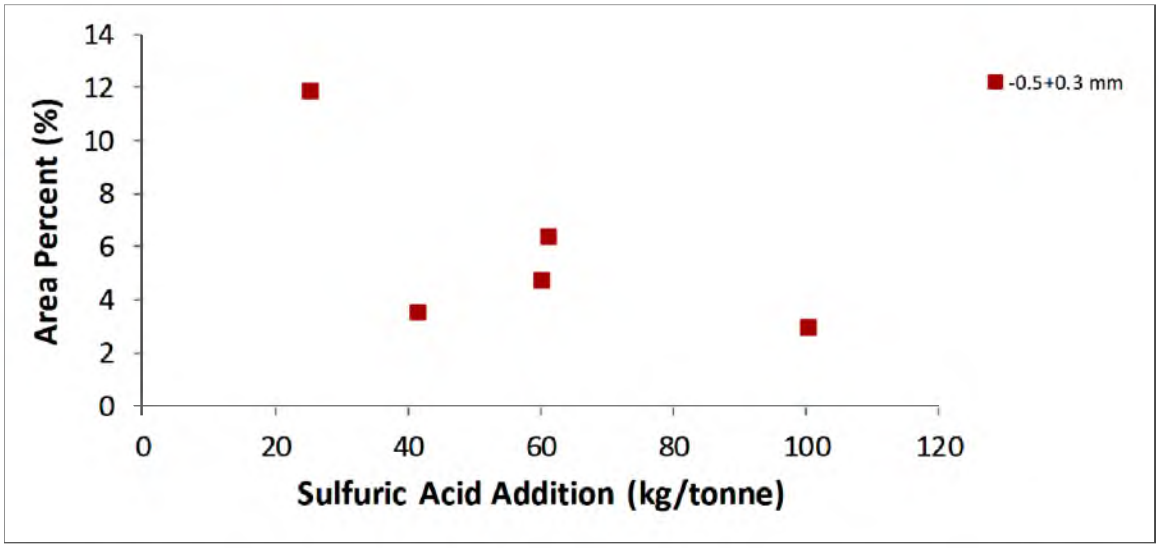

Figure 82. The relationship between acid addition and area percent of clay minerals.

Higher sulfuric acid addition during agglomeration results in a higher amount of sulfur in the agglomerates, as illustrated in Table 26. The average of SO_3 amount in the agglomerates at 61.3 and 25.4 kg/tonne acid addition rate are 10.3 and 6.0%, respectively.

The relationship between the sulfate phase and agglomerate properties are given in Table 35. As acid addition during agglomeration increases, the sulfate phase also increases until it reaches the maximum point at 100.5 kg/tonne acid addition rate. The electrical conductivity of agglomerates, hydraulic conductivity and breakthrough time have an inconclusive relationship with the sulfate phase. The sulfuric acid electrical conductivity seems to have a larger effect on the electrical conductivity of agglomerates. The permeability of the agglomerate bed is affected more by the amount of agglomeration solution rather than the amount of the sulfate phase in the agglomerate body. The amount of sulfate phase may affect agglomerate strength, but that was not examined in this study.

Table 35. The relationship between the sulfate phase and agglomerate properties.

Acid Addition (kg/tonne)	Sulfate Phase Area Percent (%)		Hydraulic Conductivity (cm/s)	Electrical Conductivity (mS/m)		Breakthrough Time (hrs)
	1	2		No Load	20.45 kg Load	
25.4	13.0	35.9	$2.2x10^{-5}$	32.38	66.86	11
41.6	22.9	48.0	$1.3x10^{-1}$	66.79	303.10	5
60.2	43.0	46.2	$1.0x10^{-2}$ (+/- 0.01)	60.31 (+/- 21.69)	147.72 (+/- 52.10)	8 (+/- 2.0)
61.3	32.6	52.1	$1.7x10^{-2}$	9.64	26.06	16
100.5	33.2	52.0	$2.9x10^{-2}$	12.28	60.33	10

1 is -2.0 +0.9 mm size fraction and 2 is -0.5 +0.3 size fraction

Phase Transformation during Leaching

After the column leaching experiments were completed, leach residual samples were collected from each column to investigate the mineralogy. The samples were collected from the top, center and bottom of the column to study the mineralogical changes within the column at different depths. The x-ray pattern of feed, agglomerate and leach residual samples are illustrated in Figure 83. The smectite appearing in the feed and agglomerate samples disappears in leach residual samples. Leaching has dissolved the smectite phase.

Figure 84 illustrates the x-ray pattern of leach residual samples at different acid addition rates during agglomeration. Most of the mineral phases present in the feed and agglomerate samples were also present in the leached residual samples. The difference in phase amount at different acid addition rates cannot be distinguished by x-ray diffraction.

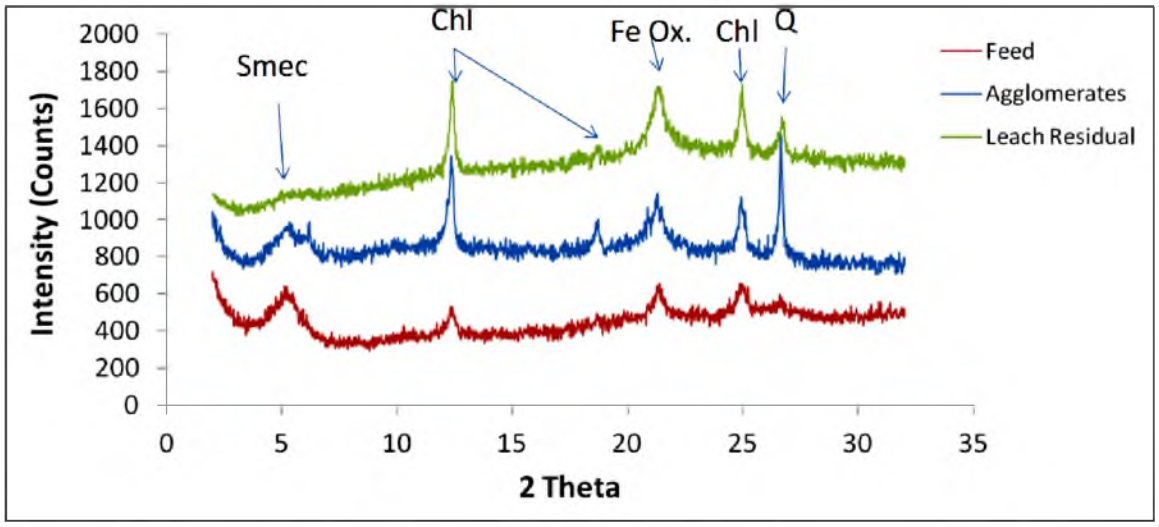

Figure 83. X-ray diffraction pattern of glycolated feed, agglomerates and leach residual samples.

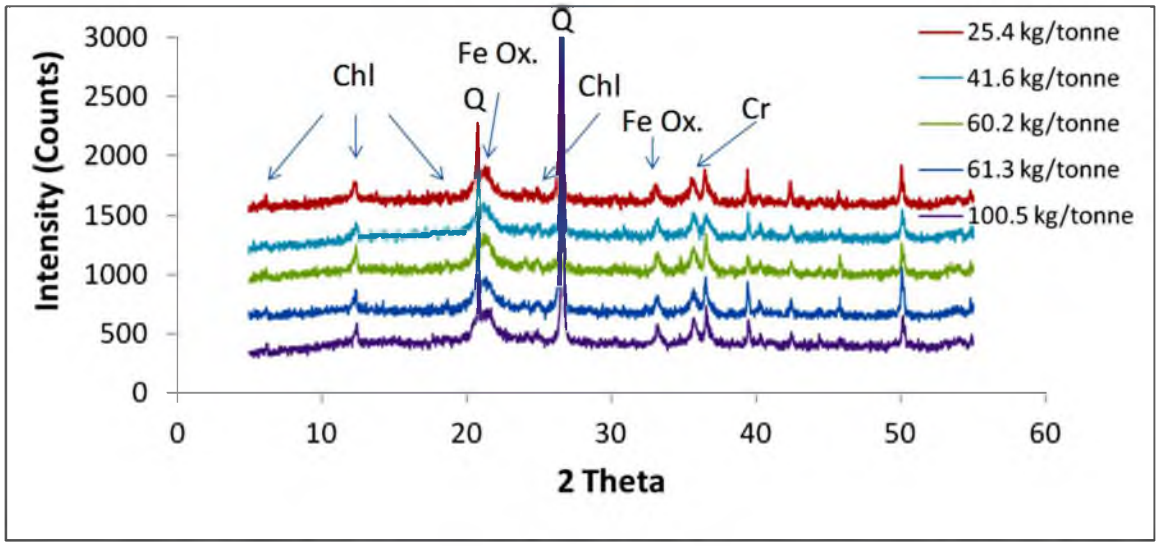

Figure 84. X-ray diffraction pattern of leached residual samples at different acid addition rates from the same column depth.

Coarser particles were then removed from the leach residual samples by centrifugal forces. The samples were then saturated with ethylene glycol. Figure 85 shows the x-ray pattern of leached residual samples after the coarser particles were removed and the samples were saturated with ethylene glycol. As the acid addition rates increase from 25.4 to 61.3 kg/tonne, the clay amount in each sample is almost identical. However, when the acid addition rate reaches 100.5 kg/tonne, the clay amount in the sample decreases. Clay minerals are dissolved during agglomeration by sulfuric acid solution and form a sulfate-associated phase. The more sulfuric acid is added to agglomeration, the more sulfate phase is produced during agglomeration. This sulfate phase is likely to dissolve in the relatively weak sulfuric acid solution used in the column leaching experiment (65 g/L sulfuric acid). Therefore, the clay in high sulfuric acid used during agglomeration is less than the clay in lower sulfuric acid used during agglomeration.

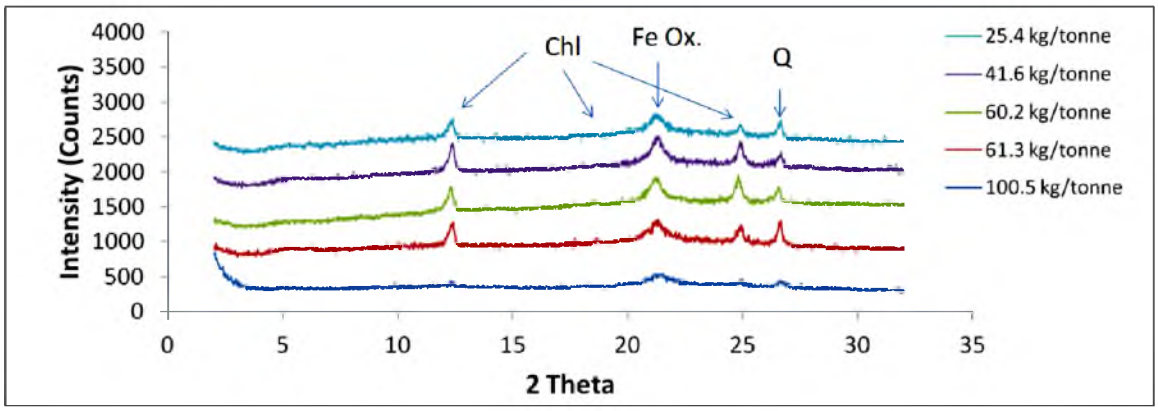

Figure 85. X-ray diffraction patterns of leached residual samples with different acid addition rates during agglomeration after coarser particles were removed and samples were saturated with ethylene glycol.

QEMSCAN results of leached residual samples are given in Table 36. Comparing with the agglomerate samples, quartz, silico-ferruginous plasma and iron oxy-hydroxide phases increased. Sulfate, nickel and clay minerals decreased. Chromite, talc, kaolinite and phlogopite phases were relatively stable. Chromite, talc and phogopite were quite stable in dilute acid; therefore, these phases changed minimally after the leaching experiment. Sulfate and clay were easily dissolved in dilute acid solution so the amount of these two phases decreased after the column leaching experiment. Since nickel was contained in sulfate and clay, the amount of nickel in the leached residual sample also decreases.

The soluble elements such as nickel, magnesium and manganese within clays and other phases were dissolved and carried out by the acid solution. Iron, silicon and other elements remained behind due to their insolubility. Nickel, manganese and magnesium were not completely leached, remaining in the quartz, silico-ferruginous plasma, iron oxy-hydroxide and the products of the leached clays and other soluble phases.

Table 36. Area percent of phases in leach residuals at different acid addition rates.

Phases	Area Percent (%)									
	Acid Addition (kg/tonne)									
	25.4		41.6		60.2		61.3		100.5	
	1	2	1	2	1	2	1	2	1	2
Sulfate phase	0.1	1.0	0.4	2.2	0.1	0.2	0.1	0.1	0.0	0.1
Quartz	46.5	27.6	23.2	24.6	40.7	39.3	37.1	27.9	41.7	33.0
Silico-ferruginous plasma	41.3	42.0	61.4	57.1	36.9	47.8	46.9	47.7	43.1	43.0
Chlorite/Smectite/Vermiculite/Serpentine	3.2	4.1	5.5	4.9	3.4	3.6	3.5	3.9	2.9	3.6
Iron oxy-hydroxides	2.9	10.7	2.4	4.1	9.9	2.2	4.4	10.7	4.1	8.4
Manganese oxides	0.3	0.7	0.5	0.0	0.3	0.1	0.0	0.0	1.4	0.0
Kaolinite	0.9	1.9	1.6	1.1	2.5	3.1	1.3	1.9	2.8	2.6
Chromite	3.6	10.3	3.3	4.1	4.5	2.8	3.0	5.1	3.1	5.6
Talc	0.4	0.6	0.5	0.7	0.6	0.4	0.7	0.5	1.0	0.6
Phlogopite	0.4	0.7	0.5	0.7	0.5	0.2	0.5	0.5	1.1	0.7
Nickel	0.1	0.3	0.3	0.1	0.5	0.1	0.1	0.1	0.0	2.2
Other phases	0.2	0.2	0.4	0.4	0.2	0.2	0.2	0.4	0.2	0.3

1 is -2.0 +0.9 mm size fraction and 2 is -0.5 +0.3 size fraction. Nickel can be any mineral with more than ~ 5% nickel

The x-ray patterns of leached residuals from different positions within the column show some differences in minerals phases, especially for the clay minerals (Figures 86 and 87 and Table 37). QEMSCAN results show that there were only small differences in the amounts of phases within the column. The columns used in the leaching experiment are 1.5 m tall. The agglomerates filled only about 1.0 m. The interval between each sample was about 30 cm. Since the sulfuric acid concentration at each column depth was different, the mineralogy at each column position could also be different. The sulfuric acid reacted with the surrounding minerals as it flowed down the column and reduced its strength early in the leaching experiments. Near the end of the column tests, the feed and exit pH were approximately the same. This result indicates that there was minimal difference in mineralogy between column depths. The agglomerate body height in the column leaching experiment may not be enough to see any difference in mineralogy.

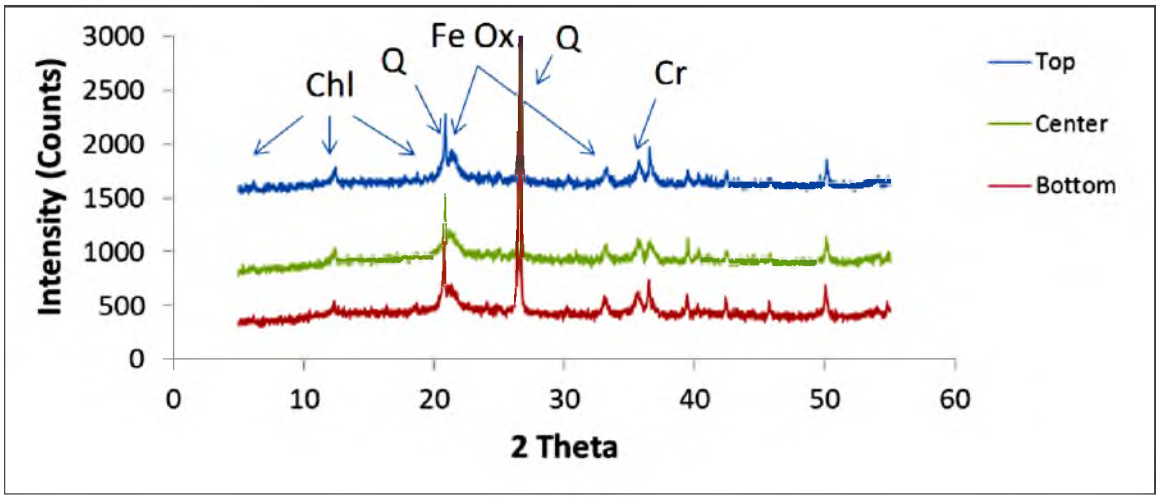

Figure 86. X-ray diffraction pattern of leached residual samples agglomerated with 313 g/L sulfuric acid solution and 19% moisture content at different column depth.

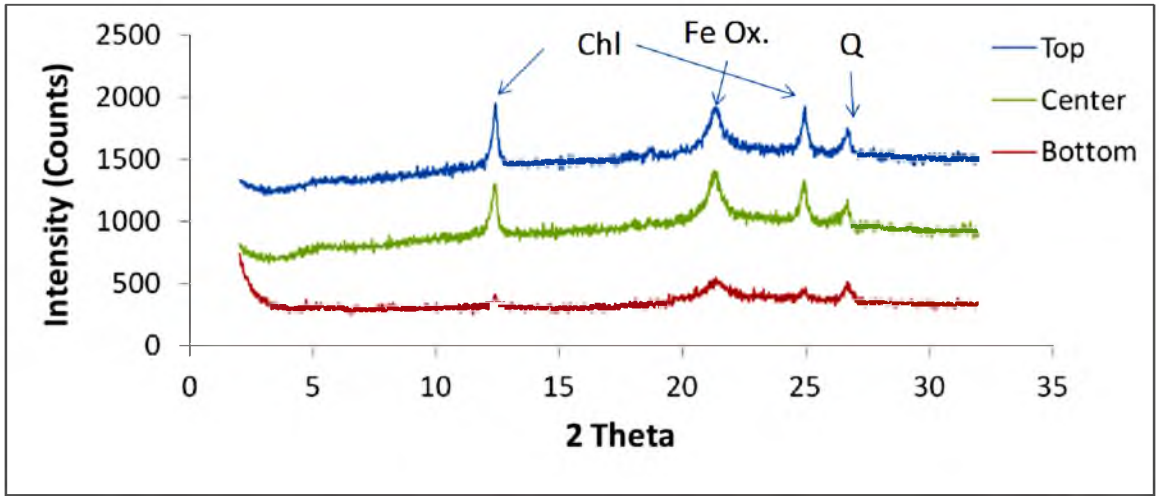

Figure 87. X-ray diffraction patterns of leached residual samples agglomerated with 313 g/L sulfuric acid solution and 19% moisture content at different column depth after coarser particles were removed and samples were saturated with ethylene glycol.

Table 37. Area percent of phases in leach residuals with 41.6 kg/tonne acid addition rate.

Mineral phases	Area Percent (%)					
	Sample Positions					
	Top		Center		Bottom	
	1	2	1	2	1	2
Sulfate phase	0.4	2.2	0.1	0.3	0.1	0.1
Quartz	23.2	24.6	26.1	24.4	39.5	22.2
Silico-ferruginous plasma	61.4	57.1	58.9	57.1	44.1	59.2
Chlorite/Smectite/Vermiculite/Serpentine	5.5	4.9	4.1	4.8	3.5	5.3
Iron oxy-hydroxides	2.4	4.1	3.7	5.4	3.9	5.0
Manganese oxides	0.5	0.0	0.2	0.0	0.1	0.0
Kaolinite	1.6	1.1	2.7	1.8	1.2	2.0
Chromite	3.3	4.1	3.0	4.5	6.2	4.8
Talc	0.5	0.7	0.3	0.4	0.4	1.2
Phlogopite	0.5	0.7	0.5	0.7	0.7	0.8
Nickel	0.3	0.1	0.1	0.2	0.1	0.2
Other phases	0.4	0.4	0.4	0.4	0.2	0.4

1 is -2.0 +0.9 mm size fraction and 2 is -0.5 +0.3 size fraction. Nickel can be any mineral with more than ~ 5% nickel

After leaching, the nickel concentration in the samples decreased. In the agglomerates, nickel occurred in chlorite, smectite, vermiculte, serpentine, silico-ferruginous plasma and sulfate phases. In the leached residuals, nickel was mostly found in silico-ferruginous plasma. It was also present in clay mineral phases and iron oxy-hydroxides phases. However, the amount of nickel found in clay minerals and iron oxy-hydroxide was very low.

As illustrated in Figure 88, the sulfate phase present in agglomerates disappeared in the leach residual, leaving unattached fines. The nickel associated with the sulfate phase also disappeared in the leached residual samples. Nickel can be found in the silico-ferruginous plasma phase in leached residual samples, as shown in Figure 89. The silico-ferruginous plasma may be hard to dissolve; therefore, it can withstand the acid used in the leaching experiment. Leaching solution needs to diffuse through the silico-ferruginous plasma particles to leach nickel. If the particles are dense, the solution will require long diffusing times to reach the nickel-bearing particles.

The electron microprobe results for leach residual samples are shown in Table 38. Nickel appears to still be trapped in silico-ferruginous plasma and an unidentified phase. The nickel content in the silico-ferruginous plasma in leached residuals minimally changes from the agglomerates and feeds. Plasma phase in feed, agglomerate and leach residual consistently shows 0.13-0.21% NiO on average, implying that the nickel in the plasma phase is very difficult to extract using the methods employed in this study. The silico-ferruginous plasma is a quartz-like phase and quite stable in the dilute acid solution. Therefore, the nickel which is trapped inside silico-ferruginous plasma particles did not come into contact with the acid solution and remained in the particles.

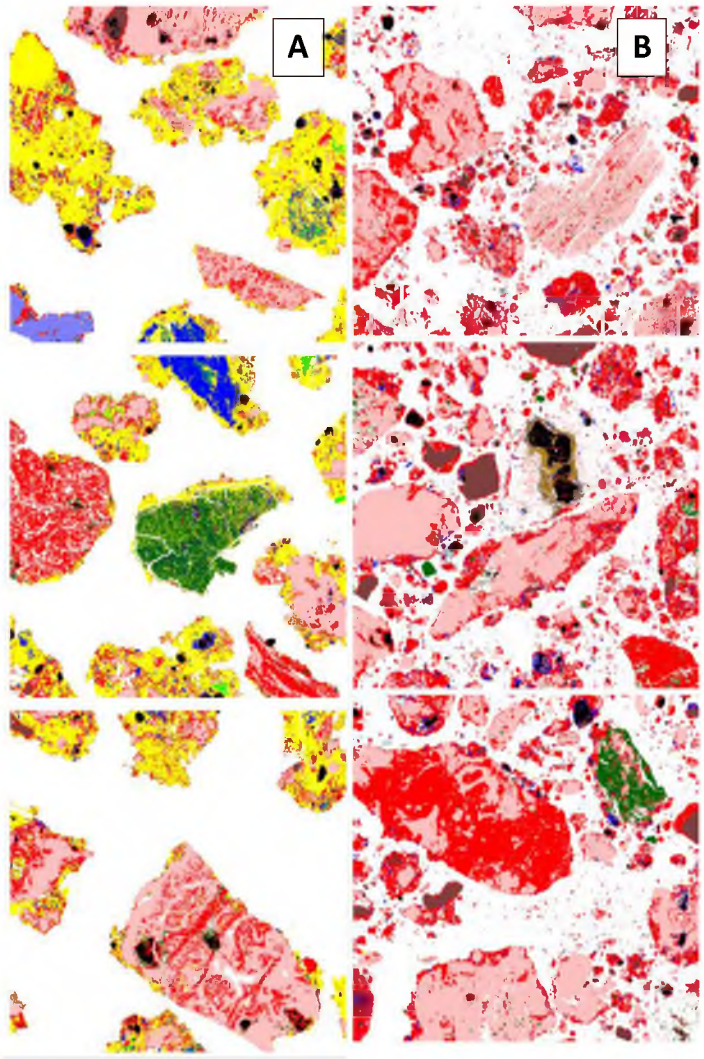

Figure 88. QEMSCAN images of agglomerate (A) and leached residual (B) samples of 972 g/L sulfuric acid concentration and 19 % moisture content agglomeration condition.

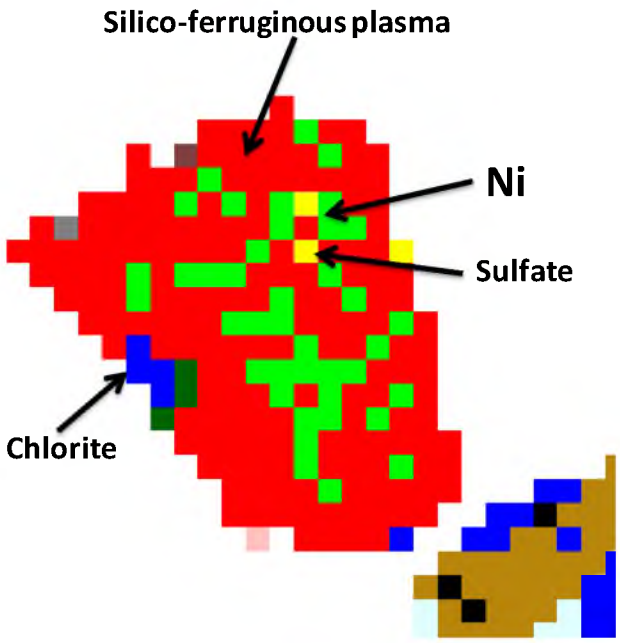

Figure 89. QEMSCAN image illustrates the silico-ferruginous plasma phase containing nickel after leaching experiment

The unidentified phase contained various amounts of nickel. This phase may be the leached sulfate phase, or leached clays and a precipitated amorphous phase.

The nickel extraction rates during the leaching experiment have been affected by the acid addition rates. Tables 39 and 40 illustrate the relationship between nickel extraction rate, acid addition amount and mineral phases. As the acid addition rates increased, the nickel extraction rates also increased. However, when the acid addition reached 100.5 kg/tonne, the nickel extraction did not increase further. The 61.3 kg/tonne of acid addition may have been enough for predissolving the acid-consuming phases in the agglomerate body. Further additional acid did not increase the dissolution rate of acid-consuming phases.

Table 38. Example of electron microprobe data of leached residual samples.

Sample	NiO (%)	CoO (%)	Fe_2O_3 (%)	Al_2O_3 (%)	SiO_2 (%)	MgO (%)	MnO (%)	Cr_2O_3 (%)	SO_3 (%)	Sum (%)	Phases
1	0.28	0.00	14.66	0.36	78.63	0.29	0.25	0.50	0.03	95.00	Plasma
2	0.21	0.00	3.12	0.51	92.80	0.08	0.01	0.02	0.00	96.77	Plasma
3	0.21	0.04	1.09	0.65	94.59	1.78	0.02	0.03	0.03	98.45	Plasma
4	0.08	0.00	2.23	0.03	93.97	0.02	0.00	0.05	0.00	96.37	Plasma
5	0.06	0.00	0.29	0.01	87.05	0.42	0.00	0.03	0.01	87.88	Plasma
6	5.59	0.00	28.19	0.56	20.80	0.78	0.02	0.29	0.40	56.63	Un-Identified
7	0.41	0.00	27.74	12.59	23.96	0.22	0.10	0.87	0.53	66.42	Un-Identified
8	0.53	0.00	19.23	4.66	24.75	0.88	0.03	0.54	0.21	50.84	Un-Identified
9	0.15	0.00	6.32	10.96	36.07	18.25	0.03	0.44	0.15	72.35	Un-Identified
10	0.49	0.00	4.24	6.19	43.37	1.16	0.00	0.13	0.10	55.67	Un-Identified

Table 39. The relationship between nickel extraction rate, acid addition amount and sulfate and silico-ferruginous plasma phases.

Nickel Extraction rate (%)	Nickel Extraction Rate within First Week (%)	Acid Addition (kg/tonne)	Sulfate Phase Area Percent (%)				Silico-ferruginous plasma Phase Area Percent (%)			
			Agglomerates		Leached Residuals		Agglomerates		Leached Residuals	
			1	2	1	2	1	2	1	2
48.9	18.0	25.4	13.0	29.8	0.1	1.0	20.1	19.4	31.7	29.5
48.2	20.4	41.6	22.9	48.0	0.4	2.2	11.4	9.1	47.2	45.0
49.2	25.6	60.2	43.0	46.2	0.1	0.2	11.0	17.8	27.8	36.9
58.7	31.6	61.3	32.6	52.1	0.1	0.1	16.1	14.2	37.3	36.3
54.8	34.2	100.5	33.2	52.0	0.0	0.1	20.0	12.6	36.2	31.2

Table 40. The relationship between nickel extraction rate, acid addition amount and clays.

Nickel Extraction rate (%)	Nickel Extraction Rate within First Week (%)	Acid Addition (kg/tonne)	Chlorite/Smectite/Vermiculite/Serpentine Phase Area Percent (%)			
			Agglomerates		Leached Residuals	
			1	2	1	2
48.9	18.0	25.4	4.9	11.8	3.2	4.1
48.2	20.4	41.6	9.5	3.5	5.5	4.9
49.2	25.6	60.2	2.5	4.7	3.4	3.6
58.7	31.6	61.3	8.0	6.3	3.5	3.9
54.8	34.2	100.5	5.1	2.9	2.9	3.6

The amount of sulfate phase in the agglomerates also has the same trend as the nickel extraction rates. The sulfate phase resulted from the reaction of sulfuric acid solution and fine particles to create agglomerates. It increased as the acid addition rates increased until the acid addition rate reached 100.5 kg/tonne.

The extraction rates of nickel were highest in the first week of leaching (Chapter 5). This is related to the amount of sulfate phase in the agglomerates. The more sulfate phases in the agglomerates, the greater the extraction rate was.

Clay minerals and silico-ferruginous plasma phases do not have distinct relationships with acid addition rates. However, the clay amount in the leached residual samples decreased from agglomerate samples. On the other hand, the amount of silico-ferruginous plasma in leached residuals increase from agglomerates. The clay minerals left in agglomerates were further leached by leaching solution; therefore, the amount of clays in the leached residuals decreased. Since the clays dissolved, the phases left in leached residual samples are the relatively insoluble minerals which are quartz, chromite and silico-ferruginous plasma phases. Therefore, the silico-ferruginous plasma phase in leached residual samples seems to increase from agglomerates samples.

CHAPTER 7

CONCLUSIONS

The agglomeration, leaching and mineralogy of a nickel laterite ore from Brazil were investigated. Agglomeration was examined as a function of solution addition volume, acid concentration, drum rotation speed and mixing time. Leaching was studied as a function of agglomeration conditions and evaluated in terms of breakthrough time, draw down volumes and metal extraction rates. Finally, the mineralogy of the feed ore, agglomerates and leach residual was investigated to understand the underlying effects of agglomeration.

Agglomeration was evaluated in terms of size distribution, electrical conductivity and bed permeability. Agglomerate size distributions (ASDs) were affected by solution addition volume, acid concentration and mixing time. Agglomerate size (D_{10} and D_{50}) increased as the amount of solution addition during agglomeration increased. More solution added during agglomeration provides more liquid phase to fill the void between and inside the particles, creating capillary forces to attach the particles together. However, agglomerate sizes decreased as the acid concentration of the solution added during agglomeration increases since the liquid volume introduced to the agglomeration decreases as the acid concentration increases at constant moisture. The amount of fines (-1.7 mm) in the ores decreased as more solution was added during agglomeration.

However, mud did form when excess liquid was added during agglomeration. Drum speed had minimal effect on size distribution. Increasing mixing time increased agglomerate sizes slightly.

Electrical conductivity of agglomerates was affected by the acid concentration, solution volume, compaction and nature of the ores. The sulfuric acid concentration and moisture content had strong effects on electrical conductivity of the nickel laterite agglomerates. The electrical conductivity of nickel laterite agglomerates follows a similar trend as the electrical conductivity of sulfuric acid. The electrical conductivity increases as more solution volume was added during agglomeration. The electrical conductivities of agglomerates are less varied when 20.4 kg of load was applied.

Permeability of agglomerate beds was related to the agglomerate sizes. Coarser agglomerates create more void spaces within the agglomerate bed and allow more solution to flow through. Agglomerate strength is another factor that affected permeability. Agglomerates produced from high acid concentration tend to disintegrate during permeability test and had low permeability.

After leaching, the sizes of leached residuals were smaller than those of agglomerates before leaching. However, the leach residual sizes were still coarser than the feed sizes. It is obvious that the agglomerates were deteriorated during the leaching experiments. More fine particles were found in the leached residuals than in the agglomerated feed ore. The amount of fines at different column depths of each column showed significant variation. Agglomerates produced with stronger acid were weaker than those produced with weaker acid.

The density of pregnant leaching solution (PLS) was influenced by the agglomeration solution density and mineral dissolving. However, the effects of these two factors on the PLS density are not obvious. The pH of PLS started low due to the high concentration of acid used during agglomeration, then increased as leaching times increased and then slowly decreased toward the pH of leaching solution as mineral dissolution slowed. The ORP decreased slightly within the first week of leaching and then remained stable.

Within 90 days of leaching, the maximum extraction rates of nickel, cobalt, iron, aluminum, magnesium and manganese were 58%, 38%, 22%, 28%, 48% and 28%, respectively. The amount of acid addition during agglomeration affected the extraction rate of nickel, iron, aluminum, magnesium and manganese, especially within the first week. Higher acid concentration of the agglomeration solution resulted in higher extraction rates. The solution volume added during agglomeration seemed to have little effect on the extraction rate of interested elements.

The leach selectivity between nickel and other elements such as iron, aluminum and magnesium can be observed via Ni:Fe, Ni:Al and Ni:Mg ratios. The Ni:Fe ratios of the PLS are significantly decreased from those in the feed ore which indicated preferential Ni dissolution to Fe. The Ni:Al and Ni:Mg ratios decrease slightly from the feed ore ratios, showing less preferential leaching.

The shrinking core model was examined and did not fit the leaching kinetics of nickel laterite column leaching for the entire 90 days. The metal leach kinetics of nickel laterite agglomerates are complicated and hard to predict. The agglomerate size distribution changed during leaching; the variation of leaching solution strength,

liberation of metals and porosity of agglomerates likely contribute to the leaching kinetics and should be studied in order to understand the leach kinetics of nickel laterite agglomerates.

The main minerals in the feed ore are quartz, silico-ferruginous plasma and clays. Clays, including smectite and chlorite, are the main nickel-bearing minerals. Nickel can also be found in silico-ferruginous plasma. After agglomeration, a new "sulfate phase" was formed. This phase is the intimate mixture of Fe-Alunogen, plasma and clays. As expected, the amount of sulfate phase increases as the amount of acid addition during agglomeration increases. Two types of agglomerates, layered and coalesced, can be observed using QEMSCAN.

After leaching, the percentages of quartz, silico-ferruginous plasma and iron oxy-hydroxide phases increased as the "sulfate phase" and clay minerals were dissolved. Chromite, talc, kaolinite and phlogopite phases are relatively stable. Nickel remains in the silico-ferruginous plasma and some unidentified phases. The nickel content within silico-ferruginous plasma is quite constant in the feed, agglomerates and leached residuals. Therefore, the nickel extraction cannot reach 100% unless the nickel trapped inside silico-ferruginous plasma is liberated.

APPENDIX A

THE ASDs OF AGGLOMERATES IN COLUMN LEACHING EXPERIMENT

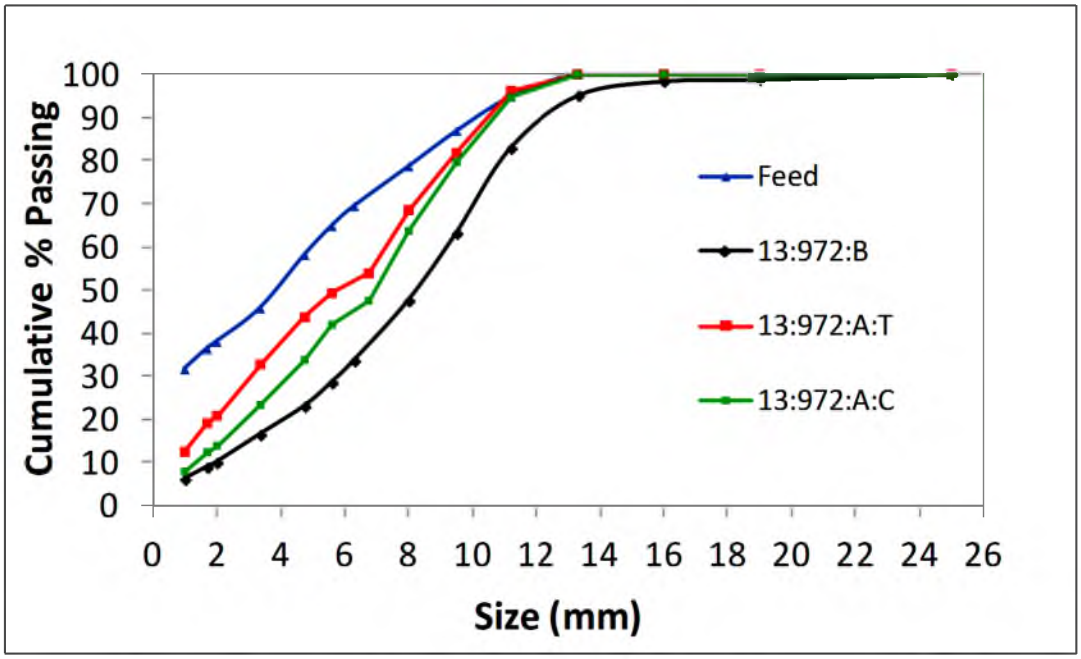

Figure 90. The agglomerate size distributions of the agglomerates at 13% moisture content and 972 g/L acid concentration condition after column leaching experiments were completed are compared with the agglomerate size distributions prior to leaching and the ore feed distribution prior to agglomeration.

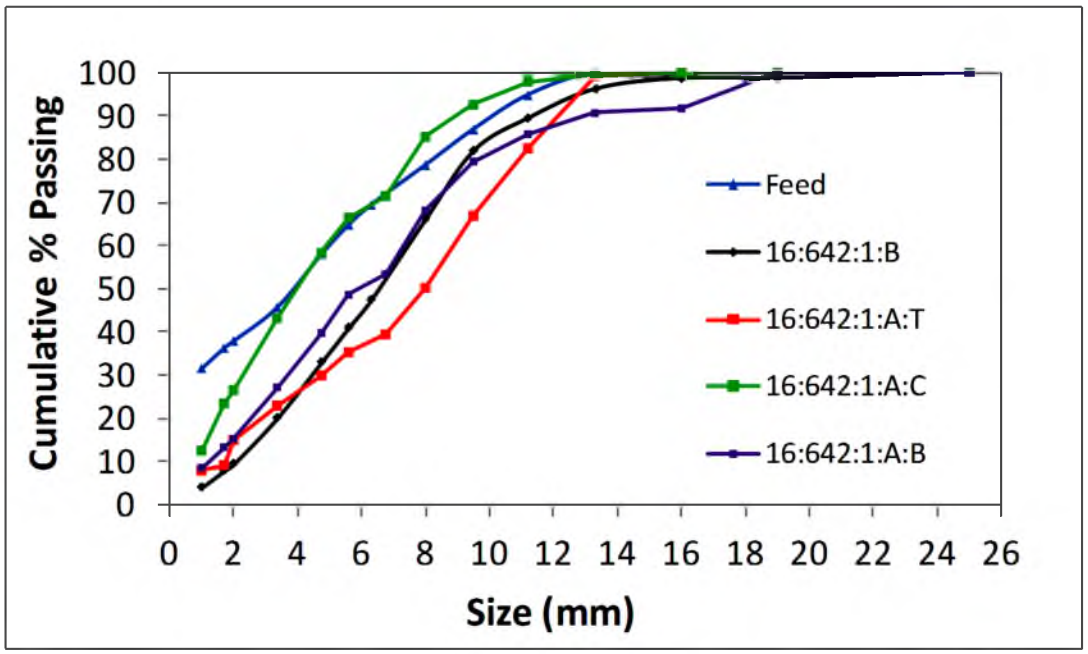

Figure 91. The agglomerate size distributions of the agglomerates at 16% moisture content and 642 g/L acid concentration condition (first replicate) after column leaching experiments were completed are compared with the agglomerate size distributions prior to leaching and the ore feed distribution prior to agglomeration.

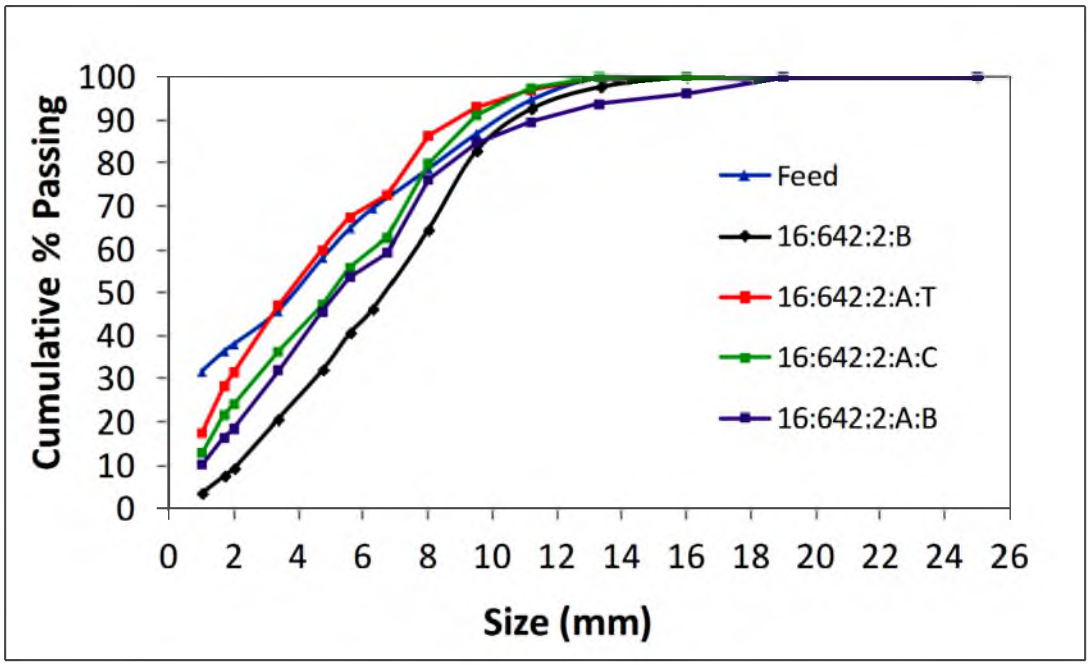

Figure 92 . The agglomerate size distributions of the agglomerates at 16% moisture content and 642 g/L acid concentration condition (second replicate) after column leaching experiments were completed are compared with the agglomerate size distributions prior to leaching and the ore feed distribution prior to agglomeration.

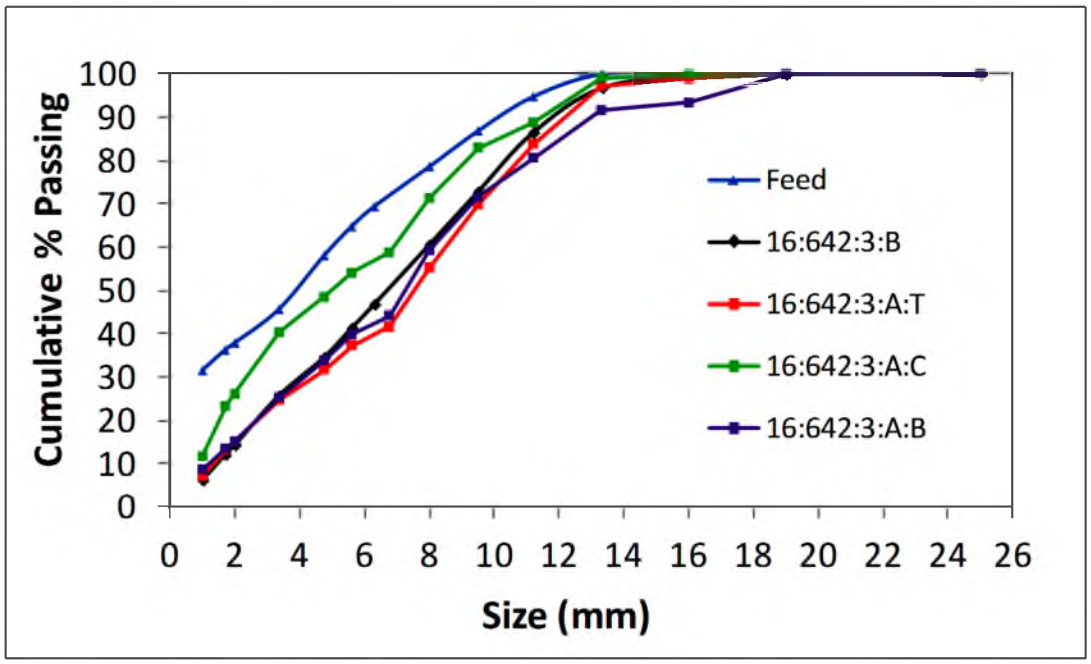

Figure 93. The agglomerate size distributions of the agglomerates at 16% moisture content and 642 g/L acid concentration condition (third replicate) after column leaching experiments were completed are compared with the agglomerate size distributions prior to leaching and the ore feed distribution prior to agglomeration.

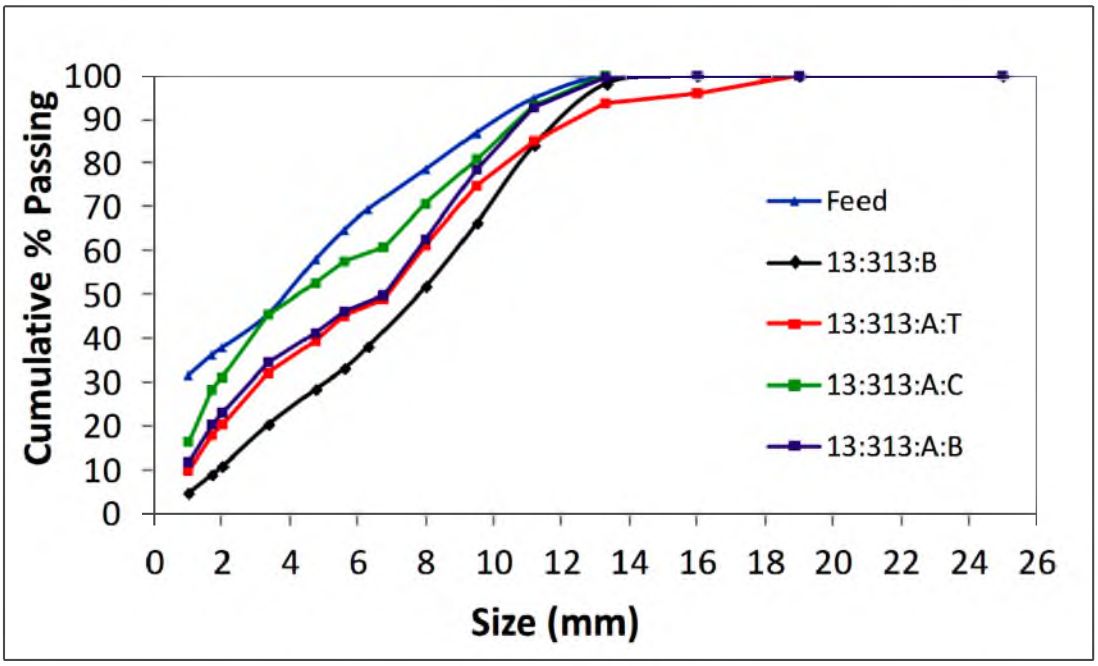

Figure 94. The agglomerate size distributions of the agglomerates at 13% moisture content and 313 g/L acid concentration condition after column leaching experiments were completed are compared with the agglomerate size distributions prior to leaching and the ore feed distribution prior to agglomeration.

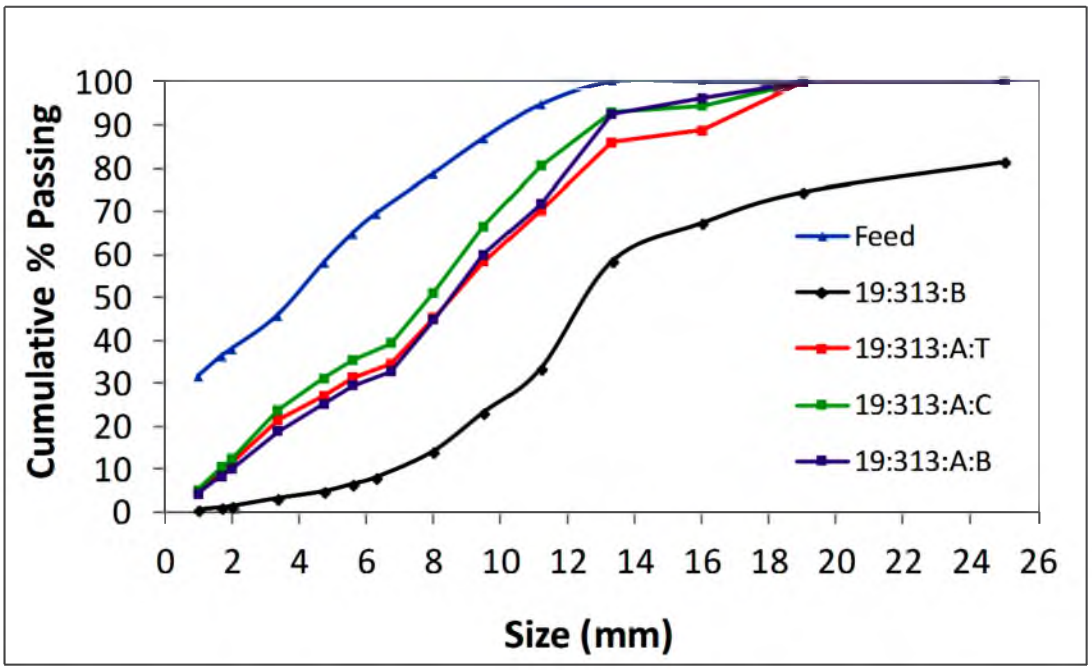

Figure 95. The agglomerate size distributions of the agglomerates at 19% moisture content and 313 g/L acid concentration condition after column leaching experiments were completed are compared with the agglomerate size distributions prior to leaching and the ore feed distribution prior to agglomeration.

APPENDIX B

THE EXTRACTIONS OF ANALYZED ELEMENTS AT DIFFERENT AGGLOMERATION CONDITIONS

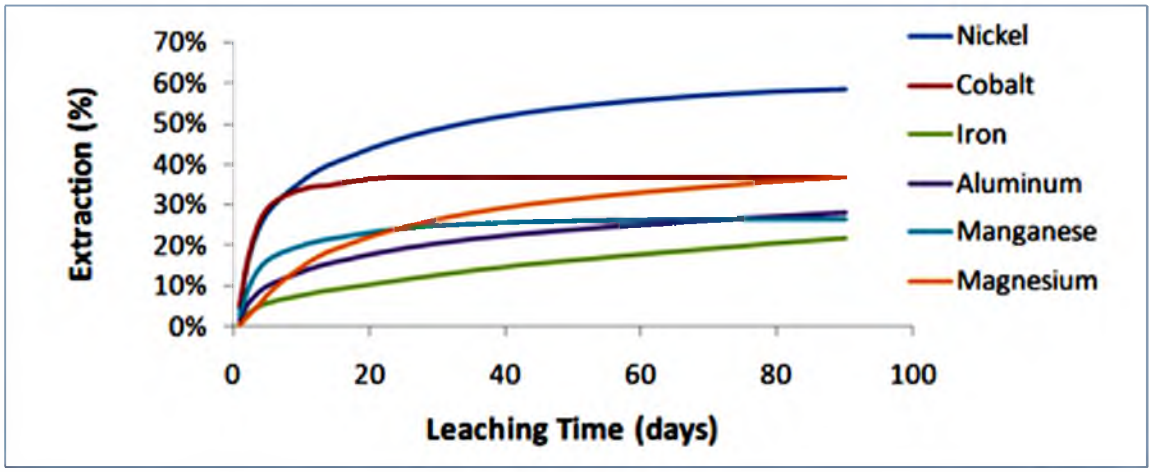

Figure 96. The extraction of analyzed elements of 972 g/L acid concentration and 13% moisture content.

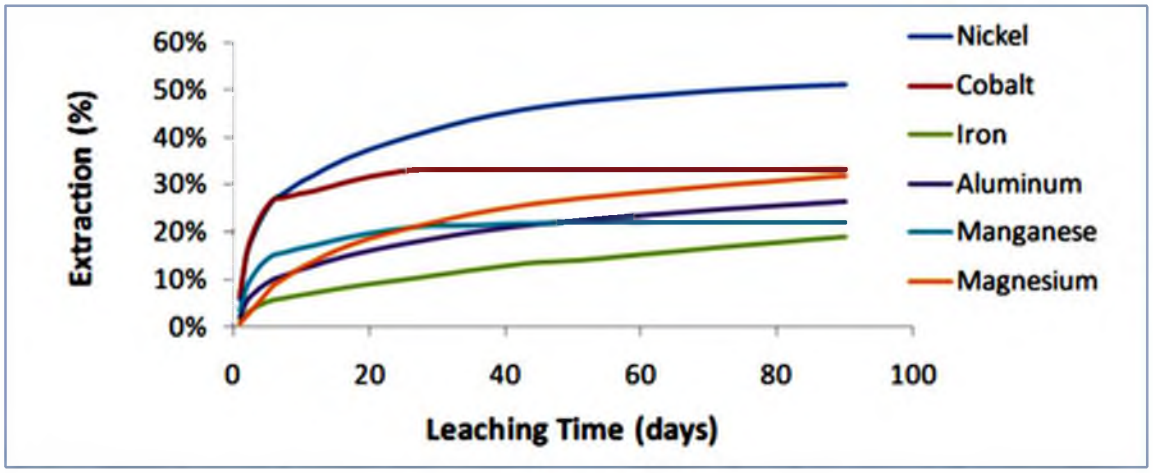

Figure 97. The extraction of analyzed elements of 642 g/L acid concentration and 16% moisture content (first replicate).

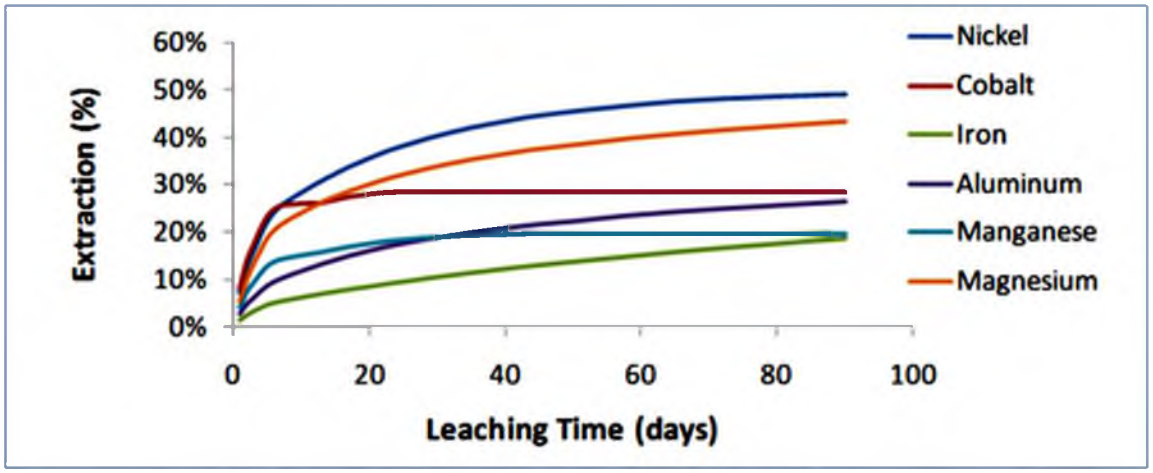

Figure 98. The extraction of analyzed elements of 642 g/L acid concentration and 16% moisture content (second replicate).

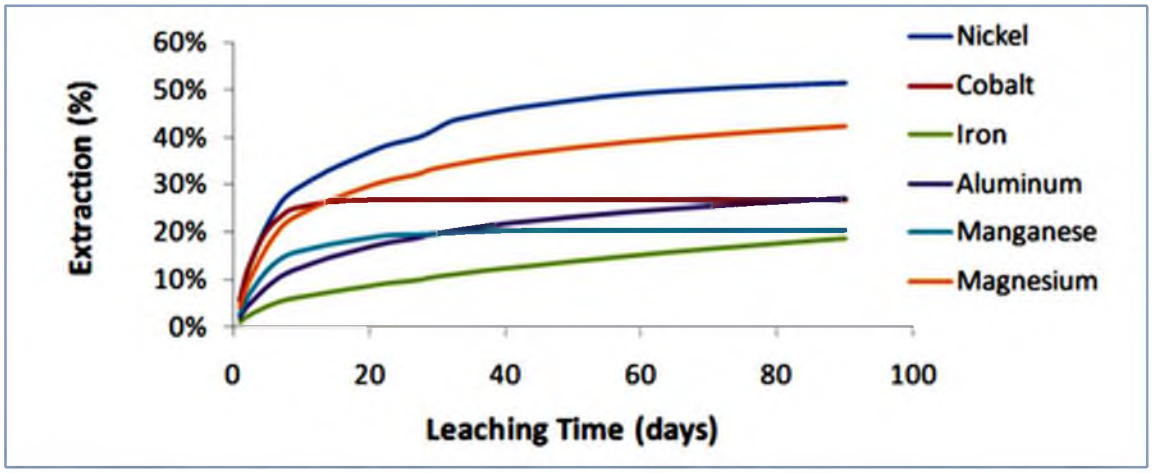

Figure 99. The extraction of analyzed elements of 642 g/L acid concentration and 16% moisture content (third replicate).

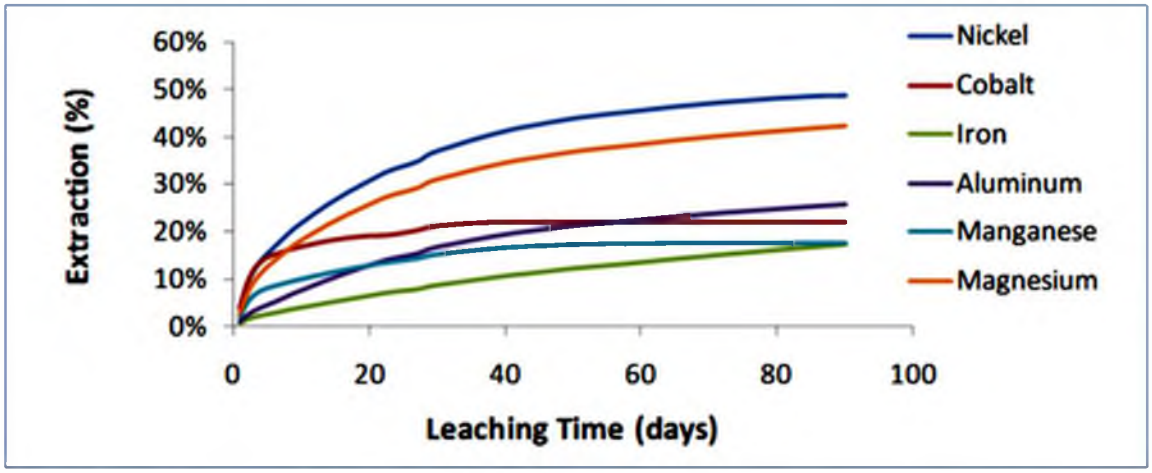

Figure 100. The extraction of analyzed elements of 313 g/L acid concentration and 13% moisture content.

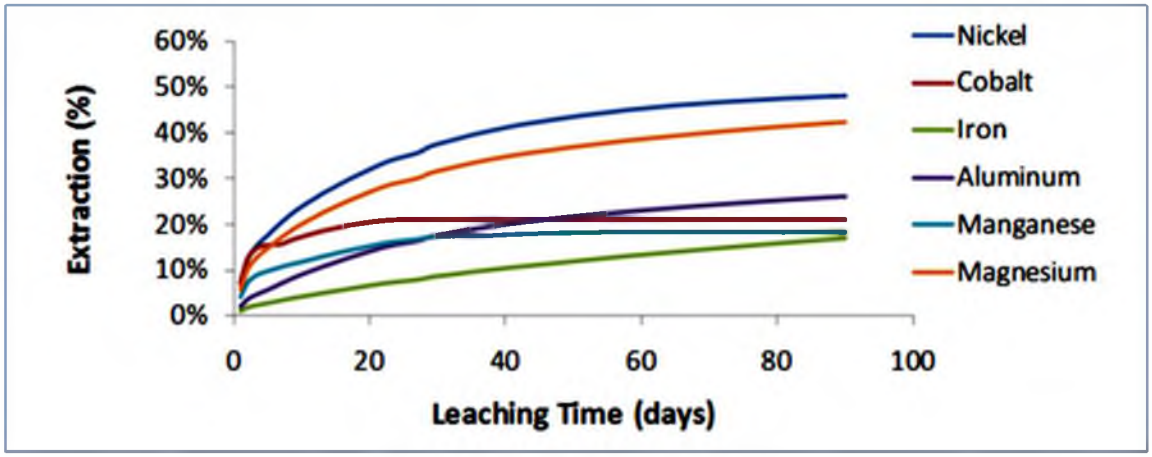

Figure 101. The extraction of analyzed elements of 313 g/L acid concentration and 19% moisture content.

APPENDIX C

THE EXTRACTION OF INTERESTED ELEMENTS AT DIFFERENT ACID CONCENTRATION USED DURING AGGLOMERATION

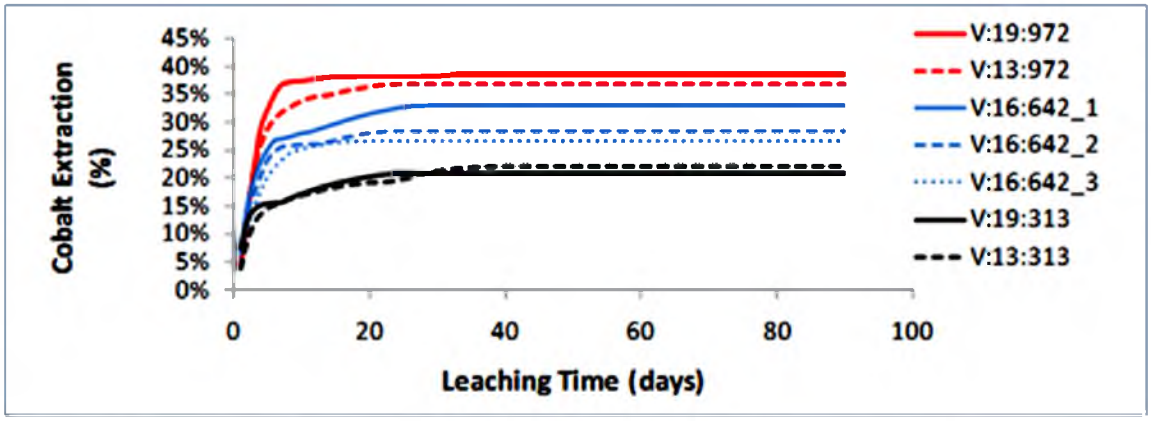

Figure 102. The extraction of cobalt at different agglomeration conditions.

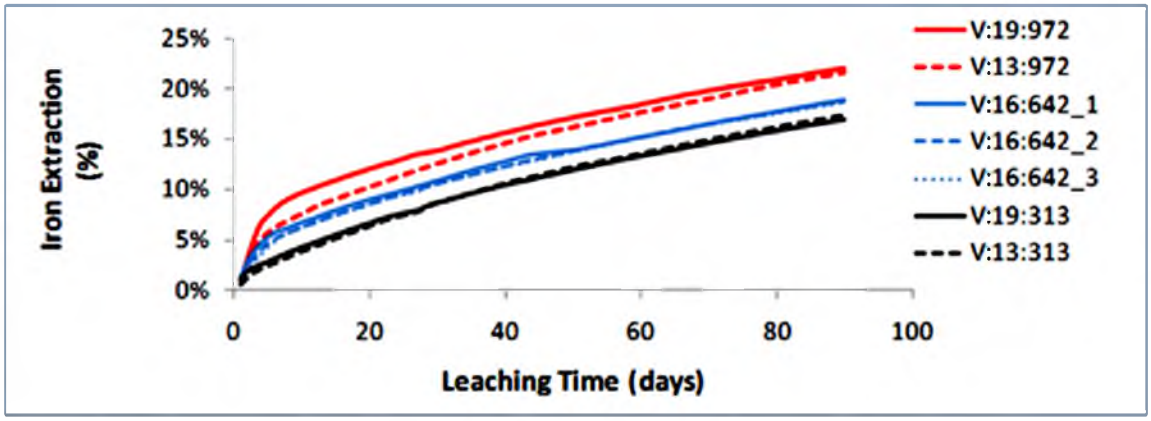

Figure 103. The extraction of iron at different agglomeration conditions.

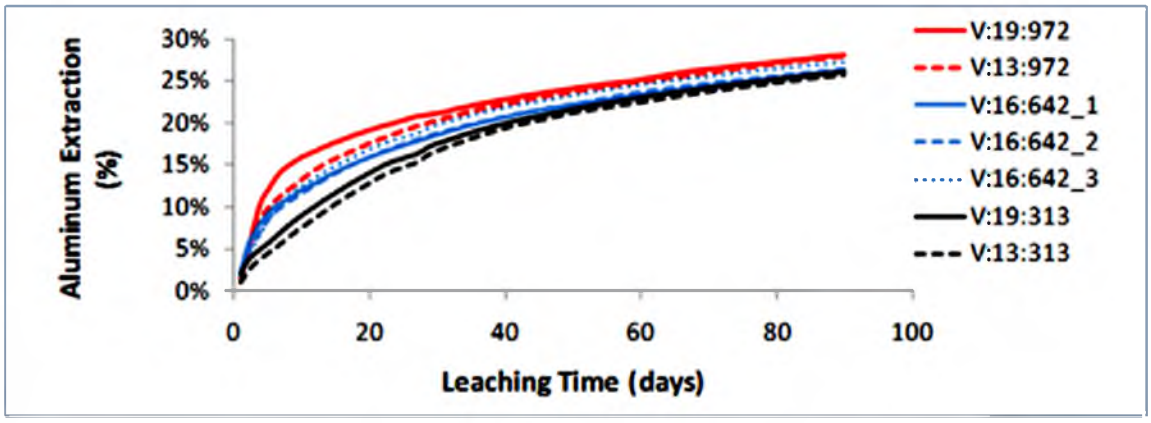

Figure 104. The extraction of aluminum at different agglomeration conditions.

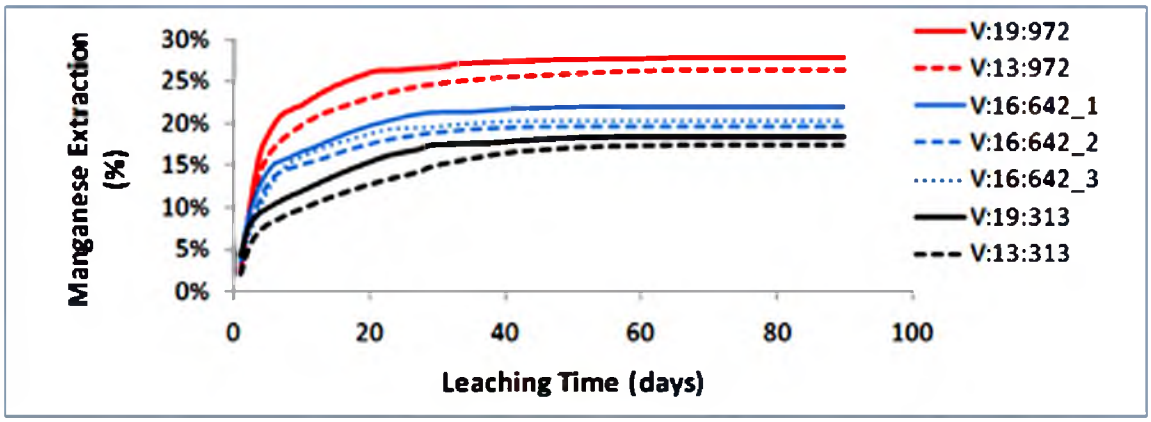

Figure 105. The extraction of manganese at different agglomeration conditions.

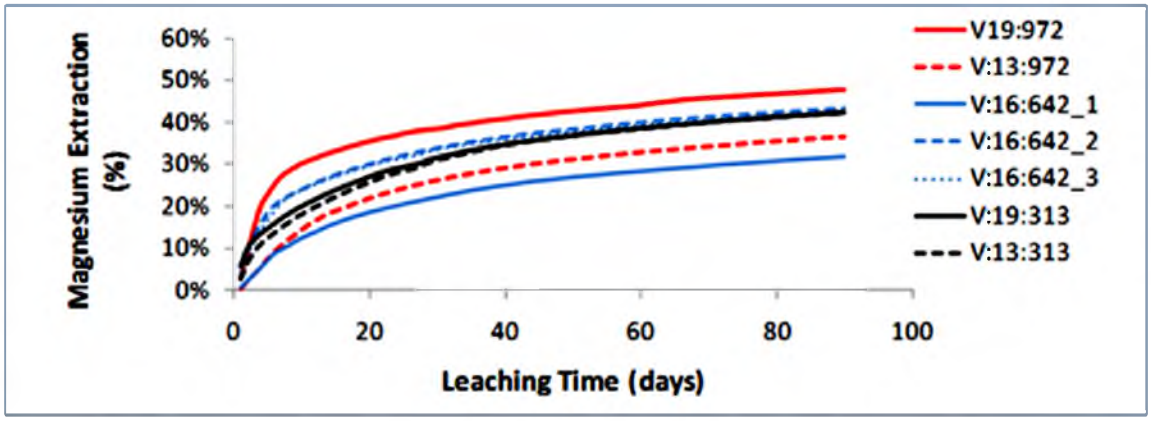

Figure 106. The extraction of magnesium at different agglomeration conditions.

APPENDIX D

THE RELATIONSHIP BETWEEN WATER AMOUNT ADDITION DURING AGGLOMERATION AND EXTRACTION RATE OF INTERESTED ELEMENTS

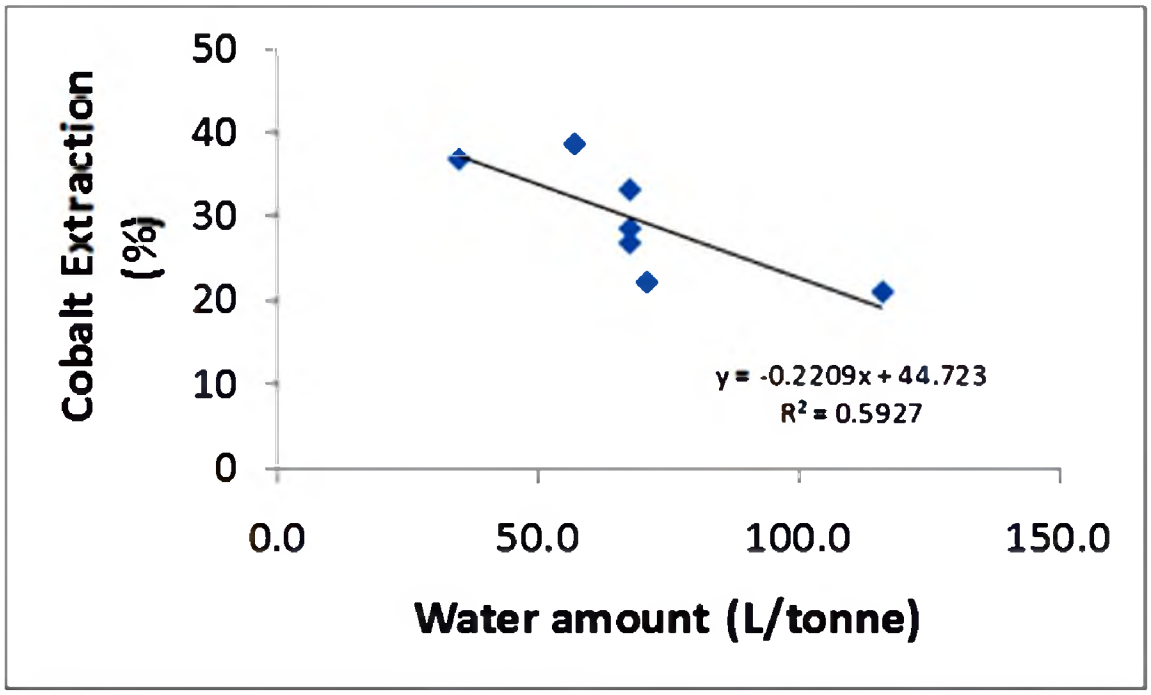

Figure 107. The relationship between water amount addition during agglomeration and cobalt extraction.

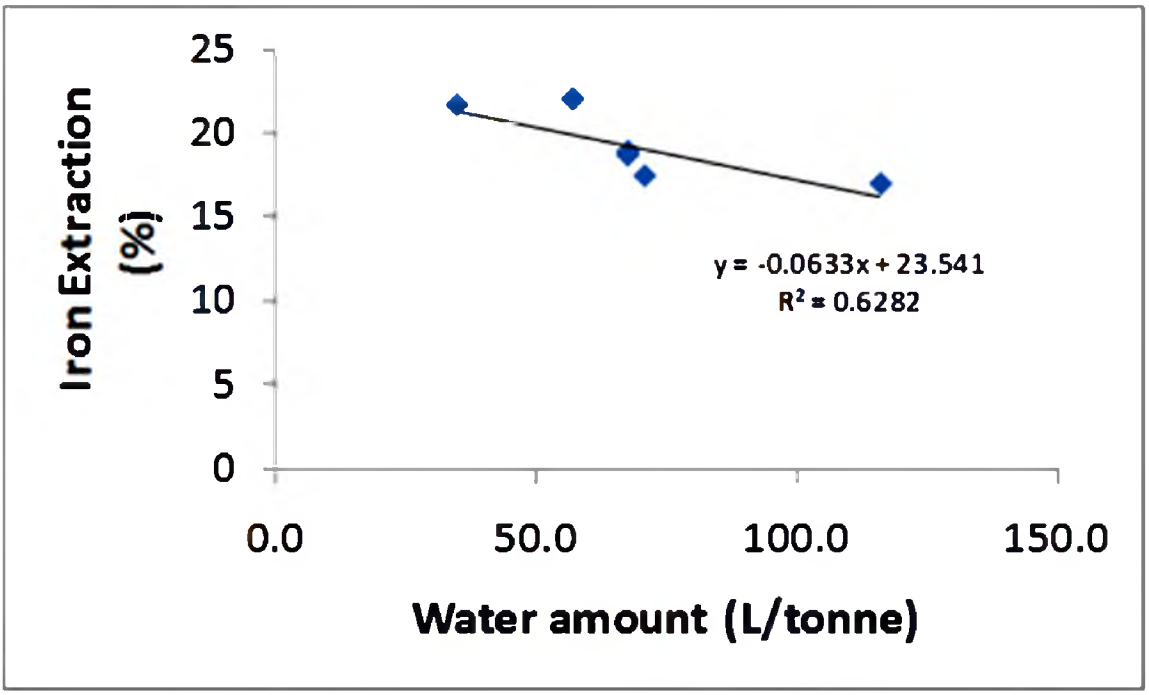

Figure 108. The relationship between water amount addition during agglomeration and iron extraction.

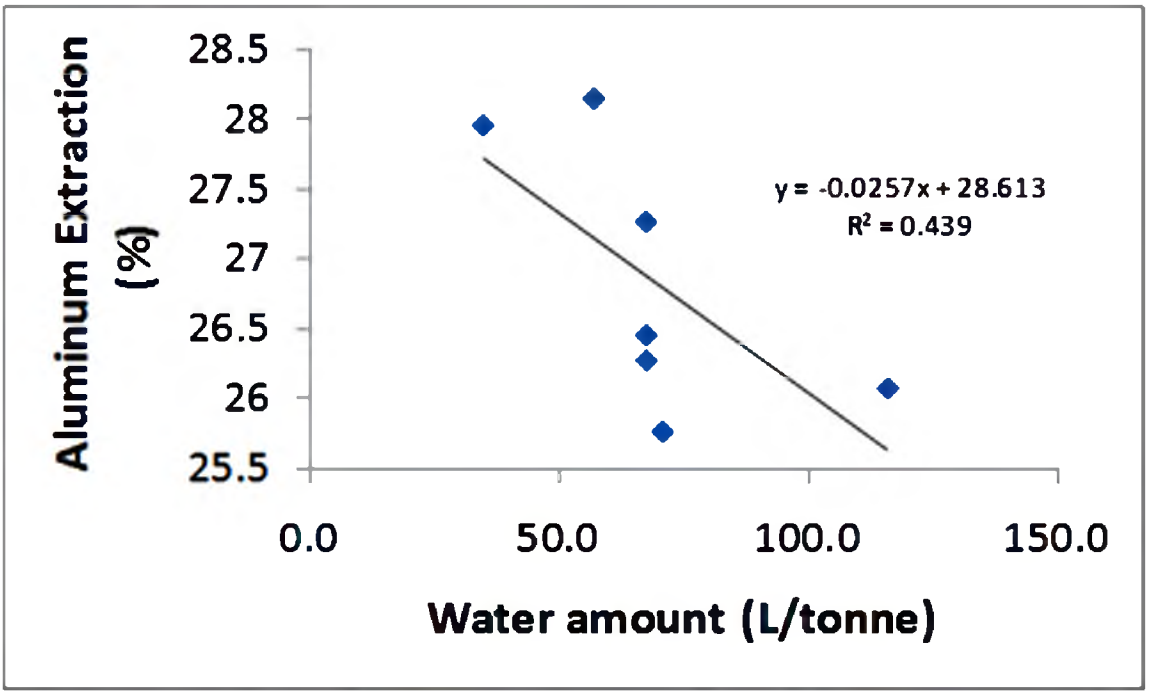

Figure 109. The relationship between water amount addition during agglomeration and aluminum extraction.

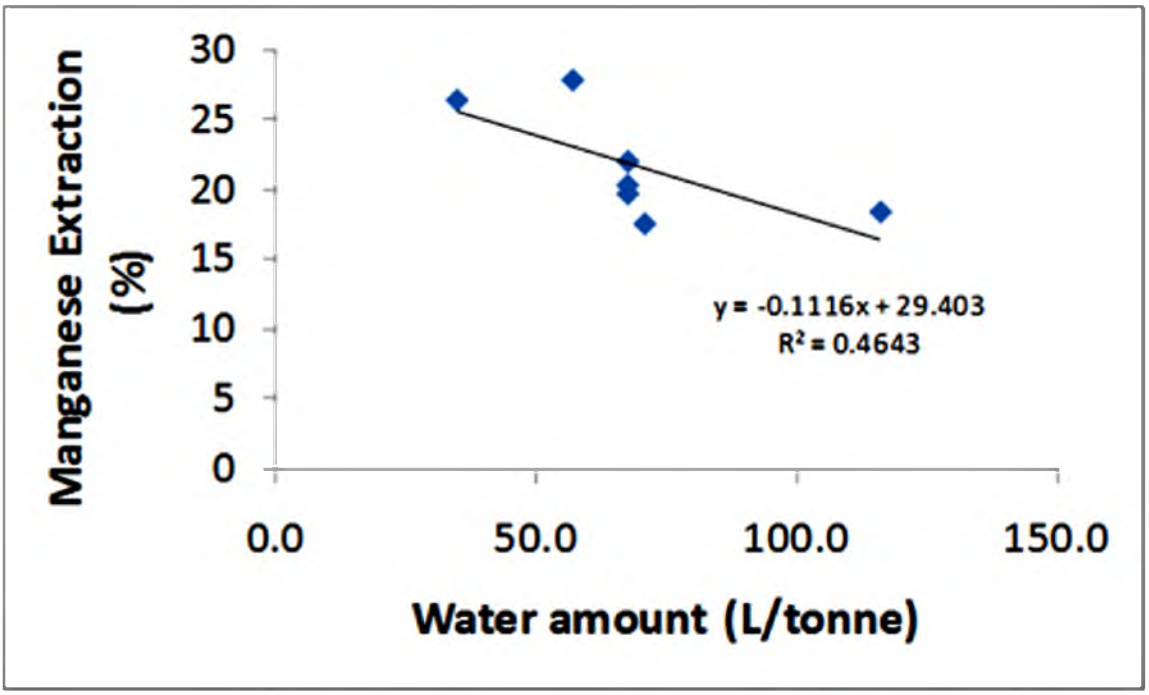

Figure 110. The relationship between water amount addition during agglomeration and manganese extraction.

REFERENCES

1. Agatzini-Leonardou, S. & Dimaki, D., 1994, "Heap leaching of poor nickel laterites by sulphuric acid at ambient temperatures", *Hydrometallurgy* 94, 193-208

2. Agatzini-Leonardou, S. & Zafiratos, I. G., 2004, 'Benefication of a Greek serpentinic nickeliferous ore part II. Sulfuric acid heap and agitation leaching', *Hydrometallurgy* 74, 267-275

3. Agrawal, R. & Naveen, Y., 2011, 'Pharmaceutical processing: A review on wet granulation technology', *International Journal of Pharmaceutical Frontier Research* 1(1), 65-83

4. Amer, A. M. & Ibrahim, I. A., 2001, 'Aspects of leaching and kinetics of some Egyptian iron ore", *Erzmetall* 54, 619-624

5. Bear, J., 1988, *Dynamics of Fluids in Porous Media*, Dover Publication, New York.

6. Boldt Jr., J. R., 1967, *The Winning of Nickel*, The Hunter Rose Company.

7. Bouffard, S. C., 2005, 'Review of agglomeration practice and fundamentals in heap leaching', *Mineral Processing & Extractive Metallurgy Review* 26, 233-294

8. Bouffard, S. C., 2008, 'Agglomeration for heap leaching: Equipment design, agglomerate quality control, and impact on the heap leach process'. *Mineral Engineering* 21, 1115-1125

9. Butt, C. R. M., Morris, R. C. & Piantone, P., 2005, 'Ore forming processes related to lateritic weathering', *2005 Society of Economic Geologists, Inc., Economic Geology 100th Anniversary Volume*, 681-722

10. Capes, C. E., 1980, *Handbook of Powder Technology Volume 1: Particle Size Enlargement*, Elsevier Scientific Publishing Company, New York

11. Castro, F. & Pereira, G., 2009, 'Characterization of the nickel laterite sample and guidelines for column leach tests project AMIRA P986', Vale Mineral Development Center, Brazil.

12. Chamberin, P. D., 1986, 'Agglomeration: Cheap insurance for good recovery when heap leaching gold and silver ores', *Mining Engineering*, 1986, 1105-1109

13. Chander, S., 1982, 'Atmospheric pressure leaching of nickeliferous laterites in acidic media', *Transactions of Indian Institute of Metals* 35(4), 366-371

14. Crundwell, F., Moats, M., Ramachandran, V., Robinson, T. & Davenport, W., G., 2011, *Extractive Metallurgy of Nickel, Cobalt and Platinum Group Metals*, Elsevier

15. Curlook, W., 2004, 'Direct atmospheric leaching of saprolitic nickel laterite ores with sulphuric acid', *The Minerals, Metals & Materials Society: International Laterite Nickel Symposium 2004 Atmospheric Leaching*, 385-392

16. Dalvi, A. D., Bacon, W. G. & Osborne, R. C., 2004, 'The past and the future of nickel laterites', *PDAC 2004 International Convention, Trade Show and Inventors Exchange*, 1-27

17. Duyvesteyn, W. P. C., Liu, H. & Davis, M., 2001, *Heap Leaching of Nickel Containing Ore*, United States Patent, US 6312500 B1

18. Eisele, T. C., Gurtler, J. A, Hardison, C. A. & Kawatra, S. K, 2005, 'Determination of acid resistance of agglomerates in copper heap leaching', *SME Annual Meeting Preprint 05-37*, Feb. 28-Mar. 2, Salt Lake City, Utah

19. Elliot, A., Fletcher, H., Li, J., Watling, H. & Robinson, D. J., 2009, "Heap leaching of nickel laterites-A challenge and an opportunity", *Hydrometallurgy of Nickel and Cobalt 2009, Proceeding of the 39th Annual Hydrometallurgy Meeting held in the conjunction with the 48th Annual Conference of Metallurgists of CIM,* 537-549

20. Free, M. L., 2004, *Chemical Processing and Utilization of Metals in Aqueous Media,* 2nd edn, Copley Custom Textbooks, Michigan

21. Garcia, J. A. & Jorgensen, M. K., 1997, 'Agglomeration and heap testing requirements for high clay ores', *Randol Gold Forum 97 Conference and Exhibition*, 143-146

22. Georgiou, D. & Papangelakis, V. G., 1998, 'Sulphuric acid pressure leaching of a limonite laterite: Chemistry and kinetics', *Hydrometallurgy* 49, 1998, 23-46

23. Gibson, R. W. & Rice, N. M., 1997, 'A hydrochloric acid process for nickeliferous laterites', *Proceedings of the Nickel-Cobalt 97 International Symposium: Hydrometallurgy and Refining of Nickel and Cobalt* 1, pp. 247-261

24. Gillies, A., 2005, 'NORNICO heap leach nickel laterite metallurgy testwork update – Positive results', ASX Announcement and Press Release, Metallica Minerals Limited

25. Golightly, J. P., 1979, 'Nickeliferous laterites: A general description', *International Laterite Symposium*, 3-23

26. Golightly, J. P., 1981, 'Nickeliferous laterite deposits', *Economic Geology 75th Anniversary Volume*, 710-735

27. Guo, X., Shi, W. T., Li, D. & Tian Q. H., 2011, 'Leaching behavior of metals from limonitic laterite ore by high pressure acid leaching', *Transactions of Nonferrous Metals Society of China* 21, 191-195

28. Halikia, I., 1991, 'Parameters influencing kinetics of nickel extraction from a Greek laterite during leaching with sulfuric acid at atmospheric pressure', *Transactions of the Institution of Mining and Metallurgy, Section C: Mineral Processing and Extractive Metallurgy* 100, 154-164

29. Harris, B. & Magee, J., 2003, 'Atmopheric chloride leaching: The way forward for nickel laterites', *Hydrometallurgy 2003: Fifth International Conference in Honor of Professor Ian Ritchie, Vol. 1: Leaching and Solution Purification*, 501-515

30. Harris, B., Lakshmanan, V. I. & Sridhar, R., 2004, *Process for the Recovery of Value Metals from Material Containing Base Metal Oxides*, United State Patent, US 2004/0228783 A1

31. Harris, B., White, C., Jansen, M. & Pursell, D., 2006a, 'A new approach to the high concentration chloride leaching of nickel laterites', *ALTA Nickel/Cobalt 11*, 1-20

32. Harris, B., White, C. & Demopoulos, G. P., 2006b, 'Iron control in high concentration chloride leach processes', *Third International Symposium on Iron Control in Hydrometallurgy*

33. Head, K. H., 1994, *Manual of Soil Laboratory Testing Volume 2: Permeability, Shear Strength and Compressibility Tests*, Pentech Press Limited, London

34. Horizonte, S. G. & Horizonte D. O., 2007, *Process for Extraction of Nickel, Cobalt, and Other Base Metals from Laterite Ores by Using Heap Leaching and Product Containing Nickel, Cobalt, and Other Metals from Laterite Ores*, European Patent, EP 1790739 A1

35. Hubler, W. G. & Ratcliffe, F., 1938, *Method of Treating Lateritic Ores*, United State Patent, 2105456

36. Kawatra, S. K., Eisele, T. C., Gurtler, J. A. & Lewandowski, K. A., 2005, 'Novel binders and methods for agglomeration of ore' Semiannual Technical Progress Report, Department of Chemical Engineering, Michigan Technological University

37. Kinard, D. T. & Schweizer, A. A., 1987, 'Engineering properties of agglomerated ore in a heap leach pile', *Geotechnical Aspects of Heap Leach Design*, 55-64

38. King, M. G., 2005, 'Nickel laterite technology - finally a new dawn?', *Journal of the Minerals, Metals & Materials Society* 57(7), 35-39

39. Lewandowski, K. A., Gurtler, J. A., Eisele, T. C. & Kawatra, S. K., 2006, 'Determination of acid resistance of copper ore agglomerates in heap leaching', *Sohn International Symposium Advanced Processing of Metals and Materials, Vol. 6: New, Improved and Existing Technologies: Aqueous and Electrochemical Processing*, 109-124

40. Lewandowski, K. A. & Kawatra, S. K., 2007a, 'Agglomeration for copper heap leaching', *Cu2007 The John E. Dutrizac International Symposium on Copper Hydrometallurgy, Vol. IV (Book 1)*, 439-451

41. Lewandowski, K. A. & Kawatra, S. K., 2007b, 'Agglomeration binders to improve efficiency of copper heap leaching', *SME Annual Meeting Preprint 07-119*, Feb. 25-Feb. 28, Denver, Colorado

42. Lewandowski, K. A. & Kawatra, S. K., 2008, 'Development of experimental procedures to analyze copper agglomerate stability', *Minerals & Metallurgical Processing* 25(2), 110-116

43. Lewandowski, K. A. & Kawatra, S. K., 2009, 'Binders for heap leaching agglomeration', *Minerals & Metallurgical Processing* 26(1), 1-24

44. Lipiec, I. A. & Bautista, R. G., 1998, 'Considerations in the extraction of metal from heap leaches', *Transactions of the Indian Institute of Metals* 51(1), 7-16

45. Liu, H., Gillaspie, J. D., Lewis, C. A., Neudorf, D. & Barnett S., 2005, *Atmospheric Pressure Leach Process for Lateritic Nickel Ore*, United States Patent, US 2005/0226797 A1

46. Liu, H., 2006, *An Improved Process for Heap Leaching of Nickeliferous Oxidic Ores*, World Intellectual Property Organization, WO 2006/119559 A1

47. Maclver, B. N. & Hale, G. P., 1986, *Engineering and Design: Laboratory Soils Testing*, Office of the Chief Engineers, Dept. of the Army, Washington D. C.

48. McDonald, R. G. & Whittington, B. I., 2008a, 'Atmospheric acid leaching of nickel laterites review part I. sulphuric acid technologies', *Hydrometallurgy* 91, 35-55

49. McDonald, R. G. & Whittington, B. I., 2008b, 'Atmospheric acid leaching of nickel laterites review part II. chloride and bio-technologies', *Hydrometallurgy* 91, 56-69

50. Mihaylov, I., Krause, E., Colton, D. F., Okita, Y., Duterque, J. P. & Perraud, J. J., 2000, 'The development of a novel hydrometallurgical process for nickel and cobalt recovery from Goro laterite ore', *The Canadian Institute of Mining, Metallurgy and Petroleum Bulletin* 93, 124-130

51. Miller, G., 2006, 'The effective particle size in heap leaching', *Alta Copper* 12, 1-23

52. Miller, G. W. & Liu, H., 2005, *Process for Recovery of Nickel and Cobalt by Heap Leaching of Low Grade Nickel or Cobalt Containing Material*, World Intellectual Property Organization, WO 2005/005671 A1

53. Milligan, D. A. & Engelhardt, P. R., 1983, 'Agglomerated heap leaching at Anaconda's Darwin silver recovery project', Hiskey, J. B. (Ed.), *Gold and Silver Heap and Dump Leaching Practice*, *Society of Mining Engineers*, Colorado, 29-39

54. Mitarai, N. & Nori, F., 2006, 'Wet granular material', *Advances in Physics* 55(1-2), 1-45

55. Moats, M. S. & Janwong, A., 2008, 'The art and science of crushed ore agglomeration for heap leaching', *Hydrometallurgy 2008: Proceeding of the Sixth International Symposium in honor of Robert S. Shoemaker*, 912-917

56. Moore, D. M. & Reynolds Jr., R. C., 1989, *X-ray Diffraction and the Identification and Analysis of Clay Minerals*, Oxford University Press, New York

57. Mora, N., Moroney, A. S. & Thomas, S., 2010, *Method of Agglomeration*, World Intellectual Property Organization, WO 2010/085857 A1

58. Moskalyk, R. R., & Alfantazi, A. M., 2002, 'Nickle laterite processing and electrowinning practice', *Minerals Engineering* 15, 593-605

59. Munroe, N. D. H., 1997, 'The leaching of nickeliferous laterite with ferric chloride', *Metallurgical and Materials Transactions B* 28B, 995-1000

60. Norgate, T., & Jahanshahi, S., 2010, 'Low grade ores – smelt, leach or concentrate?', *Mineral Engineering* 23, 65-73

61. Nossen, E. S., 1959, *Extraction of Metals from Ores*, Canadian Patent, CA 576372

62. Oxley, A., Sirvanci, N. & Purkiss, S., 2007, 'Caldag nickel laterite atmospheric heap leach project', *Association of Metallurgical Engineering of Serbia* 13(1), 5-10

63. Pietsch, W., 1991, *Size Enlargement by Agglomeration*, John Wiley & Sons Ltd, England

64. Readett, D., Meadows, N. & Rodriguez, M., 2006, 'Murrin Murrin heap leaching project', *Metallurgical Plant Design and Operating Strategies (MetPlant 2006)*, 367-372

65. Reid, J. G., 1996, 'Laterite ores - nickel and cobalt resources for the future', *Proceeding of the 1996 Nickel Conference*, Kalgoorlie, Australia, November 27-29, pp 11-16

66. Robertson, S. W. & Van Staden, P. J., 2009, 'The progression of metallurgical testwork during heap leach design', *Hydrometallurgy Conference 2009*, 31-42

67. Robertson, S., Seyedbagheri, A., Van Staden, P. & Guzman, A., 2010, 'Advances in heap leach research and development', *ALTA 2010 Nickel-Cobalt-Copper*, 1-16

68. Rodriguez, M. & Wedderburn, B. J., 2007, *Hydrometallurgical Method for the Extraction of Nickel and Cobalt from Laterite Ores*, World Intellectual Property Organization, WO 2007/016737 A1

69. Rumpf, H., 1962, 'The strength of granules and agglomerates in agglomeration', *Proceedings of First International Symposium on Agglomeration*, 379-418

70. Sarojini, B., Rao, P. K. & Sant, B. R., 1972, 'Extraction of nickel from laterites of Orissa using dilute nitric acid', *Indian Journal of Technology* 10, 155-156

71. Schaafsma, S. H., 2000, Down-scaling of a fluidized bed agglomeration process, PhD Dissertation, University of Groningen

72. Sherrington, P. J. & Oliver, R., 1981, *Granulation*, Heyden & Son Ltd, London

73. Southwood, A. J., 1985, *The Agglomeration of Fine Material for Bacterial Heap Leaching,* Council for Mineral Technology, South Africa

74. Standard Test Method for Permeability of Granular Soils (Constant Head), ASTM D 2434- 68 (Reapproved 2006), ASTM International, Pennsylvania, 224-228

75. Steyl, J. D. T., Pelser, M. & Smit, J. T., 2008, 'Atmospheric leach process for nickel laterite ores", *Hydrometallurgy 2008: Proceeding of the Sixth International Symposium in honor of Robert S. Shoemaker*, 540-550

76. Tibbals, R. L., 1987, 'Agglomeration practice in the treatment of precious metal ores', *Proceedings of the International Symposium on Gold Metallurgy*, 77-86

77. Velde, B., 1992, *Introduction to Clay Minerals*, Chapman & Hall, London

78. Velarde, G., 2005, 'Agglomeration control for heap leaching processes', *Mineral Processing and Extractive Metallurgy Review 26*, 219-231

79. Weast, C., R., 1973, *CRC Handbook of Chemistry and Physics,* 54th edn., CRC Press, Ohio

80. William, J., 2005, *Process for Refining Lateritic Ore*, Australian Patent, 2005100146

81. Wray, W. K., 1986, *Measuring Engineering Property of Soils*, Prentice-Hall, New Jersey